Dynamical Analysis and Robust Control Synthesis for Water Treatment Processes

Bui Duc Hong Phuc

A Dissertation Submitted in Partial Fulfillment of Requirements
For the Degree of Doctor of Philosophy

February 2017

Korea Maritime and Ocean University
Ocean Science and Technology School
Department of Convergence Study on Ocean Science and Technology

Supervisor Sam Sang You

본 논문을 BUI DUC HONG PHUC 의 공학박사

학위논문으로 인준함

위 원장 임태우 (인)

위 원 유삼상 (인)

위 원 최형식 (인)

위 원 김환성 (인)

위 원 정석권 (인)

2017 년 1 월

한국해양대학교 해양과학기술전문대학원

Acknowledgement

First and foremost I would like to express my special appreciation and thanks to my advisor Professor Sam-Sang You. I would like to thank you for your encouraging my research and for allowing me to grow as a research scientist. Thank to your guidance, I can develop my best talent and improve quickly in my research. Your advices on both research and my future career have been priceless. I would also like to thank the committee members, professor Seok-Kwon Jeong, professor Hyeung-Sik Choi, professor Hwan-Seong Kim and professor Tae-Woo Lim for serving as my committee members even at hardship.

I would like to thank my family, my father, my mother, my older sister and my younger brother for all of the sacrifices that you've made for me. Your prayers from home help me stand firmly so far. I would also like to thank all of my friends who supported me in writing, and contribute ideas to complete my dissertation. At the end, a special thanks to my beloved wife. She is always beside me, takes care of and encourages me in my hard time. Being with her, I have enough strength to step over any barrier.

Korea Maritime and Ocean University, Busan, Korea

December 23rd 2016

Bui Duc Hong Phuc

Dynamical Analysis and Robust Control Synthesis for Water Treatment Processes

Bui Duc Hong Phuc

Korea Maritime and Ocean University

Department of Convergence Study on Ocean Science and Technology

Abstract

Nowadays, water demand and water scarcity are very urgent issues due to population growth, drought and poor water quality all over the world. Therefore, water treatment plants are playing a vital role for good living condition of human. Water area needs more concentration study to increase water productivity and decrease water cost. This dissertation presents the analysis and control of water treatment plants using robust control techniques. The applied control algorithms include H_∞, gain scheduled and observer-based loop-shaping control technique. They are modern control algorithms and very powerful in robust controlling of systems with uncertainties and disturbances. The water treatment plants include a desalination system and a wastewater process. Since fresh water scarcity is getting more serious, the desalination plants are to produce drinking water and wastewater treatment plants give the reusable water. The desalination system is a RO one used to produce drinking water from seawater and brackish water. The nonlinear behaviors of this system is carefully analyzed before the linearization. Due to the uncertainty caused by concentration polarization, the system is linearized using linear state-space parametric uncertainty framework. The system also suffer from

many disturbances which water hammer is one of the most influential one. The mixed robust H_∞ and μ-synthesis control algorithm is applied to control the RO system coping with large uncertainties, disturbances and noises. The wastewater treatment process is an activated sludge process. This biological process use microorganisms to convert organic and certain inorganic matter from wastewater into cell mass. The process is very complex with many coupled biological and chemical reactions. Due to the large variation in the influent flow, the system is modelized and linearized as a linear parametric varying system using affine parameter-dependent representation. Since the influent flow is quickly variable and easily to be measured, the robust gain scheduled robust controller is applied to deal with the large uncertainty caused by the scheduled parameter. This control algorithm often gives better performances than those of general robust H_∞ one. In the wastewater treatment plant, there exist an anaerobic digestion, which is controlled by the observer-based loop-shaping algorithm. The simulations show that all the controllers can effectively deal with large uncertainties, disturbances and noises in water treatment plants. They help improve the system performances and safeties, save energy and reduce product water costs. The studies contribute some potential control approaches for water treatment plants, which is currently a very active research area in the world.

Key words: Desalination, Reverse osmosis, Wastewater treatment, Activated sludge, H_∞ robust control, Robust gain scheduling control, Water hammer, Uncertainty modeling, Linear parameter-varying system, Observer-based controller.

Contents

List of Tables

List of Figures

Chapter 1. Introduction

Freshwater makes up a very small fraction of all water in the world. While 70 percent of the earth surface is covered by water, only 2.5 percent of it is freshwater. However, almost of freshwater is entrapped in glaciers and snowfields. Essentially, only 0.007 percent of the water in our planet is available for 7 billion people. Nowadays, when world population increases rapidly, the lack of fresh water is becoming a more and more urgent issue in many areas of the world. Currently, nearly 1 billion people in the developing world don't have safe drinking water.

Water demand includes some major parts: domestic, public, industrial and agriculture demand. The domestic demand is the water required in private building for drinking, bathing, gardening, sanitary purpose, etc. The public demand represents the water demand for public utility purpose such as washing of public parks, gardening, washing on roads, public fountain. The industrial demand is the water demand for plants, factories and the agricultural demand is the water used for the irrigation of crops or the watering of livestock. Water demand of human cannot decrease, but the freshwater source is decreasing due to pollutant and climate change.

There have been many water treatment plants operating to produce freshwater. However, due to the efficiency, the price of product water is still high for most of world population who are poor. Furthermore, the demand side seem to be higher than the supply side. Therefore, water treatment is one of the most important areas that needs more investment. Water treatment is a process making water more acceptable for a specific end-use. The end-use may be drinking, industrial water supply, irrigation, river flow maintenance or other uses. The water treatment compromises two main branches, sea and brackish water desalination, and wastewater treatment. The desalination is mostly for producing drinking water and wastewater treatment is mainly to convert wastewater into reusable water which is safely for people and surrounding environment. The current major techniques in those two branches include reverse osmosis (RO) and activated sludge process (ASP), respectively.

In water area, control techniques mostly call the name of simple ones such as PID control, fault tolerant control…However, under higher disturbances, those kinds of controller may not guarantee the robustness of the control system. In order to guarantee system performance in harsh working conditions having more uncertainties, disturbances or noises and to lower product water cost, it is necessary to apply some powerful control method. In this dissertation, the robust H_∞ and gain scheduled control technique are applied to control RO and ASP system, respectively, to contribute some significant advantages. In the following sections, some comprehensive introductions are first given to provide some overviews of the control systems.

1.1 Reverse osmosis process

Historically, desalination developed as a means of providing freshwater in arid countries such as Saudi Arabia, Qatar, UAE…Recently, due to the growing populations, desalination has been spread out all over the world and become important source of fresh water in many places such as major cities in Australia, Singapore, Spain, India, California…The annual world production of desalination illustrated in Fig.1 showing that this kind of filtration is growing very fast and it will be the main source of fresh water in future.

Some desalination technologies have been developed during the last decades to produce low cost and qualified water. Two of the most important technologies are multi-stage flash distillation (MSF) and RO process (Alatiqi *et al*., 1999). MSF is a water desalination technology that distills sea water by flashing a portion of the water into steam in multiple stages arranged as countercurrent heat exchangers. RO is a water purification technology that uses semipermeable membranes to remove ions, molecules, and larger particles from drinking water. In reverse osmosis, an applied pressure is used to overcome osmotic pressure so that the pure solvent is allowed to pass to the membrane whereas the solute is retained on the pressurized side. Reverse osmosis can remove many types of dissolved and suspended species from water,

including bacteria, and is used widely in the production of potable water. In recent years, the market share of RO desalination has widely expanded because of significant improvements and advantages in membrane technology. RO plants have lower energy consumption, investment cost, space requirements and maintenance than other desalination processes (Gambier, 2006).

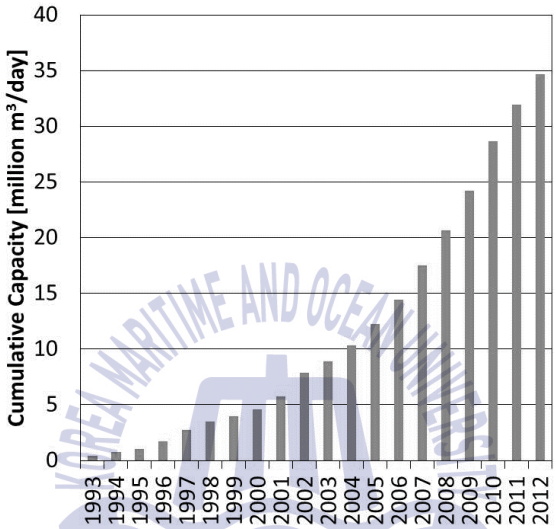

Fig. 1 Growth in world water production from seawater desalination. Source desaldata.com

In 1748, the process of osmosis through semipermeable membranes was first discovered by Jean-Antoine Nollet, a French scientist-cleric. Initial 200 years, it was only a phenomenon observed in the laboratory. In 1950, the desalination of seawater using semipermeable membranes was first carried on by the University of California at Los Angeles (UCLA). At that time the permeate flux was too low to be commercially used until the discovery of asymmetric membranes by Sidney Loeb (UCLA) and Sourirajan at the National Research Council of Canada. They used cellulose acetate polymer as the material for the asymmetric membranes which includes an effectively thin "skin" layer supported atop a highly porous and much thicker substrate region. The invention was so effective that it let fresh water pass

through at a good enough flux for reverse osmosis to be proven available for commercial use. Hereafter, John Cadotte, of FilmTec Corporation developed the process by discovering that membranes with particularly high flux and low salt passage could be made by interfacial polymerization of *m*-Phenylenediamine and trimesoyl chloride. This kind of membrane are very strong and durable. Nowadays, almost all commercial reverse osmosis membrane is made by this method.

In 1965, Coalinga, California became the first site of the RO plant.

In 1977, Cape Coral, Florida became the first municipality to use the RO process on a large-scale with an initial operating capacity of 3 million gallons per day.

By the end of 2001, there were about 15,200 desalination plants in operation or under construction all over the world. Nowadays, RO technique has been conquered the desalination market. It spreads out from the large-scale plants for cities, mid-scale plants for small communities and small-scale systems for home water purification. (wikipedia.org)

In literature, many studies and mathematical models about RO have been reported. They are mainly classified into two categories: the membrane transport model and the lumped parameter model. Some earlier models were presented separately by many authors like Johnson (1980b), Soltaniesh and Gill (1981), Mazid (1984). Slater *et al*. (1985) used non-linear differential equations to present a transient membrane mass transfer model for a small scale RO unit, representing the system conditions, fluxes, solute concentrations and rejections. Davis and Leighton (1987) described the transport of the concentrated boundary layer under laminar flow. Alatiqi *et al*. (1989) introduced a MIMO transfer function model for the desalination process from the experimental data for closed-loop control. Fountoukidis (1989) developed transient models for membrane fouling phenomena. Masahide and Shoji (2000) estimated the transport parameters of RO membranes for sea water desalination. Riverol and Pilipovik (2005) used the feed forward neural network to predict the performance of RO systems. Gambier *et al*. (2007) introduced a lumped parameter dynamic MIMO model for the fault diagnosis purpose. Chaaben *et al*. (2008) developed a MIMO model relating input and output variables by empirical transfer

matrix through a small photovoltaic reverse osmosis desalination unit. The above models describe either the steady state mass transfer phenomena, or the transient dynamics of membrane concentration polarization, and can be used to evaluate the process performance. Hence, some mathematical models and transfer functions have been ready for control purposes.

In RO plants, the system parameters change fast because of fouling. Consequently, membrane cleaning has to be carried out often and process parameters obtained before and after cleaning are very different. Hence, if the controller was optimally adjusted, the control performance will not be acceptable in some operational stages. Furthermore, in a typical RO unit, membranes are very sensitive to feed water temperature, salinity and pressure variations. Therefore, RO systems often operate under many uncertainties. Besides, due to the change in global weather, uncertainties and disturbances are getting larger for desalination plants. Since the hardware and software in RO controlling is now powerful enough, it's necessary to apply a powerful control strategy that can simultaneously deal with large uncertainties, disturbances and noises; rather than fixed proportional-integral-derivative (PID) controller.

Several contributions with varying approaches have been made in the literature to automatic stabilize RO systems. Among the control methods, conventional PID is the most popular due to its simplification. PID can be used as a standard PID controller or redesigned into multiple single-input single-output structure for a more effective control strategy (Alatiqi *et al.* 1989). Many other researchers also develop their control approaches based on PID, such as Kim *et al.* (2009) applied Immune-Genetic Algorithm to get PID parameters for RO system, Gambier & Badreddin (2011) designed multi objective optimization based PID controller so that the control loop was less sensitive to parameter changes, and Rathore *et al.* (2013) used PID tuning in RO to self-tune the parameters of the controller. Another common control algorithm is model predictive control (MPC) which has the ability to allow RO plant to operate with various permeate fluxes (Robertson *et al.*, 1996; Abbas, 2006; Ali *et al.*, 2010). This approach has some

robustness characteristics, but the uncertainty level allowed is not high. Less common controllers for RO system include fuzzy logic (Jafar & Zilouchian, 2002), optimal control (Gambier, 2006), fault tolerant control and feed-forward/feed-back based on Lyapunov control law (McFall *et al*., 2007, 2008). However, at this stage there has been no work on a robust H_∞ controller that simultaneously deals with uncertainties, disturbances and measurement noises in RO system.

1.2 Activated sludge process

Desalination plants often produce drinking water while wastewater treatment plants convert wastewater into reusable water or safely water for environment. There are two wastewater treatment plants namely chemical and biological wastewater treatment plant. They are built for treating sewage, industrial wastewater or agricultural wastewater. In this dissertation, activated sludge process is studied, which is the main section of a biological wastewater treatment plant.

Activated sludge is a process in which a mass of microorganisms is cultivated to break down organic matter into carbon dioxide, water, and other inorganic compounds. Basically, the activated sludge process includes an aeration tank, clarifier, biomass return, and waste biomass disposal. The separation of the active biomass from the treated wastewater is performed by settling in clarifiers but may also be done by other methods, including flotation and membrane filtration. The activated sludge process was discovered in 1913 in the United Kingdom by Ardern and Lockett. Initially, the design and operation of ASPs were mostly based on the empirical rules of thumb. Since the 1950's, many researchers and engineers have applied theories of reactor design and microorganism growth to wastewater treatment systems, making it possible to describe substrate degradation, microorganism growth, and plant performance in terms of mathematical models (wikipedia.org). In particular, the Eckenfelder (1955) and Lawrence-McCarty (1970) activated sludge models gained widespread practical application due to their ability to predict the plant performance (Huo, 2005). The two models set the basis for many

others developed models. Especially, the Monod's formulation introduced in Lawrence-McCarty model plays a core role to modelize the growth of microorganisms.

Based on the models above, many other advanced models have been created. Up to this end, Activated Sludge Models ASM family (ASM1, ASM2-ASM2d, ASM3) proposed by the International Water Association (IWA) are the most commonly applied mathematical models for the modelling of the biological wastewater treatment plants.

The Activated Sludge Model No. 1 (ASM1) (Henze *et al.*, 1986) is considered as the reference model, since this model triggered the general acceptance of WWTP modelling, first in the research community and later on also in industry. The ASM1 essentially describes a single-stage activated sludge system performing simultaneous COD (Chemical Oxygen Demand) oxidation, nitrification and denitrification processes. (Gernaey, 2004)

In 1995, the Activated Sludge Model no. 2 was introduced. This model included nitrogen removal and biological phosphorus removal. The ASM2 model was expanded in 1999 into the ASM2d model, where denitrifying phosphorus-accumulating organisms were included.

The ASM3 model (Gujer *et al.*, 1999) was also developed for biological N removal WWTPs, with basically the same goals as ASM1. The ASM3 model is intended to become the new standard model, correcting for a number of defects that have appeared during the usage of the ASM1 model (Gujer *et al*., 1999). The major difference between the ASM1 and ASM3 models is that the latter recognises the importance of storage polymers in the heterotrophic activated sludge conversions (Gernaey, 2004).

Three models have been successfully applied to full-scale treatment plants and shown to be a good compromise between the complexity of the activated sludge processes and prediction of the plant behavior under dynamic conditions (Hassanpour, 2014). Among these models, the ASM1 is one of the most important models. Since its first development in 1986, it has been well and widely applied in

many practicing projects. It has become a reference for many scientific and practical projects, and has been implemented (in some cases with modifications) in most of the commercial software available for modelling and simulation of WWTPs (Gernaey, 2004). It come to a conclusion that through its developments and contributions, nowadays, ASP is currently the best documented and most widely used process for the control of secondary wastewater treatment plants.

The control of ASP is challengeable, due to the complexity in biochemical reactions and the variation in flow and concentration at the influent. Several control strategies have been reported to be applied for ASP. They include the conventional PI, PID and cascade control algorithms. The common method was the feed-forward of influent ammonia to handle disturbance rejection in combination with cascade control such as in the study of Ingildsen *et al*. (2002), Krause *et al*. (2002), Vrecko *et al*. (2003), Yong *et al*. (2005), Vrecko *et al*. (2006), Zhang *et al*. (2008) and Thornton *et al*. (2010); Fuzzy control (Meyer and Pöpel, 2003; Serralta, 2002; Baroni *et al*., 2006; Yong *et al*., 2006) is also popular in ASP control. It has been widely used in combination with PI controller. Meyer and Pöpel (2003) applied a fuzzy controller to control the DO (dissolved oxygen) set-point and the ratio of aerobic and anoxic zones for a pilot plant. The control system is a combination of feed-forward of influent ammonia with feedback effluent ammonia and nitrate as well as the effluent ammonia time variation. A similar control strategy was also found in the study of Serralta *et al*. (2002) and Yong *et al*. (2006), where DO and nitrate are controlled with fuzzy controller. Influent and effluent ammonia was used as inputs to the controller. Baroni *et al*. (2006) implemented of a fuzzy logic controller with full scale in a predenitrification system. Both the DO set-point and the air supply was controlled through fuzzy logics. The performance was stable and good in energy saving.

In robust control aspect, Georgieva (1999) applied state-space H_∞ control to an ASP system, dealing with parametric uncertainty in the system. The controlled and manipulated variable was chosen as the biomass and recycle flow rate, respectively. The performance of the control system is better comparing to the PI controller.

Recently, model predictive control (MPC) has been widely used since its ability to handle constraints and to include multiple variables (Weijers, 2000; Sanchez & Katebi, 2003; Holenda *et al*., 2008; O'Brien *et al*., 2011). The set-point of DO was controlled by Sanchez & Katebi (2003) using MPC. The authors compare three different MPC controllers with a single PI controller with constant set-point. The result showed that there were some improvement in the performance the controller structure was easy to implement. Holenda *et al*. (2008) used MPC for DO tracking with a process model incorporating classical DO dynamics. The result compared to standard PI control only shows marginal improvements on effluent quality. A full-scale plant was controlled using MPC in O'Brien *et al*. (2011). In this work, the improvement is that the on/off control strategy for the surface aerators in an activated sludge process for BOD-removal is replaced by a black-box model of the aeration in combination with feedforward of the influent BOD load.

Along with MPC, Generic algorithm (GA) also gives some benefits for ASP control (Yamanaka *et al*.; 2006 and Beraud *et al*.; 2009). Yamanaka *et al*. (2006) used the Benchmark Simulation Model to evaluate a cost minimization control problem. The set-points of the process based on optimization using a simplified process model and GA. The optimizer determined an appropriate ammonia set-point which the lower level PI controller tracks. Beraud *et al*. (2009) also applied Multi-objective GA to optimize the set-point for ASP in three consecutive aerobic zones. Comparing to the conventional GA, the obtained energy reduction is of 10-20 % with maintained treatment performance. Besides the mentioned control approaches, less popular algorithms applied for ASP control includes linear quadratic optimal control, self-tuning control, adaptive linearizing control (Bastin, 1990; Ferreira, 1996).

Till now, the existing controllers for ASP have not addressed the large variation of the influent flow and concentration. Due to this variation, the ASP dynamics has big changes during it operation time, acting like a nonlinear system. Under the robustness point of view, the current most powerful H_∞ control still has some limitations in controlling of ASP, since the controller is designed for linear system. Therefore, the robust gain scheduling controller will be designed to deal with

nonlinear behavior of ASP, driving the system stably to the optimal energy consumption.

1.3 Robust H_∞ and gain scheduling control

It is known that to design a control system for a water treatment plant satisfying the control requirements, it needs a reasonably accurate model of the real system. However, real plants are hard to be described exactly by mathematical models. Furthermore, the designed controller must handle the uncertainties which make the state of the real plant differs from its mathematical model. A controller that is able to handle model uncertainties and disturbances is said to be robust, and the theory to design that controller is called robust control theory.

H_∞ (i.e. "*H*-infinity") methods are used in control theory to control uncertain systems achieving robust stabilization with guaranteed performance. In this framework, the control problem is expressed as a mathematical optimization problem and then the controller is calculated to solve this optimization. H_∞ techniques have the advantage over classical control techniques in that they are readily applicable to multivariate systems with coupling channels and they can deal with uncertain systems and modelling errors as well as exogenous disturbances. These methods were introduced into control theory in the late 1970s-early 1980s by George Zames (1981), and Zames and Francis (1983), known as the H_∞ optimal control theory. The H_∞ optimization approach and the μ-synthesis/analysis method have been well developed and applied. The label H_∞ is related to the fact that a proper rational matrix function is stable if and only if it is analytic and uniformly bounded in the open right half plane defined by $\mathrm{Re}(s) > 0$. The H_∞ norm is the maximum singular value of the function over that space. μ-synthesis is the representation of the structured singular value define by Doyle (1982).

In the early of 1990s, the succeed of H_∞ robust control technique in control systems such as distillation columns, hard-disk drives, and the inverted-pendulum made the industrial community see how to apply the new method and enjoy the

benefits brought from this control technique. Till now, it has proved its abilities through many complex applications, especially in control of systems that operate in the environment existing much disturbance such as satellites, airplanes, vehicles, ships.

The robust control theory is well established for linear systems but almost all real plants have nonlinear characteristics. If the plant operates in a narrow region, the robust control methods can be applied to design a linear robust controller for a respective linear system achieved from linearization and the nonlinearities are treated as model uncertainties. However, for real nonlinear processes, where the operating region is large, the linear robust controller may not be able to meet the performance specifications. Therefore, nowadays the control design for nonlinear systems is very concentrate and important.

Gain scheduling is one of the most common used controller design approaches for nonlinear systems and has a wide range of use in industrial applications. Gain scheduling appears in the 1960s. Most of its early applications were in flight control and aerospace areas. Then, gradually, this approach has been used almost everywhere in control engineering, which was greatly advanced with the introduction of linear parameter-varying (LPV) systems by Jeff. S. Shamma (1988). The reason is using the LPV paradigm, ones can describe nonlinear system as a family of linear systems and hence can investigate the stability of these systems. Nowadays, when gain scheduling controller is designed using robust control theory, the performance has been much improved.

Packard (1994) and Apkarian *et al.* (1995) consider LPV design approaches which are based on small gain theory, which allowed to construct a robust gain scheduled controller. The robust GS controller is more powerful but still conservative for real parameters. Becker *et al.* (1993, 1994) generalized the approach to seek a single quadratic Lyapunov function to ensure H_∞-like performance for all possible trajectories of the LPV plant. The improvement essentially comes from the ability of the quadratic H_∞ performance formalism to handle real parameters. Due to the ability to deal with the varying parameters and the combination with advanced stability

criterions, nowadays the robust LPV gain scheduling belongs to the most popular approaches to nonlinear control design.

In this dissertation, based on the parametric uncertainties, the operating range, and the indirect measurement of concentration polarization, the RO system is controlled by a robust H_∞ controller. With the large variation of the influent flow of the ASP and the availability of the measurement of this parameter, the robust gain scheduling controller is applied to control the DO concentration in the system. The result of the dissertation will be remarkable contributions for water treatment industry.

The sequel of this dissertation is organized as follows:

Chapter 2: The introduction about robust H_∞ and μ-synthesis theory.

Chapter 3: The introduction about Robust gain scheduling theory.

Chapter 4: The introduction and modeling of the reverse osmosis system and the application of the mixed robust H_∞ and μ-synthesis controller on the RO system.

Chapter 5: The introduction and modeling of the activated sludge process and the application of the robust gain scheduling controller on the ASP.

Chapter 6: The observer-based loop-shaping control of anaerobic digestion.

Chapter 7: Conclusion.

Chapter 2. Robust H_∞ controller

2.1 Introduction

Throughout 1960s and 1970s, the optimal linear quadratic (LQ) control was popular, largely applied in controlling with the work of Kalman. In the late 1970s, the control practice showed some limitations of LQ control. Doyle (1978) showed that there are no assurance for stability of LQG, which is an LQR control combined with a Kalman filter.

The control theory literature started to look for a more robust approach. Zames (1981) developed H_∞ control which is more robust than LQ control. Since in LQ control, the performance is measured with a 2-norm across frequencies, while H_∞ control uses a ∞-norm that cares the peak of the losses across frequencies. It can be interpreted as the maximum magnitude of the disturbances affects the outputs.

The uncertainty sets in the H_∞ approach are unstructured. They illustrate perturbations of the model. These perturbation are bounded but have no particular form. Recently, the structured perturbations have been studied such as parametric uncertainty, diagonal uncertainty or uncertainty in some particular channel. The robust control theory with structured uncertainty use the structured singular value (μ-synthesis) rather than the ∞-norm as a measure of performance. μ-synthesis has been getting some important stability and performance achievements. However the design procedure is a more daunting task and the theory is not as fully developed as the unstructured case.

2.2 Uncertainty modelling

Uncertainties are unavoidable in every real system. Uncertainties can be classified into two types: disturbance and dynamics perturbations. The former includes exogenous disturbance and sensor noises. The latter comes from the gap between mathematical model and the actual dynamics of the system. It is known that

mathematical model is just an approximation with some assumptions to simplify the real system. Furthermore, in the modeling, some nonlinearities is ignored and there is no varying parameters as in real systems. The dynamics perturbations may adversely affect the stability and performance of a control system. Therefore, this kind of uncertainty is described in this section so that they are well considered under robust control analysis.

2.2.1 Unstructured uncertainties

Dynamics perturbations such as unmodelled dynamics can occur at different parts in a system. However, they can be lumped into a single uncertainty block Δ. Since there is no information about the uncertainty except it bound, it is also referred as unstructured uncertainty. This uncertainty can be described by different frameworks, as following, where $G_p(s)$ denotes perturbed uncertain system and $G_o(s)$ refers to the nominal system:

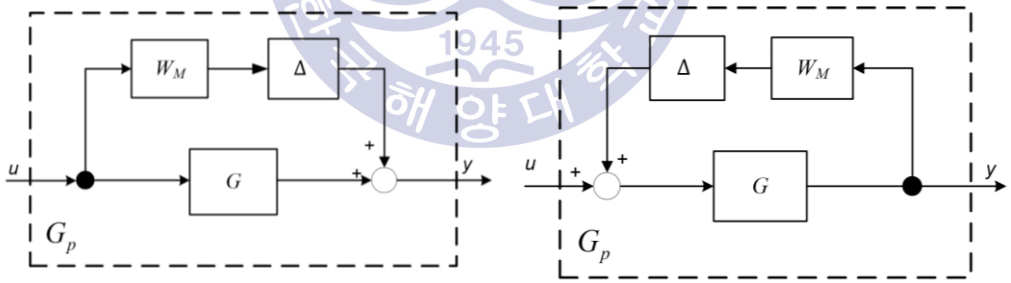

a) *Additive uncertainty*

$$G_p(s) = G(s) + \Delta(s)W_M(s)$$

b) *Inverse additive uncertainty*

$$G_p(s) = G(s)(I - \Delta(s)W_M(s)G(s))^{-1}$$

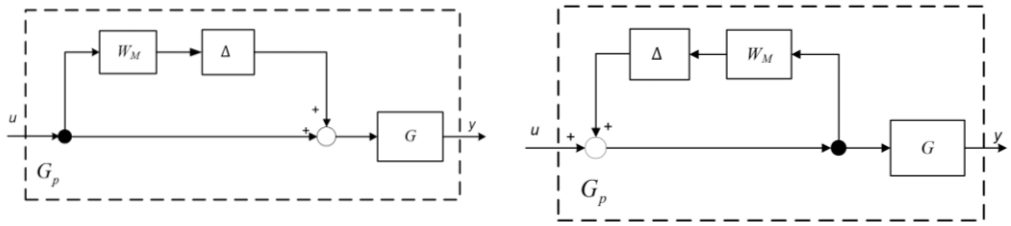

c) *Input multiplicative uncertainty*

$$G_p(s) = G(s)(I + \Delta(s)W_M(s))$$

d) *Inverse input multiplicative unc.*

$$G_p(s) = G(s)(I - \Delta(s)W_M(s))^{-1}$$

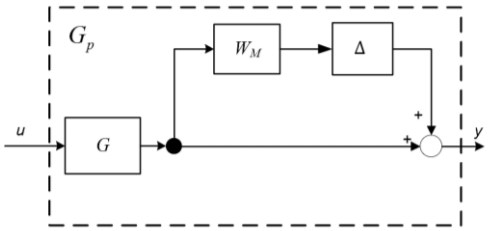

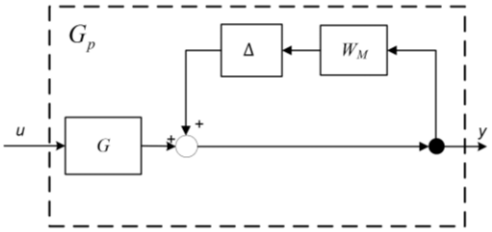

e) *Output multiplicative uncertainty*

$$G_p(s) = (I + \Delta(s)W_M(s))G(s)$$

f) *Inverse output multiplicative unc.*

$$G_p(s) = (I - \Delta(s)W_M(s))^{-1}G(s)$$

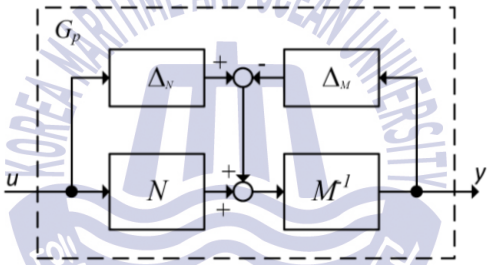

g) *Left coprime factor uncertainty*

$$G_p(s) = (M(s) + \Delta_M(s))^{-1}(N(s) + \Delta_N(s))$$

Fig. 2 Some common kinds of unstructured uncertainty

2.2.2 Parametric uncertainties

The unstructured uncertainty describes unmodelled dynamics and neglected nonlinearities occurring mostly in high frequency ranges. However, in real system, the dynamics perturbations also come from variations of certain parameters. They occur in low frequency ranges and is called “parametric uncertainties”. Parametric uncertainty is sometime called “structured uncertainty” since it models the uncertainty is a structured manner. It is often expressed along with transfer function

or state-space representation. For example, the parametric uncertainties of three components in a mass spring damper system can be represented in the following structure, using state-space representation:

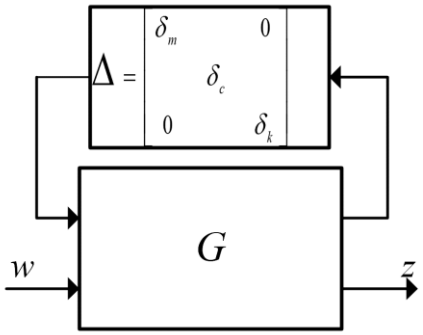

Fig. 3 Parametric uncertainty

2.2.3 Structured uncertainties

In some robust design problem, the uncertainties would include structured uncertainties, such as unmodeled dynamics as well as parametric uncertainty. The whole system then can be rearranged in a standard configuration of linear fractional transformation $F(M,\Delta)$. The uncertainty block now has the structure:

$$\Delta = diag[\delta_1 I_{r_1}, ..., \delta_s I_{r_s}, \Delta_1, ..., \Delta_f], \quad \delta_i \in C, \Delta_j \in C^{m_j x m_j} \tag{1}$$

where $\sum_{i=1}^{s} r_i + \sum_{f=1}^{f} m_j = n$, and n is the dimension of the uncertainty block Δ.

The total uncertainty block Δ now has two kinds of uncertainty: s is the repeated scalar blocks and f full blocks.

2.2.4 Linear fractional transformation

Linear fractional transformation (LFT) is a standard configuration to account the uncertainties into a system. There are two categories, say upper and lower LFT.

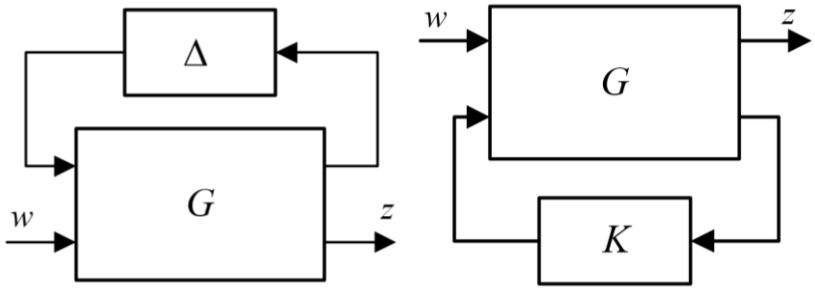

Fig. 4 Upper linear fractional transformation (left) and lower LFT (right)

Providing that the system G is partitioned as $G = \begin{bmatrix} G_{11} & G_{12} \\ G_{21} & G_{22} \end{bmatrix}$, the input and output relation in upper LFT is derived as:

$$z = \left[G_{22} + G_{21}\Delta(I - G_{11}\Delta)^{-1}G_{12} \right] w = F_u(G, \Delta)w \tag{2}$$

The lower LFT is calculated using:

$$F_l(G, K) = \left[G_{11} + G_{12}K(I - G_{22}K)^{-1}G_{21} \right] \tag{3}$$

2.3 Stability criterion

2.3.1 Small gain theorem

Consider a feedback configuration as in Fig. 5. Providing that G_1 and G_2 are the transfer function of LTI system.

Theorem 2.3.1: If G_1 and G_2 are stable, i.e $G_1, G_2 \in \mathcal{H}_\infty$, then the closed-loop system is internally stable if and only if $\|G_1 G_2\|_\infty < 1$ and $\|G_2 G_1\|_\infty < 1$.

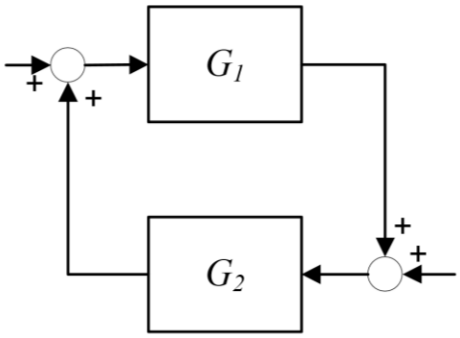

Fig. 5 A feedback configuration

Note that the small theorem consider the norm of the closed loop system, therefore it is independent on the sign of feedback.

The theorem actually came from Nyquist stability condition as stated in the following. Consider an uncertain feedback system as in Fig. 6 where there is input multiplicative uncertainty magnitude of $\|W_M(j\omega)\|_\infty$.

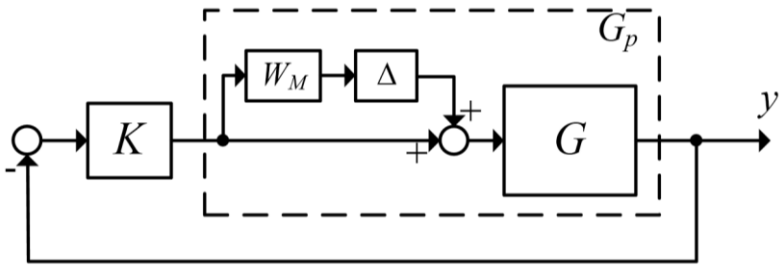

Fig. 6 Uncertain feedback system

The uncertainty loop transfer function becomes:

$$L_p = G_p K = GK(1+W_M\Delta) = L + W_M L\Delta, |\Delta(j\omega)| \le 1, \forall\omega \quad (4)$$

According to Nyquist stability condition, the closed-system is robust stable if L_p does not encircle the point -1 in the Nyquist diagram,

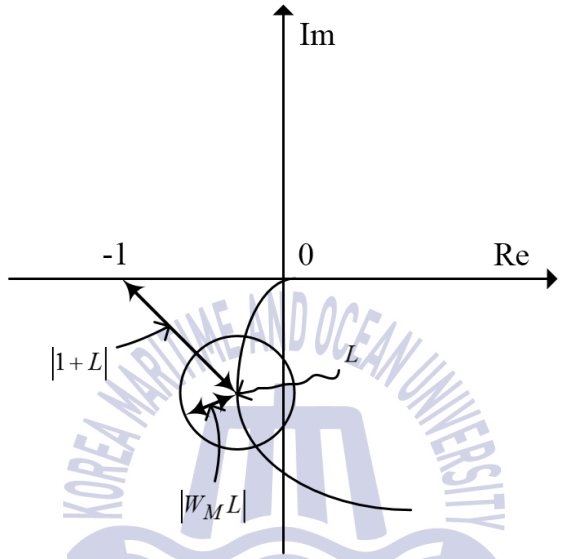

Fig. 7 Nyquist plot of closed-looop system for robust stability

From the Fig. 7, one can see that $|1+L|$ is the distance from the point -1 to the center of the disc representing L_p, and that $|W_M L|$ is the radius of the disc. Encirclements are avoided if none of the discs cover -1, it is also expressed as:

$$\begin{aligned} &\text{RS} <=> |W_M L| < |1+L|, \forall\omega \\ &<=> \left|\frac{W_M L}{1+L}\right| < 1, \forall\omega <=> |W_M T| < 1, \forall\omega \\ &<=> \|W_M T\|_\infty < 1 \end{aligned} \quad (5)$$

2.3.2 Structured singular value (μ) synthesis brief definition

If there exist a M - Δ structure as in Fig. 8

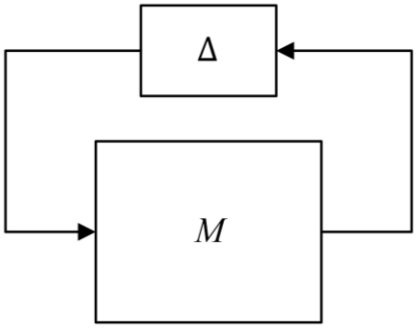

Fig. 8 M - Δ structure

For $M \in C^{n_x n}$, the structured singular value w.r.t M, μ_Δ is defined as in Doyle (1982):

$$\mu_\Delta(M) = \frac{1}{\min\{\bar{\sigma}(\Delta) \mid \Delta \in \Delta, \det(I - M\Delta) = 0\}}$$
$$\Rightarrow \min\{\bar{\sigma}(\Delta) \mid \Delta \in \Delta, \det(I - M\Delta) = 0\} = \frac{1}{\mu_\Delta(M)} \quad (6)$$

where $\bar{\sigma}(\Delta)$ is the maximum value of the uncertainty matrix Δ.

Suppose the peak (across frequency ω) of the $\mu_\Delta(M)$ is β. This means that for all perturbation matrices Δ with the appropriate structure, and satisfy $\max_\omega \bar{\sigma}[\Delta(j\omega)] < 1/\beta$, the perturbed system is stable. Normally, $\beta < 1$ is the requirement for a maximum perturbation size 1.

2.4 Robustness analysis and controller design

2.4.1 Forming generalised plant and N-$\hat{\Delta}$ structure

Consider a typical control system as in Fig. 9 with the nominal system G, the multiplicative input uncertainty expressed by W_M and Δ, the controller K. Inputs to the system include r, d, n, which are reference, disturbance at system output, and noise, respectively. These three inputs are weighted by their respective weighting function, W_r, W_d, W_n. They may be constant or dynamic which respectively describe the frequency content of the set points, disturbances, and noise signals. u is the control signal, e is the error and y is the measured output.

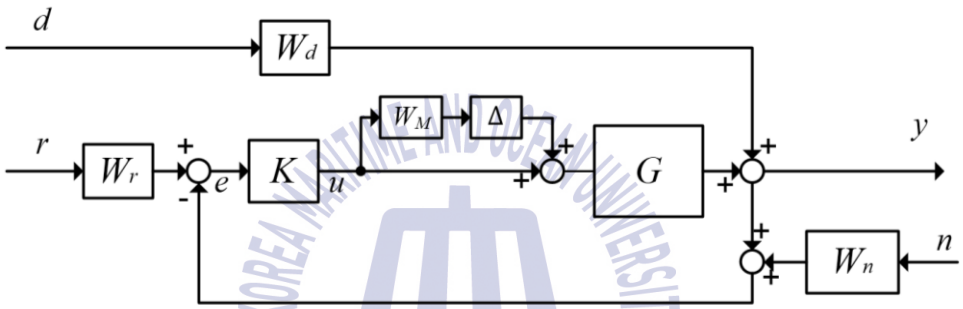

Fig. 9 A typical control system

In the procedure to create the M-Δ-like structure as in Fig. 8, the block diagram in Fig. 9 is reconstructed as in Fig. 10. In this new formulation, a weighting function W_P is added at the output to represent the performance requirement level. Δ_p is the fictitious perturbation used in case of robust performance analysis. The uncertainty block Δ is isolated and form generalised plant P blocked in the dashed rectangular. Z is the regulated output.

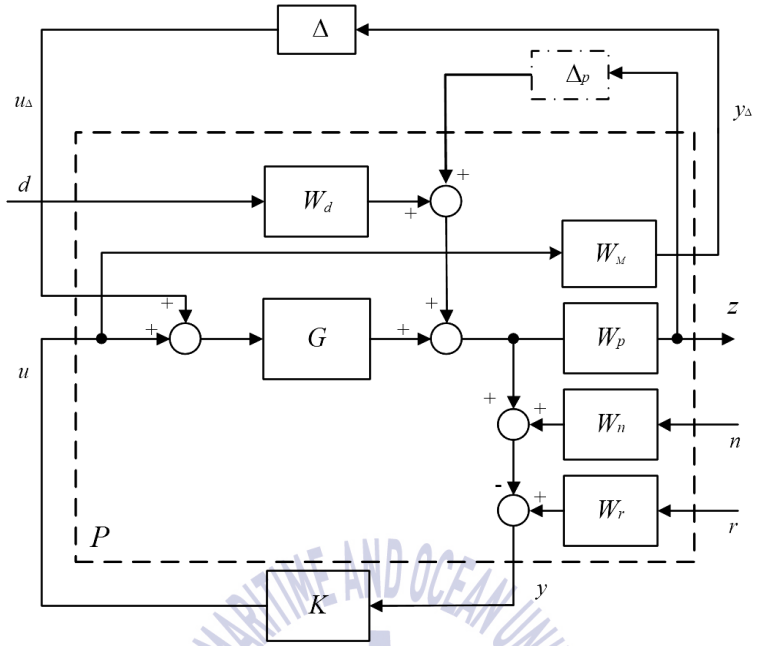

Fig. 10 Block diagram of generalised plant *P*

From the block diagram in Fig. 10, a generalised *P* block can be formed by grouping the blocks in the dashed rectangular. It shows that the generalised plant *P* is further written as

$$\begin{bmatrix} y_\Delta \\ z \\ \hline y \end{bmatrix} = \underbrace{\left[\begin{array}{cccc|c} 0 & 0 & 0 & 0 & W_M \\ W_p G_{de} & W_p W_d & 0 & 0 & W_p G_{de} \\ \hline -G_{de} & -W_d & -W_n & W_r & -G_{de} \end{array}\right]}_{P} \begin{bmatrix} u_\Delta \\ d \\ n \\ r \\ \hline u \end{bmatrix} \tag{7}$$

with $u_\Delta = \Delta y_\Delta$ and $u = Ky$

The current block diagram is then redrawn in a compact form as in Fig. 11

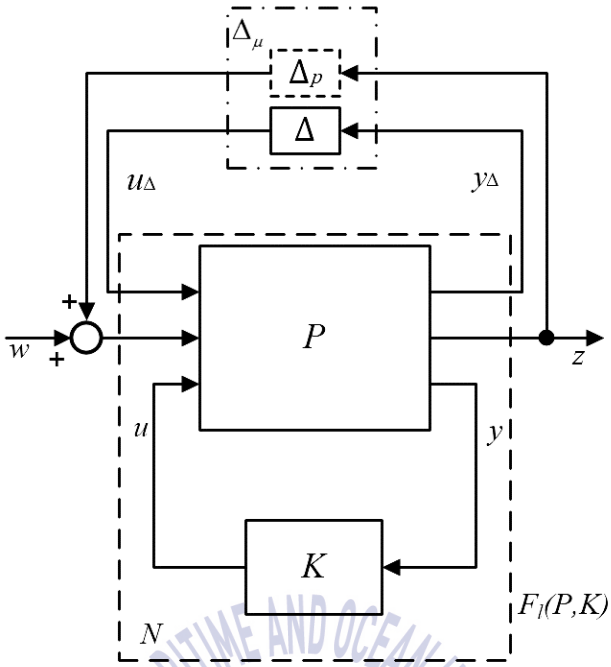

Fig. 11 *P*-*K* grouping and N - $\hat{\Delta}$ structure

In Fig. 11, the closed-loop transfer matrix N that connects the generalised plant P with the controller K via a lower linear fractional transformation (LFT), is defined by

$$\begin{bmatrix} y_\Delta \\ z \end{bmatrix} = \underbrace{F_L(P,K)}_{N} \begin{bmatrix} u_\Delta \\ w \end{bmatrix} \tag{8}$$

where $w = \begin{bmatrix} d & n & r \end{bmatrix}^T$

$$N = F_l(P,K) = P_{11} + P_{12}K(I - P_{22}K)^{-1}P_{21} \tag{9}$$

$$= \left[\begin{array}{c|ccc} -W_M T_i & -W_M K S_o W d & -W_M K S_o W_n & W_M K S_o W_r \\ \hline W_P S_o G_{de} & W_P S_o W_d & -W_P T_o W_n & W_P T_o W_r \end{array}\right]$$

$$= \left[\begin{array}{c|ccc} N_{11} & N_{12} & N_{13} & N_{14} \\ \hline N_{21} & N_{22} & N_{23} & N_{24} \end{array}\right] = \left[\begin{array}{c|c} N_{y_\Delta u_\Delta} & N_{y_\Delta w} \\ \hline N_{zu_\Delta} & N_{zw} \end{array}\right]$$

with $T_i = KG_{de}(I + KG_{de})^{-1}$, $T_o = G_{de}K(I + G_{de}K)^{-1}$ and $S_o = (I + G_{de}K)^{-1}$. $N_{y_\Delta u_\Delta}$ is the transfer matrix from u_Δ to y_Δ, $N_{y_\Delta w}$ the transfer matrix from w to y_Δ, N_{zu_Δ} the transfer matrix from u_Δ to z and N_{zw} the transfer matrix from w to z.

In this final form, the N - $\hat{\Delta}$ structure is similar to M- Δ one, so that the robust control synthesis based on small gain theorem and structured singular value can be applied. Note that $\hat{\Delta}$ block includes the unmodelled block Δ and the fictitious block Δ_p.

2.4.2 Robustness analysis

The objectives of the H_∞ robust controller for any control system include:

- Nominal stability (NS): The system is internally stable with the nominal model (no model uncertainty). A system is internally stable if all the transfer functions of the closed-loop system are stable, i.e. there is no pole staying in the right half plane of the complex plane.
- Nominal Performance (NP): The system satisfies the performance specifications with the nominal model (no model uncertainty). The nominal system performance depends on the sensitivity (S_o), which is a very good indicator of the disturbance attenuation ability. To attenuate the disturbance effects, the singular value of S_o in the element N_{22} in Eq. (9) must be small. Therefore, to limit the value of S_o, the performance weighting function W_P is selected and the controller is designed so that

$$\left\|W_P S_o W_d\right\|_\infty < 1 \Leftrightarrow \mu_\Delta(N_{22}(j\omega)) < 1, \ ^\forall\omega \tag{10}$$

where $\mu_\Delta(N_{22}(j\omega))$ is the structured singular value of the nominal system that respects to the uncertainty Δ.

Nominal performance includes disturbances and noises attenuation. To reduce noises, the singular value of complementary sensitivity (T_o) in the element N_{23} in Eq. (9) must be small. Note that T_o+S_o=1. This implies that, the disturbances and noises reduction cannot be achieved in the same frequency range. Depending on the characteristics of disturbances and noises, disturbances attenuation should be achieved in low-frequency range and noises reduction should be achieved in high-frequency range.

- Robust stability (RS): The system is stable for all perturbed plants about the nominal model, up to the worst-case model uncertainty (including the real plant). The robust stability criterion is written as

$$\left\|W_M T_i\right\|_\infty < 1 \ \Leftrightarrow \ \mu_\Delta(N_{11}(j\omega)) < 1, \ ^\forall\omega \tag{11}$$

where $\mu_\Delta(N_{11}(j\omega))$ is the structured singular value of the system that respects to parametric uncertainty Δ.

- Robust performance (RP): The system satisfies the performance specifications for all perturbed plants about the nominal model, up to the worst-case model uncertainty (including the real plant). The robust performance property is guaranteed if

$$\begin{aligned} &\left\|F_u(N,\Delta)\right\|_\infty = \left\|N_{zw} + N_{zu_\Delta}\Delta(I - N_{y_\Delta u_\Delta}\Delta)^{-1}N_{y_\Delta w}\right\|_\infty < 1, \quad \forall\Delta, \left\|\Delta\right\|_\infty < 1, \\ &\text{and robust stability} \\ &\Leftrightarrow \mu_{\hat{\Delta}}(N) < 1, \ ^\forall\omega, \ \hat{\Delta} = \begin{bmatrix} \Delta & 0 \\ 0 & \Delta_P \end{bmatrix} \end{aligned} \tag{12}$$

where uncertain perturbation $\hat{\Delta}$ includes Δ and fictitious perturbation Δ_P that represents the H_∞ performance specification in the framework of μ approach. $\mu_{\hat{\Delta}}(N)$ is the structured singular value of the system that respects to $\hat{\Delta}$.

After having all the initial weighting functions, the DK-iteration of μ-synthesis toolbox in Matlab is applied to design the μ controller for the system in case of structured uncertainty. Otherwise, *hinfsyn* command in robust control toolbox will be applied to design the H_∞ robust controller.

The key design issue is to choose reasonable weighting functions W_M and W_P satifying all the above requirements. The controller design procedure is a loop including tries and tuning. The steps to design the controller are summarized as follow:

Step 1. Model the uncertainty

Step 2. Weight the input signals by reasonable dynamics weighting functions or constants

Step 3. Choose the uncertainty weighting function W_M and performance weighting function W_P

Step 4. Create a generalized plant and forming M- Δ structure

Step 5. Design a robust controller using Matlab toolboxes, check the performance, if not satisfied, go back to step 3.

2.5 Reduced controller

The achieved controller is efficient, however, its order is very high. This high-order controller is very complex to be implemented practically. A high-order controller will lead to high cost, difficult commissioning, poor reliability and potential problem in maintenance. Therefore, it's necessary to simplify the controller into lower-order controller that achieves the same level of performance, so that it is easier to be applied in RO system.

The basis of model reduction is addressed as following. Given a stable model *G(s)* of order *n*, with state space form is given as:

$$\begin{aligned} \dot{x}(t) &= Ax(t) + Bu(t) \\ y(t) &= Cx(t) + Du(t) \end{aligned} \tag{13}$$

where $x(t) \in \Re^n, A \in \Re^{n \times n}, B \in \Re^{n \times m}, C \in \Re^{k \times n}, u(t) : \Re \to \Re^m, y(t) : \Re \to \Re^k$

Assuming the system is stable, i.e matrix *A* is Hurwits. Find a reduced order model $G_r(s)$ of degree *k* (McMillan degree) such that the infinity norm of the error $\|G(s) - G_r(s)\|_\infty$ is minimized, w.r.t the same input *u*(*t*).

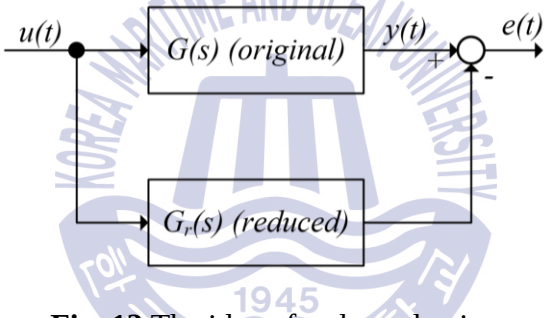

Fig. 12 The idea of order reduction

In general, there are three main methods to obtain a lower-order controller for a relatively high-order one: balanced truncation, balanced residualization and optimal Hankel norm approximation. Each method gives a stable approximation and a guaranteed bound on the error in the approximation. In this dissertation Hankel norm approximation is chosen to reduce controller's order. Therefore, the Hankel reduction algorithm will be stated carefully in this section.

2.5.1 Truncation

Let (A, B, C, D) be a minimal realization of a stable system $G(s)$, and partition the state vector x, of dimension n, into $\begin{bmatrix} x_1 \\ x_2 \end{bmatrix}$ where x_2 is the vector of n-k states that we want to remove. The state-space form become:

$$\begin{aligned} \dot{x}_1 &= A_{11}x_1 + A_{12}x_2 + B_1u \\ \dot{x}_2 &= A_{21}x_1 + A_{22}x_2 + B_2u \\ y &= C_1x_1 + C_2x_2 + Du \end{aligned} \tag{14}$$

A k^{th}-order truncation of the full system is given by G_a = (A_{11}, B_1, C_1, D). The truncated model G_a is equal to G at infinite frequency. Matrix A is in Jordan form so it is easy to reorder the states so that x_2 corresponds to high frequency or fast mode.

For simplicity, assume that A is diagonalized as:

$$A = \begin{bmatrix} \lambda_1 & 0 & \cdots & 0 \\ 0 & \lambda_2 & \cdots & 0 \\ \vdots & \vdots & \ddots & \vdots \\ 0 & 0 & \cdots & \lambda_n \end{bmatrix} \tag{15}$$

and

$$B = \begin{bmatrix} b_1^T \\ b_1^T \\ \vdots \\ b_n^T \end{bmatrix}, C = \begin{bmatrix} c_1 & c_2 & \cdots & c_n \end{bmatrix} \tag{16}$$

Then, if the eigenvalues are ordered so that $|\lambda_1|<|\lambda_2|$..., the fastest modes are removed from the model after truncation. The error between G and G_a is given as follow (Skogestad and Postlethwaite, 2005):

$$\|G - G_a\|_\infty \le \sum_{i=k+1}^{n} \frac{\bar{\sigma}(c_i b_i^T)}{|\mathrm{Re}(\lambda_i)|} \tag{17}$$

2.5.2 Residualization

In truncation as stated above, all states and dynamic associated with x_2 are removed. In residualization, $\dot{x}_2$ is set to zero in the state space. Then x_2 can be calculated based on x_1 and u, back substitution of x_2 gives:

$$\begin{aligned} \dot{x}_1 &= (A_{11} - A_{12}A_{22}^{-1}A_{21})x_1 + (B_1 - A_{12}A_{22}^{-1}B_2)u \\ y &= (C_1 - C_2A_{22}^{-1}A_{21})x_1 + (D - C_2A_{22}^{-1}B_2)u \end{aligned} \tag{18}$$

Providing that A_{22} is invertible and define

$$A_r \triangleq A_{11} - A_{12}A_{22}^{-1}A_{21} \tag{19}$$

$$B_r \triangleq B_1 - A_{12}A_{22}^{-1}B_2 \tag{20}$$

$$C_r \triangleq C_1 - C_2A_{22}^{-1}A_{21} \tag{21}$$

$$D_r \triangleq D - C_2A_{22}^{-1}B_2 \tag{22}$$

then the residualization of $G(s)$ is the reduced order model $G_a(s)= (A_r, B_r, C_r, D_r)$

It is noted that truncation is better for the systems that require accuracy at high frequency while residualization works well for low-frequency system.

2.5.3 Balanced realization

Balanced realization is an asymptotically stable minimal realization where the controllability and observability Gramians are equal and diagonal.

Let (*A, B, C, D*) be a minimal realization of a stable, rational transfer function *G(s).* Then, (*A, B, C, D*) is called balanced if the controllability and observability Gramian (*P, Q)* satisfy following Lyapunov equations:

$$A^T Q + QA = -C^T C \tag{23}$$

$$AP + PA^T = -BB^T \tag{24}$$

where

$$Q \triangleq \int_0^\infty e^{A^T t} C^T C e^{At} dt \tag{25}$$

$$P \triangleq \int_0^\infty e^{A^T t} B B^T e^{At} dt \tag{26}$$

Any minimal realization of a stable transfer function can be balanced by state similarity transformation, in other word, by changing of the basis of state and Gramians into quadratic forms:

$$x \to Tx, P \to TPT^T, Q \to (T^T)^{-1} Q T^{-1} \tag{27}$$

Then the balanced realization between controllability and observability Gramian can be achieved as:

$$P = Q = diag(\sigma_1, \sigma_2, ..., \sigma_n) \triangleq \Sigma = \begin{pmatrix} \Sigma_1 & 0 \\ 0 & \Sigma_2 \end{pmatrix}, \sigma_1 \geq \sigma_2 \geq ... \geq \sigma_n > 0 \tag{28}$$

The σ_i are the ordered Hankel singular value of $G(s)$, defined as:

$$\sigma_i = \sqrt{\lambda_i (PQ)} \tag{29}$$

A full model then can be reduced by using balanced truncation, balanced residualization or optimal Hankel norm approximation. The latest is the most popular so it will be well stated in the next section.

2.5.4 Optimal Hankel norm approximation

Given a stable model *G(s)* of order *n*, with state space form is given as:

$$\begin{aligned} \dot{x}(t) &= Ax(t) + Bu(t) \\ y(t) &= Cx(t) + Du(t) \end{aligned} \tag{30}$$

where

$x(t) \in \Re^n, A \in \Re^{n\times n}, B \in \Re^{n\times m}, C \in \Re^{k\times n}, u(t) : \Re \to \Re^m$: inputs, $y(t) : \Re \to \Re^k$:outputs

The Hankel norm of a system $G = (A,B,C,D)$ is defined by:

$$\|G\|_H^2 = \sup \frac{\int_0^\infty y(t)^2 dt}{\int_{-\infty}^0 u(t)^2 dt} \tag{31}$$

Note that for any G and G_r,

$$\|G - G_r\|_\infty \geq \left\|\Gamma_{G-G_r}\right\| = \left\|\Gamma_G - \Gamma_{G_r}\right\| = \|G(s) - G_r(s)\|_H \tag{32}$$

The problem equals to find a Hankel operator $\Gamma_G : L_2(-\infty, 0] \to L_2[0, \infty)$ which solves:

Minimize $\left\|\Gamma_G - \Gamma_{G_r}\right\|$ subject to Γ_{G_r} is the Hankel operator for some G_r that rank (Γ_{G_r}) = r, or it equals to find a reduced order model $G_r(s)$ of degree k (McMillan degree) such that the Hankel norm of the approximation error, $\left\|G(s) - G_r(s)\right\|_H$ is minimized, where the Hankel norm of a stable transfer function $E(s)$ is defined as:

$$\left\|E(s)\right\|_H = \sqrt{\rho(PQ)} = \sqrt{\lambda_{\max}(PQ)} \tag{33}$$

where P and Q are the controllability and observability Gramians of $E(s)$. ρ is the spectral radius (maximum eigenvalue) of PQ.

The Hankel operator maps past inputs to future system outputs. It ignores any system response before time 0. In Hankel operator, the interest is to know how energy is transferred between input to state and to output of the system. In other words, the problem is to observe how much energy is released from some state $x(0)$ to the output and what is the minimal energy of input signal needed to drive system to the state $x(0)$.

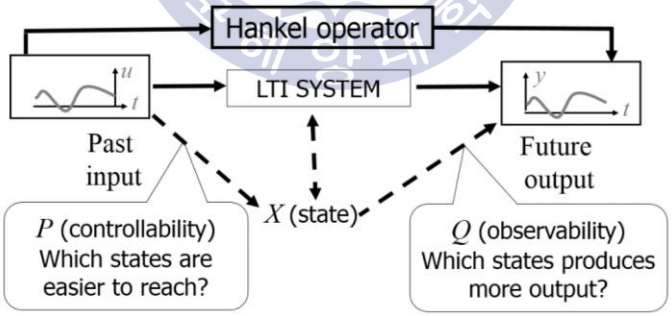

Fig. 13 Hankel operation

Let $G(s)$ be a stable, square, transfer function with Hankel singular values such as

$$\sigma_1 \geq \sigma_2 \geq \ldots \geq \sigma_k \geq \sigma_{k+1} = \sigma_{k+2} = \ldots = \sigma_{k+l} > \sigma_{k+l+1} \geq \ldots \geq \sigma_n > 0 \tag{34}$$

then an optimal Hankel norm approximation of order $k, G_r(s)$, can be calculate as follows:

Let (A, B, C, D) be a balanced realization of $G(s)$ with the Hankel singular values reordered so that the Gramian matrix is

$$\begin{aligned}\Sigma &= diag(\sigma_1, \sigma_2, ..., \sigma_k, \sigma_{k+l+1}, ..., \sigma_n, \sigma_{k+1}, ..., \sigma_{k+l}) \\ &\triangleq diag(\Sigma_1, \sigma_{k+1} I)\end{aligned} \tag{35}$$

Partition matrices (A, B, C, D) to fit with Σ:

$$A = \begin{bmatrix} A_{11} & A_{12} \\ A_{21} & A_{22} \end{bmatrix}, B = \begin{bmatrix} B_1 \\ B_2 \end{bmatrix}, C = \begin{bmatrix} C_1 & C_2 \end{bmatrix} \tag{36}$$

Define $(\hat{A}, \hat{B}, \hat{C}, \hat{D})$ by:

$$\hat{A} \triangleq \Gamma^{-1}(\sigma_{k+1}^2 A_{11}^T + \Sigma_1 A_{11} \Sigma_1 - \sigma_{k+1} C_1^T U B_1^T) \tag{37}$$

$$\hat{B} \triangleq \Gamma^{-1}(\Sigma_1 B_1 - \sigma_{k+1} C_1^T U) \tag{38}$$

$$\hat{C} \triangleq C_1 \Sigma_1 - \sigma_{k+1} U B_1^T \tag{39}$$

$$\hat{D} \triangleq D - \sigma_{k+1} U \tag{40}$$

where U is a unitary matrix which satisfies:

$$B_2 = -C_2^T U \tag{41}$$

and

$$\Gamma \triangleq \Sigma_1^2 - \sigma_{k+1}^2 I \tag{42}$$

Then

$$G_r(s) = {}^{s}\left[\begin{array}{c|c} \hat{A} & \hat{B} \\ \hline \hat{C} & \hat{D} \end{array}\right] - F(s) \tag{43}$$

where $G_r(s)$ is the stable optimal Hankel norm approximation of order *k*, and $F(s)$ is an antistable (all poles in the RHP) transfer function of order *n-k-l*. F(s) contains the unstable modes, hence, it should be removed then only the stable modes remain.

When apply optimal Hankel norm approximation, the optimal simplified controller is the one with minimum order while remains almost the same characteristics with the original one. For example, given a full order controller with 34 orders. After applying optimal Hankel norm approximation, a 7-order controller is achieved that has not much difference in frequency and closed-loop time response, comparing to the full-order controller. In order to check whether the 7-order controller is the lowest-order one that preserves system performance, the frequency response of 6-order controller and its closed-loop time response are simulated and the result shows that there are large differences from the original one. It can be observed from Figs. 14 and 15 that the frequency and time response of the full-order and 7-order controller have almost the same appearances. Meanwhile, the frequency response of 6-order controller of the first channel has big deviation from the full-order one. This leads to very bad closed-loop time response as in Fig. 15(c). Therefore, it is safe to implement the 7-order controller instead of the full-order one.

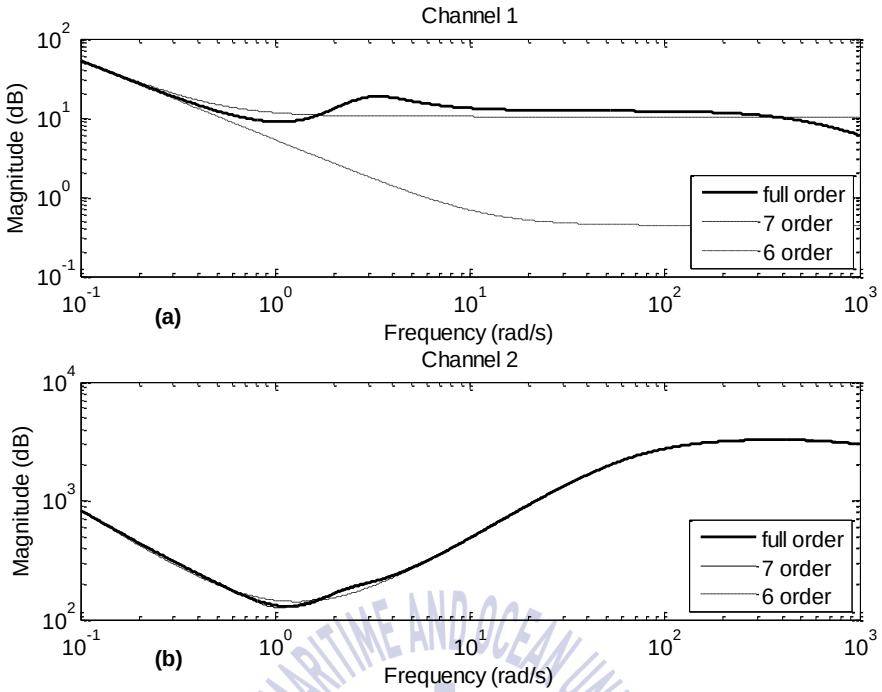

Fig. 14 Frequency responses of full-order, 7-order and 6-order controller: (a) channel 1; (b) channel 2

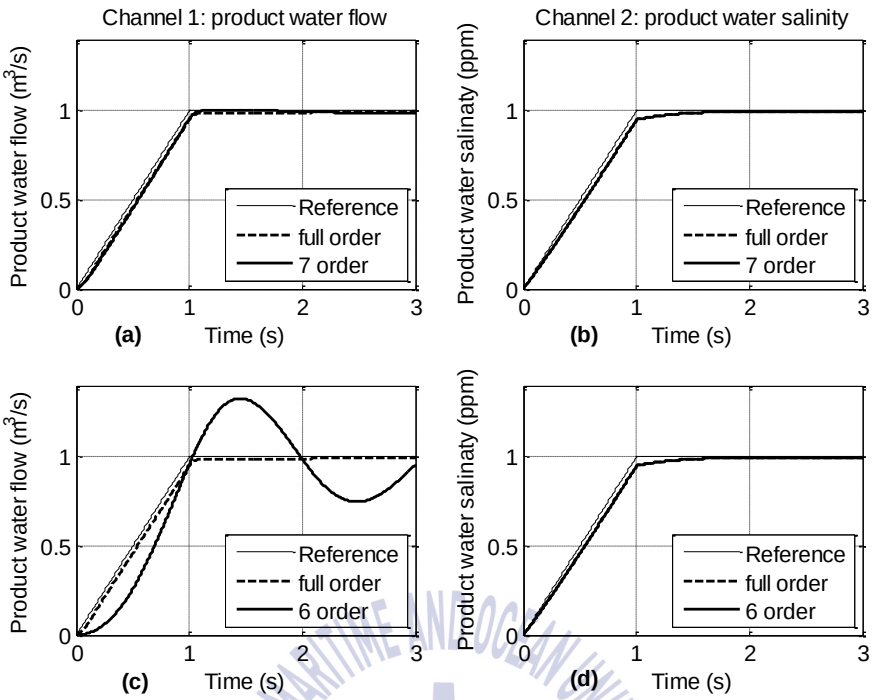

Fig. 15 Closed-loop time responses of full-order and reduced-order controller: (a) and (b) the closed-loop time responses of full-order and 7-order controller; (c) and (d) the closed-loop time responses of full-order and 6-order controller

Chapter 3. Robust gain scheduling controller

3.1 Introduction

The robust H_∞ controller can deal with parametric uncertainty, unmodeled dynamics and nonlinearity. However, it is still conservative since the design is only in some neighborhood of a single operating point. In many applications, the controller must accommodate a plant with changing objectives, operating conditions, and behaviors. Usually, a fixed controller cannot handle such changes without significant deterioration in performance. Gain scheduling is a technique to increase the region of attraction to a range of possible operating points so that the controller fits with new conditions. In this framework, it is possible to model the system in such a way that the operating points are parameterized by one or more variables, which we call scheduling variables. Designers can linearize the system at several equilibrium points, design a feedback controller at each point to optimize the performance and robustness of the closed-loop system, and implement the resulting family of linear controller as a single controller whose parameters are changeable by monitoring the scheduling variables. The broad appeal of this technique arises from addressing each situation individually rather than the entire set simultaneously. Consequently, the synthesized controller may be optimized and tuned for its respective situation without incurring trade-offs that compromise performance for the remaining situations. Therefore, gain-scheduling is a common engineering practice used to control nonlinear plants in a variety of engineering applications.

The classical gain scheduling needs the decomposition of the design a nonlinear controller into the design of some linear controllers, so that well-established linear control design techniques can be applied without restriction, as opposed to nonlinear methods. However, the robustness, performance and nominal stability of the closed-loop are not guaranteed. Classical gain scheduling controller design includes four steps (Rugh & Shamma, 2000):

Step 1: A family of LTI approximation of a nonlinear system at some chosen equilibrium points is computed, which is parameterized by a gain scheduled parameter $\theta(t)$. This parameter can be system parameter or exogenous signal. The approximation is the Jacobian linearization at equilibrium points.

Step 2: LTI controllers corresponding to the family of LTI models are designed to achieve required performance and stability at each equilibrium point. The set of LTI controllers is also parameterized by the gain scheduled parameter $\theta(t)$. Even though $\theta(t)$ is time-varying, the classical gain scheduling design are based on fixed values of $\theta(t)$.

Step 3: Implementation of the family of LTI controllers such that the coefficients of the controllers are scheduled according to the current value of $\theta(t)$. At each equilibrium point, the scheduled controller has to linearize to the corresponding LTI controller to give the best performance and stability. This is also known as the interpolation of the local controllers.

Step 4: Checking the nonlocal performance of the gain scheduled controller by extensive simulation.

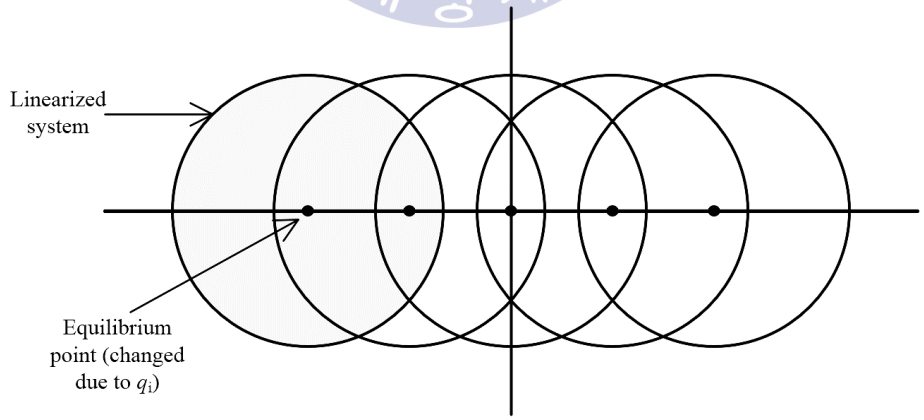

Fig. 16 Gain scheduling framework

Recently, robust gain scheduling control design has achieved new advantages. It includes LPV and LFT synthesis. Both methods yield direct synthesis of a controller by using L_2 norm based methods, guaranteeing the robustness, performance and nominal stability of the overall gain scheduling design. Furthermore, they are direct synthesis, therefore no interpolation is needed (Rugh & Shamma, 2000).

The design of the robust gain scheduling controller consists two main steps:

Step 1: This step relates to the classical approach. A family of LTI of a nonlinear system at some equilibrium points, parameterized by frozen values of gain scheduled parameter $\theta(t)$, is calculated.

Step 2: LPV and LFT control synthesis directly yield a robust gain scheduling controller. Stability and performance specifications can be guaranteed a prior as the gain scheduled parameter $\theta(t)$ instead of its corresponding frozen value is addressed in the design process.

3.2 Linear parameter varying (LPV) system

Consider a linear time invariant (LTI) system described by:

$$\begin{aligned} \dot{x} &= Ax + Bu \\ y &= Cx + Du \end{aligned} \tag{44}$$

The robustness of the LTI system can be check through linear fraction transformation (LFT) or linear matrix inequality (LMI).

Linear parameter-varying (LPV) systems are linear time-varying plants whose state-space matrices are fixed functions of some vectors of varying parameters $\theta(t)$ in the scheduling space $\mathcal{P}$. The LPV systems are written in the form:

$$\begin{aligned} \dot{x} &= A(\theta)x + B(\theta)u \\ y &= C(\theta)x + D(\theta)u \end{aligned} \tag{45}$$

The LPV systems have some interesting interpretation such as (Apkarian *et al*., 1995):

- They can be considered as LTI system plants subject to time-varying parametric uncertainty $\theta(t)$.
- They can be the results of the linearization of nonlinear systems along trajectories of the exogenous parameter $\theta(t)$.

The first class of plants falls within the scope that the LTI robust control techniques described, for example in Zhou *et al*. (1992). In the second class, the parameter $\theta(t)$ is not an uncertainty since it is measured during system operation time. The applied gain scheduling controller for this class can exploit the available measurements of $\theta(t)$ to increase control performance.

The LPV properties are global, since they concern the behavior of the system along all possible trajectories of $\theta(t)$. This problem is different from standard LTI system stabilization, since the controller dynamics are restricted to depend on the variation of gain-scheduled parameter. Note that the exogenous parameters $\theta(t)$ are supposed to be measured in real time during system operation.

3.3 Matrix Polytope

As defined in Apkarian *et al.* (1995), a matrix polytope is defined as the convex hull of a finite number of matrices M_i with the same dimensions. That is,

$$\mathrm{Co}\{M_1,\ldots M_k\} := \left\{ \sum_{i=1}^{k} \alpha_i M_i \,\middle|\, \alpha_i \geq 0, \sum_{i=1}^{k} \alpha_i = 1 \right\} \tag{46}$$

The LPV system is restricted as follow:

- The parameter dependence is affine; that is, the state-space matrices $A(\theta)$, $B(\theta)$, $C(\theta)$, and $D(\theta)$ depend affinely on $\theta(t)$;
- The time-varying parameter $\theta(t)$ varies in a polytope Θ of vertices $\omega_1, \omega_2, \ldots \omega_k$; that is,

$$\theta \in \Theta := Co\{\omega_1, \omega_2, ..., \omega_r\} \tag{47}$$

Hence, the state-space matrices $A(\theta), B(\theta), C(\theta)$, and $D(\theta)$ vary in a polytope of matrices whose vertices are the images of the vertices $\omega_1, \omega_2, \ldots \omega_k$, which can be express as:

$$\begin{pmatrix} A(\theta) & B(\theta) \\ C(\theta) & D(\theta) \end{pmatrix} \in Co\left\{ \begin{pmatrix} A_i & B_i \\ C_i & D_i \end{pmatrix} := \begin{pmatrix} A_{(\omega_i)} & B_{(\omega_i)} \\ C_{(\omega_i)} & D_{(\omega_i)} \end{pmatrix}, i = 1, ..., k \right\} \tag{48}$$

Definition 3.3 (Apkarian *et al.*, 1995)

An LPV system is called 'polytopic' if it can be represented by state-space matrices $A(\theta), B(\theta), C(\theta)$, and $D(\theta)$, where the parameter vector θ ranges over a fixed polytope, and the dependence of the state-space matrices on θ *(t)* is affine.

3.4 Polytope and affine parameter-dependent representation

There are two styles to represent the LPV system, including polytope and affine parameter-dependence representation.

3.4.1 Polytope representation

The LPV system is described by:

$$\begin{cases} E(t)\dot{x} = A(t)x + B(t)u \\ y = C(t)x + D(t)u \end{cases} \tag{49}$$

where E is non-singular matrix and satisfies (Apkarian *et al.*, 1995):

$$\left[\begin{array}{c|c} A(t)+jE(t) & B(t) \\ \hline C(t) & D(t) \end{array}\right] \in \left\{ \sum_{i=1}^{k} \alpha_i M_i \,\middle|\, \alpha_i \geq 0, \sum_{i=1}^{k} \alpha_i = 1 \right\} \\ =: \mathrm{Co}\{M_1, \ldots M_k\} \text{(convexcity)} \tag{50}$$

and M is the polytope of vertices $M_1,\ldots,M_k$ represented by:

$$M_i := \left[\begin{array}{c|c} A_i + jE_i & B_i \\ \hline C_i & D_i \end{array}\right] \tag{51}$$

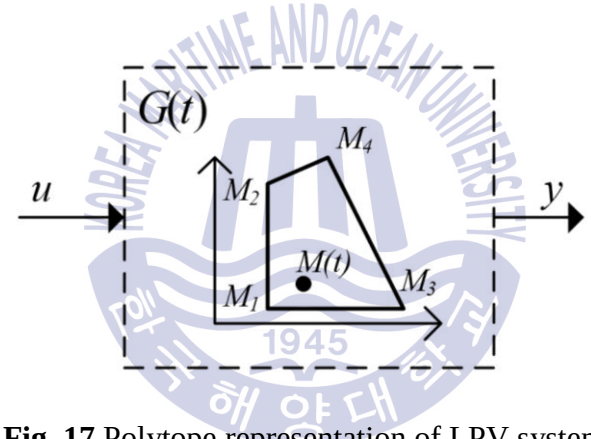

Fig. 17 Polytope representation of LPV system

3.4.2 Affine parameter-dependent representation

In this style, the LPV system is described by:

$$\begin{cases} E(p)\dot{x} = A(p)x + B(p)u \\ y = C(p)x + D(p)u \end{cases} \tag{52}$$

where $A(p)$, $E(p)$ are affine function and $p = (p_1, \ldots p_k)$ are real parameters. Let

$$\left[\begin{array}{c|c} A(p)+jE(p) & B(p) \\ \hline C(p) & D(p) \end{array}\right] = S_0 + \sum_{i=1}^{k} p_i S_i,\ S_i = \left[\begin{array}{c|c} A_i + jE_i & B_i \\ \hline C_i & D_i \end{array}\right] \tag{53}$$

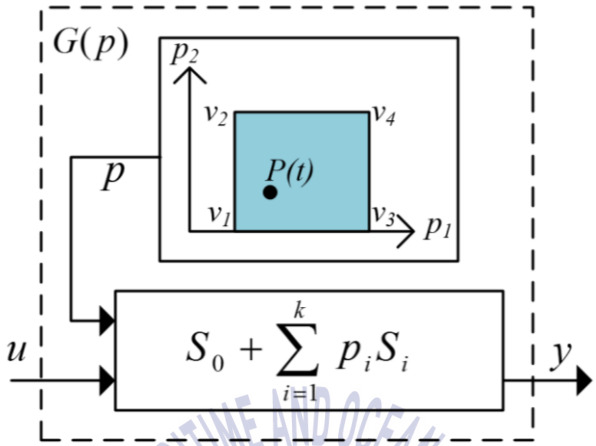

Fig. 18 Affine parameter-dependent representation of LPV system

3.5 Quadratic stability of LPV systems and quadratic (robust) H_∞ performance

Quadratic stability is actually the Lyapunov stability theorem. Lyapunov stability is the mathematical extension of the energy conservation concepts associated with a mechanical system: the motion of a mechanical system is stable if its total mechanical energy decreases all the time. The basic procedure of this direct method is to construct an energy-like function, referred to as the Lyapunov function, for the dynamic system, and to examine the time-variation of this function as time progresses.

The system $\dot{x}(t) = A(t)x(t),\ A(t) \in \mathcal{A}\ \ \forall t \geq 0$ is (Lyapunov) quadratically stable if:

$$\begin{aligned} &\exists P = P^T \succ 0 \text{ and } \varepsilon > 0 \text{ s.t.} \\ &V(x) = x^T Px,\ \dot{V}(x) = x^T \left(PA + A^T P\right) x \leq 0\ \ \forall A \in \mathcal{A} \end{aligned} \tag{54}$$

$$\Leftrightarrow \exists P = P^T \succ 0 \; s.t. \; A^T P + PA \prec 0 \quad \forall A \in \mathcal{A}$$

where $\mathcal{A} = Co\{\mathcal{A}_1, ..., \mathcal{A}_k\}$

Since the technique for parameter-dependent controller synthesis based on the small gain theorem and applicable to LPV plants with an LFT (linear fractional transformation) (Packard, 1994; Apkarian and Gahinet, 1995) is still conservative for real parameters, quadratic H_∞ performance is currently used for gain scheduling control to give significant improvements. This notion is closely related to quadratic stability (Barmish, 1985; Arzelier *et al.*, 1991), and seeks a single quadratic Lyapunov function to ensure H_∞-like performance for all possible trajectories of the LPV plant (Packard and Becker, 1992; Becker *et al.*, 1993).

In this framework, the parameter is treated as real and should enter the state-space matrices of the LPV plant in an affine fashion. The improvement essentially comes from the ability of the quadratic H_∞ performance formalism to handle real parameters.

Given the LPV system and scalar $\gamma > 0$. If there exists $X = X^T > 0$ such that,

$$\Phi_\infty(M_i, X) := \begin{bmatrix} A_i X + X A_i^T & X C_i^T & B_i \\ C_i X & -\gamma I & D_i \\ B_i^T & D_i^T & -\gamma I \end{bmatrix} < 0, \quad \forall i = 1, ..., k \tag{55}$$

then $\Phi_\infty(M_i, X) < 0, \quad \forall M \in Co\{M_1, ...M_k\}$ and the Lyapunov function $V(x) = x^T X x$ establishes asymptotic stability and the $\mathcal{L}_2$ gain of the input/output map is bounded by γ. That is $\|y\|_2 < \gamma \|u\|_2$ along all possible parameter trajectories *p*.

3.6 Robust gain scheduling

3.6.1 LPV system linearization

Consider the nonlinear plant

$$\begin{cases} \dot{x} = f(x,u,w,v) \\ z = g_1(x,u,w,v) \\ y = g_2(x,u,w,v) \end{cases} \tag{56}$$

where v is the parametric-dependent exogenous input.

The linearization is carried on around the equilibrium family:

$$\begin{cases} \dot{x}_e(p) = f(x_e(p),u_e(p),w_e(p),v_e(p)) = 0 \\ z_e(p) = g_1(x_e(p),u_e(p),w_e(p),v_e(p)) \\ y_e(p) = g_2(x_e(p),u_e(p),w_e(p),v_e(p)) \end{cases} \tag{57}$$

With the scheduling variable $p(t) \in \mathcal{P}$ is real-time measurable.

Fig. 19 The linearized LPV system

The Jacobian linearized system is written in the form:

$$\begin{bmatrix} \dot{x}_\delta \\ z_\delta \\ y_\delta \end{bmatrix} = \begin{bmatrix} A(p) & B_1(p) & B_2(p) \\ C_1(p) & D_{11}(p) & D_{12}(p) \\ C_2(p) & D_{21}(p) & D_{22}(p) \end{bmatrix} \begin{bmatrix} x_\delta \\ w_\delta \\ u_\delta \end{bmatrix} \tag{58}$$

where δ is the notion for the deviations of the respective component slightly away from equilibrium family.

3.6.2 Polytope-based gain scheduling

From this section, the LPV plant is analyzed considering the following assumptions to simplify the derivation of the control synthesis:

- $D_{22}(p) = 0$, or equivalently $D_{22i} = 0$ for $i = 1, 2, \ldots k$;
- $B_2(p)$, $C_2(p)$, $D_{12}(p)$, $D_{21}(p)$ are parameter-independent, or equivalently $B_{2i} = B_2$, $C_{2i} = C_2$, $D_{12i} = D_{12}$, $D_{21i} = D_{21}$ for $i = 1, 2, \ldots k$;
- The pairs $(A(p), B_2)$ and $(A(p), C_2)$ are quadratically stabilizable and quadratically detectable over p.

Consider the LPV plant $G(p)$:

$$\begin{bmatrix} z \\ y \end{bmatrix} = G(p) \begin{bmatrix} w \\ u \end{bmatrix}, \quad G(p) = \left[\begin{array}{c|cc} A(p) & B_1(p) & B_2 \\ \hline C_1(p) & D_{11}(p) & D_{12} \\ C_2 & D_{21} & D_{22} \end{array}\right] \tag{59}$$

where $p(t) = (p_1(t), \ldots, p_k(t))$ is real-time measurable, $G(p) \in M \triangleq Co\{M_1, \ldots, M_k\}$, A, B_1, C_1, D_{11} are affine functions of $p(t)$ and physical parameter $p_i(t)$ is bounded by $[p_{i\min}, p_{i\max}]$

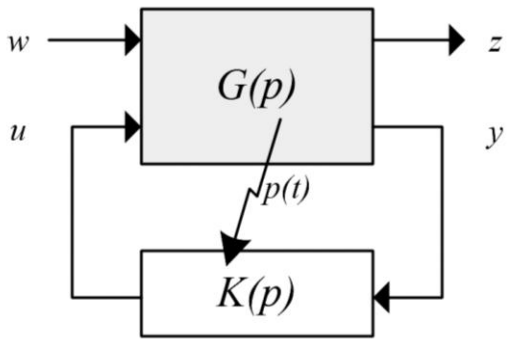

Fig. 20 Polytope-based Gain Scheduling

The LPV controller *K(p)* has the state-space representation as follow:

$$\begin{cases} \dot{\varsigma} = A_K(p)\varsigma + B_K(p)y \\ u = C_K(p)\varsigma + D_K(p)y \end{cases} \tag{60}$$

In the polytope style, the LPV controller is written in the form:

$$K(p) = \left[\begin{array}{c|c} A_K(p) & B_K(p) \\ \hline C_K(p) & D_K(p) \end{array}\right] = \sum_{i=1}^{k} \alpha_i K_i = \sum_{i=1}^{k} \alpha_i \left[\begin{array}{c|c} A_K(M_i) & B_K(M_i) \\ \hline C_K(M_i) & D_K(M_i) \end{array}\right] \tag{61}$$

The closed-loop system *T* with the corresponding closed-loop system state vector equals to $\zeta = [x, \xi]^T$. The closed-loop system becomes:

$$\begin{bmatrix} \dot{\zeta}(t) \\ z(t) \end{bmatrix} = \underbrace{\begin{bmatrix} A_{cl}(\theta(t)) & B_{cl}(\theta(t)) \\ C_{cl}(\theta(t)) & D_{cl}(\theta(t)) \end{bmatrix}}_{T} \begin{bmatrix} \zeta(t) \\ \omega(t) \end{bmatrix} \tag{62}$$

where:

$$\begin{bmatrix} A_{cl} & B_{cl} \\ C_{cl} & D_{cl} \end{bmatrix} = \left[\begin{array}{cc|c} A + B_2 D_K C_2 & B_1 C_K & B_1 + B_2 D_K D_{21} \\ B_2 C_2 & A_K & B_K D_{21} \\ \hline C_1 + D_{12} D_K C_2 & D_{12} C_K & D_{11} + D_{12} D_K D_{21} \end{array}\right] \tag{63}$$

The design objective is to find the robust gain-schedule controller *K(p)* satisfying $\|T\|_\infty = \|F_l(G(p), K(p))\|_\infty < \gamma$ for all admissible trajectories *p(t)*. In other words, the closed-loop system satisfies the quadratic H_∞ performance condition.

It turns out to solve the convex optimization problem by minimizing γ such that $R=R^T$ and $S=S^T$ satisfying the following LMIs:

$$\begin{bmatrix} \mathcal{N}_R & 0 \\ 0 & I \end{bmatrix}^T \left[\begin{array}{cc|c} A_i R + R A_i^T & R C_{1i}^T & B_{1i} \\ C_{1i} R & -\gamma I & D_{11i} \\ \hline B_1^T & D_{11i}^T & -\gamma I \end{array}\right] \begin{bmatrix} \mathcal{N}_R & 0 \\ 0 & I \end{bmatrix} < 0 \tag{64}$$

$$\begin{bmatrix} \mathcal{N}_S & 0 \\ 0 & I \end{bmatrix}^T \left[\begin{array}{cc|c} A_i^T S + S A_i & S B_1 & C_{1i}^T \\ B_{1i}^T S & -\gamma I & D_{11i}^T \\ \hline B_1^T & D_{11i}^T & -\gamma I \end{array}\right] \begin{bmatrix} \mathcal{N}_S & 0 \\ 0 & I \end{bmatrix} < 0 \tag{65}$$

and $\begin{bmatrix} R & I \\ I & S \end{bmatrix} \geq 0, \begin{bmatrix} A_i & B_i \\ C_{1i} & D_{11i} \end{bmatrix} := \begin{bmatrix} A(M_i) & B(M_i) \\ C(M_i) & D(M_i) \end{bmatrix}$, $\mathcal{N}_R$ and $\mathcal{N}_S$ are the base of the null space spanned by $(B_2^T, D_{12}^T), (C_2, D_{21})$

The following steps summarize the procedure to design a robust gain scheduling controller for an LPV system using the above LMI approach:

Step 1: Derive an analysis condition for a desired closed-loop property

Step 2: Evaluate this condition on the closed-loop LPV system

Step 3: Transform the search for control parameters into a convex search

Step 4: If the convex search is successful, extract controller parameters.

3.6.3 LFT-based gain scheduling

An LFT model is in fact a special case of an LPV model, which is transformed by an upper LFT of the know part *G* and the corresponding gain scheduling parameter Θ; and a lower LFT between the know part LPV controller *K* and the gain scheduling parameter Θ. The framework is depicted in Fig. 21.

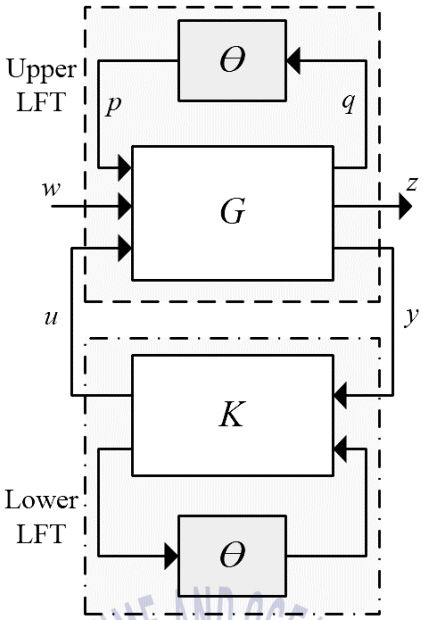

Fig. 21 LFT-based gain scheduling

Consider the LPV plant G, the upper LFT is presented by:

$$\begin{bmatrix} z \\ y \end{bmatrix} = F_u\left(G(s),\theta\right)\begin{bmatrix} w \\ u \end{bmatrix}, \ \forall \theta(t) \in \Delta$$
$$\Delta = \left\{ diag\left\{\theta_1 I_{r1},...,\theta_k I_{rk}\right\} : \theta_i(t) \in R \right\} \tag{66}$$

where

$$\begin{bmatrix} \dot{x}(t) \\ q(t) \\ z(t) \\ y(t) \end{bmatrix} = \underbrace{\left[\begin{array}{c|ccc} A & B_\theta & B_1 & B_2 \\ \hline C_\theta & D_{\theta\theta} & D_{\theta 1} & D_{\theta 2} \\ C_1 & D_{1\theta} & D_{11} & D_{12} \\ C_2 & D_{2\theta} & D_{21} & D_{22} \end{array}\right]}_{G} \begin{bmatrix} x(t) \\ p(t) \\ w(t) \\ u(t) \end{bmatrix} \tag{67}$$

As defined in Wu (2006) and depicted in Fig. 21, *w* is disturbance, *z* is the controlled output, *p*, *q* are the pseudo-input and output, *u* is the control input and *y* is the measurement for control.

The LPV plant can also be written as:

$$G(s)=\left[\begin{array}{cc|c} D_{\theta\theta} & D_{\theta 1} & D_{\theta 2} \\ D_{1\theta} & D_{11} & D_{12} \\ \hline D_{2\theta} & D_{21} & D_{22} \end{array}\right]+\left[\begin{array}{c} C_{\theta} \\ \hline \begin{array}{c} C_1 \\ C_2 \end{array} \end{array}\right](sI-A)^{-1}\left[\begin{array}{ccc} B_{\theta} & B_1 & \mid B_2 \end{array}\right] \tag{68}$$

$A \in R^{n x n}, D_{\theta\theta} \in R^{r x r}$

Specifically, the upper LFT is calculated as:

$$F_u\left(G(s),\theta\right)=\left[\begin{array}{cc|c} A & B_1 & B_2 \\ C_1 & D_{11} & D_{12} \\ \hline C_2 & D_{21} & D_{21} \end{array}\right]+\left[\begin{array}{c} B_{\theta} \\ \hline \begin{array}{c} D_{1\theta} \\ D_{2\theta} \end{array} \end{array}\right]\theta(I-D_{\theta\theta}\theta)^{-1}\left[\begin{array}{ccc} C_{\theta} & D_{\theta 1} & \mid D_{\theta 2} \end{array}\right] \tag{69}$$

The lower LFT can be called the LPV controller $u=F_l(K(s),\theta)y$ with state-space representation as follow:

$$\begin{cases} \dot{\xi}=A_K(\theta(t))\xi+B_K(\theta(t))y \\ u=C_K(\theta(t))\xi+D_K(\theta(t))y \end{cases} \tag{70}$$

Then the closed-loop interconnection of the resulting LFTs is transformed, again using a lower LFT. The transformation yields the closed-loop interconnection system *T*.

The design objective is to find the robust gain-schedule controller *K(θ)* satisfying:

$$\left\|T(G,K,\theta)\right\|_{\infty}=\left\|F_l(F_u(G,\theta),F_l(K,\theta))\right\|_{\infty}<\gamma \tag{71}$$

Chapter 4. Mixed robust H_∞ and μ-synthesis controller applied for a reverse osmosis desalination system

4.1 RO principles

4.1.1 Osmosis and reverse osmosis

Osmosis is a natural tendency of water with a low concentration of total dissolved solids (TDS) diffuses through a semi-permeable membrane into a higher solution of TDS in order to balance the concentration between two sides of the membrane. The membrane can reject most of dissolved molecules and ions, while allowing water to permeate through. The pressure that causes this natural water flow is called osmotic pressure, which is due to the difference in concentration between the both sides.

By applying a pressure that is an excess of the osmotic pressure to the high TDS side, it can force the water to flow from the high TDS side into the low TDS side. Therefore, the direction of water flow is reversed and the process is called reverse osmosis, as shown in Fig. 22.

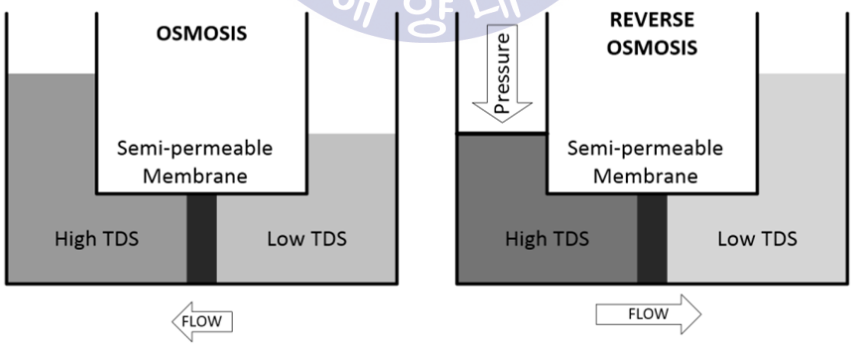

Fig. 22 Reverse osmosis principle

Reverse osmosis membrane can remove many types of molecules and ions from solutions, including bacteria, and is used in both industrial processes and the production of potable water

4.1.2 Dead-end filtration and cross-flow filtration

Dead-end technique is used in simple filtration processes, where the flow of liquid to be filtered is directed perpendicular to the membrane surface. This technique is only effective when the fluid concentration is low or the packing tendency of the filtered material does not produce a large pressure drop across the membrane medium. Some common examples of dead-end filtration are home water filters, vacuum cleaners and oil filters in automobiles. Typical industrial uses include the sterile filtration of beer, and wine.

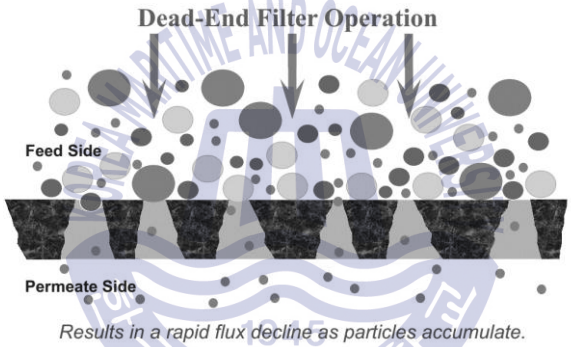

Fig. 23 Dead-end filtration. (Source wikipedia.org)

In contrast, there are many process whose fluids have high concentration of particles or macromolecules such as cells, proteins and precipitates that will rapidly compact on the membrane surface when using dead-end filtration. Consequently, the recovery ratio drops quickly to an unacceptable level. In these cases, a cross-flow membrane system provides the means to maintain stable filtration rates and reduce cleaning. The major different in cross-flow filtration process is the geometry of membranes must suit the physical characteristics of the process fluid, normally the pores are conical and smaller in the feed side. Cross-flow membranes can be provided in tubular, flat sheet, spiral wound, and hollow fiber configurations, each of which provides certain advantages for specific process needs.

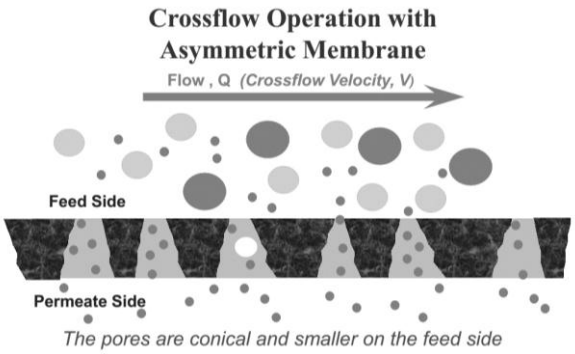

Fig. 24 Cross-flow filtration. (Source wikipedia.org)

4.2 Membranes

Reverse osmosis membranes have a pore size around 0.0001 μm. The mean size of a water molecule is about 0.097 nm. Hence, water can go through the RO membrane while the other factors with bigger sizes are prevented. After water passes through a reverse osmosis membrane, it is essentially pure water. In addition to removing all organic molecules, bacteria (sizes from 0.2 to 10 μm) and viruses (sizes from 0.02 to 0.4 μm), reverse osmosis also removes most minerals that are presented in the water. Reverse osmosis removes monovalent (eg. *NaCl)* ions, which means that it desalinates the water.

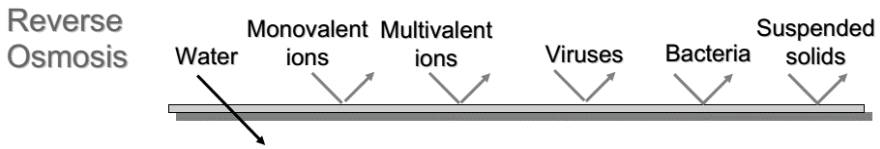

Fig. 25 RO filtration

4.2.1 Structure and material

Two materials make up the bulk of commercial RO membranes are cellulose acetate and composite. The composite membranes usually exhibit higher rejection at lower operating pressures than the cellulose acetate. The current RO membrane market is dominated by thin film composite (TFC) polyamide types. This kind of membrane consists of three layers: A polyester web acting as structural support (backing), a microporous interlayer web, and an ultra-thin barrier layer on the upper surface which is 0.2 μm (see Fig. 26). The polyester support web has almost no effect on membrane transport properties. It only has the effect on supporting the membrane's structure. Between the barrier layer and the support layer, a micro-porous interlayer of polysulfonic polymer is added to enable the ultra-thin barrier layer to withstand high pressure compression. The thickness of the barrier layer is reduced to minimize resistance to the permeate transport. Membrane pore size is normally less than 0.6 nm (0.0006 μm) to achieve salt rejection consistently higher than 99%. The selective barrier layer is often made of aromatic polyamide. With improving chemical resistance and structural robustness, it offers reasonable tolerance to impurities, enhanced durability and easy cleaning characteristics (Lee, 2011)

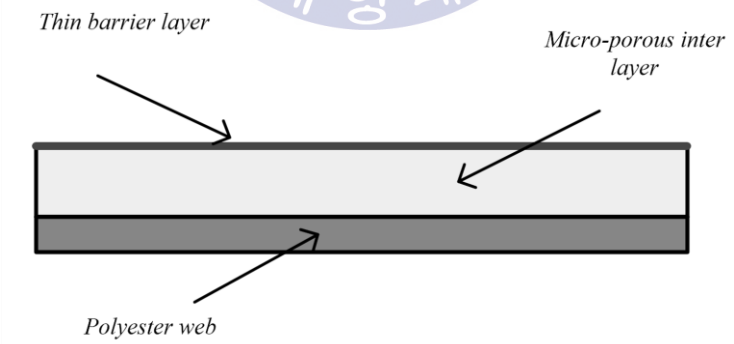

Fig. 26 The structure of RO membrane

4.2.2 Hollow fine fiber membrane module

This configuration uses membrane in the form of hollow fibers. These fibers may be extruded from cellulosic or non-cellulosic material, which have the minimum hollows size up to 42 micron (0.0016 inch). One membrane is a bundle of millions of these fibers folded in half. The bundle is packed inside a pressure tube which usually has a length about 120 cm (4 ft). The pressure tube is sealed at both ends to form a sheet-like permeate output and a brine output which prevents the feed stream from bypassing out. A perforated plastic tube in the center of the pressure tube will serve as a feed water distributor. The assembly is called a permeator. The pressurized feed saline water enters the permeator feed end through the center distributor tube, passes through the tube wall, and flows radially around the fiber bundle toward the outer permeator pressure shell. Water permeates through the outside wall of the fibers into the hollow core of fibers, and to the product end of the fiber bundle, and exits through the product connection at one end of the permeator. The left concentrate water is rejected through brine tube in the other end of permeator.

The permeability of a hollow fiber module is low. Therefore, the concentration polarization is also low at the membrane surface, resulting in a non-turbulent or laminar flow regime. Normally, a single hollow fiber permeator can be operated at up to 50-percent recovery and meet the minimum reject flow required to limit the concentration polarization. The hollow fiber unit allows a large membrane area per unit volume of permeator which results in compact structure. Hollow fiber membranes are available for brackish and seawater applications. Due to their compact structures, hollow fiber modules require feed water of lower concentration than the spiral wound module configuration.

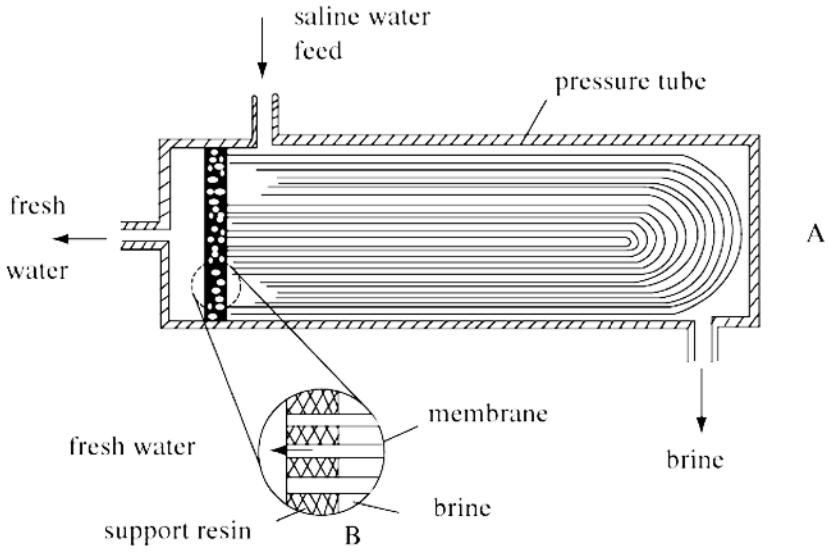

Fig. 27 The construction and flow patterns in a hollow fiber membrane system (Pfafflin, 2015)

4.2.3 Spiral wound membrane module

In spiral wound structure, a flat-sheet of composite membrane is folded in half with the membrane facing inward. A feed spacer is then put in between the folded membrane to form a membrane leaf. This assembly is sealed on three sides with the fourth side left open for permeate to exit. The mesh spacer is to provide space for feed water to flow between the membrane surfaces, and to induce turbulence and reduces concentration polarization. A permeate spacer is added between membrane leaves, forming membrane assemblies. Some of these assemblies are wound around a central plastic tube. This tube is perforated to collect the permeate water from the multiple leaf assemblies. The feed/brine flow through the element is a cross-flow from the feed end to the opposite brine end, running parallel to the membrane surface. In order to operate at acceptable recoveries, spiral systems are usually staged with three to six membrane elements connected in series in a pressure tube. The brine stream from the first element becomes the feed to the following element, and so on for each element within the pressure tube. The brine stream from the last element

exits the pressure tube to waste. The permeate water from each element enters the permeate collector tube and exits the vessel as a common permeate stream. A single pressure vessel with four to six membrane elements connected in series can be operated at up to 50-percent recovery under normal design conditions. The brine seal on the element feed end seal carrier prevents the feed/brine stream from bypassing the following element. In comparison to the hollow fiber membrane, the spiral wound membrane working under lower pressure while the recoveries are equal.

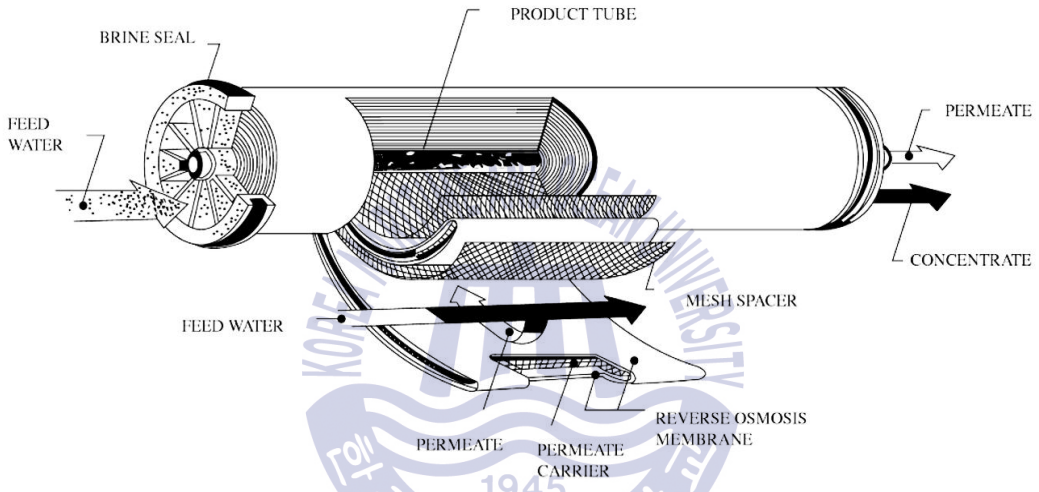

Fig. 28 The construction and flow patterns in a spiral wound membrane system (Pfafflin, 2015)

4.3 Nonlinear RO modelling and analysis

4.3.1 RO system introduction

In RO system, the cleaning process has to be carried out when the membrane permeability decreases to a threshold due to fouling. As usually, RO operation has to stop under cleaning process. Since this process can lower system productivity, a feed-flow-reversal RO system is to overcome that limitation. This kind of RO system

uses alternate valves to reverse the flow, to automatically clean the membrane. One of such model was developed by Bartman *et al*. (2009). This model based on a macroscopic kinetic energy balance and is one of the irreversible thermodynamics models. It assumes an incompressible fluid and constant internal volume and mass. Skin friction through piping and membranes are negligible relating to hydraulic losses in the throttling valves and across the membrane. The schematic of the model is depicted in Fig. 29. The system includes a high-speed pump, a membrane and two valves. The pump forces the feed seawater to go through the membrane to become product water. The left high salinity water is rejected through concentration valve to the energy recovery device, which is out of this dissertation's scope. Two outputs, the product water flow F_p and the system pressure P_s are controlled by the concentration valve and bypass valve, respectively. The control input signals are the resistances of those valves, R_{vc} and R_{vb}. Since the analysis is for the mathematical equations under normal operation, the reversal valves are not included in the block diagram.

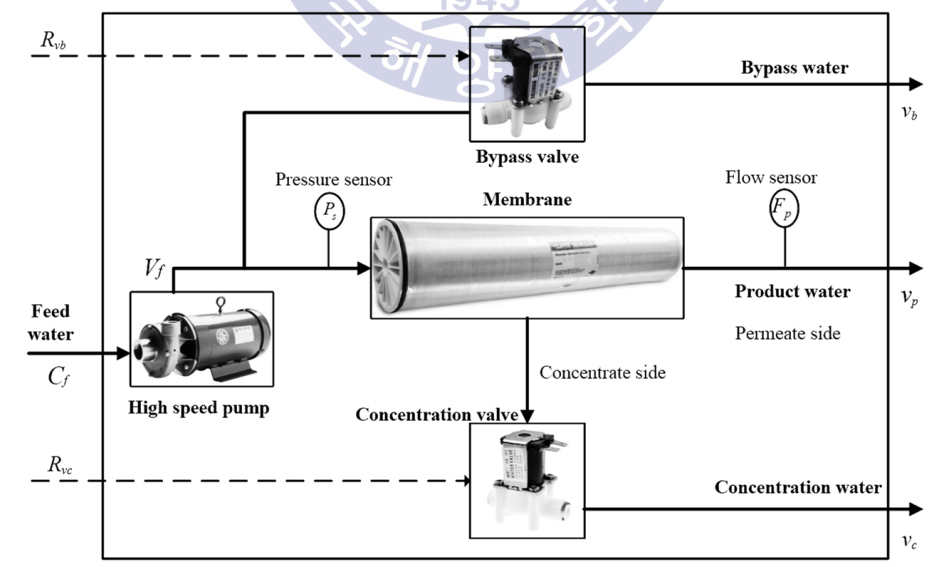

Fig. 29 Block diagram of the current RO unit

4.3.2 Modelling

Providing that the cross-sectional areas are identical for all pipes in the system, the nonlinear differential equations describing the dynamics of flow velocities through concentration and bypass valve are given in Bartman *et al*. (2009) as:

$$\frac{dv_b}{dt} = \frac{A}{V}\left(\frac{A}{SK_m}(v_f - v_c - v_b) + \frac{\Delta\pi}{\rho} - 0.5R_{v_b} v_b^2 \right) \tag{72}$$

$$\frac{dv_c}{dt} = \frac{A}{V}\left(\frac{A}{SK_m}(v_f - v_c - v_b) + \frac{\Delta\pi}{\rho} - 0.5R_{v_c} v_c^2 \right) \tag{73}$$

where V is the system volume, A pipe cross-sectional area, S membrane area, K_m overall mass transfer coefficient of the membrane, ρ fluid density, R_{vc} concentration valve resistance, R_{vb} bypass valve resistance, v water velocity, the subscript f indicates feed stream, b the bypass stream, c the concentration stream and p the product stream, $\Delta\pi$ is the osmotic pressure which is calculated using:

$$\Delta\pi = C_f \beta T \left(\alpha + (1-\alpha)\left(\frac{(1-R) + R(v_f - v_b)}{v_c} \right) \right) \tag{74}$$

where β is a constant relating effective concentration to osmotic pressure, α an effective concentration weighting coefficient, R the fractional salt rejection of the membrane, T temperature.

The valves resistance R_{vb} and R_{vc} relate to the percent of opening of the bypass and concentration valves through the following equation:

$$O_p = \mu \ln\left(\frac{1}{A_p \sqrt{0.5\rho R_v}} \right) + \phi \tag{75}$$

where R_v indicate valve resistant, μ and ϕ ate constants depending on the valve properties. The resistant increasing will decrease the valve opening. All the parameters are given in Table 1 (Bartman *et al*., 2009).

The outputs including product water flow F_p and system pressure P_s are defined as:

$$F_p = A_p(v_f - v_b - v_c).36.10^5 \tag{76}$$

$$P_s = \frac{A\rho}{SK_m}(v_f - v_c - v_b) + \Delta\pi \tag{77}$$

Note that this model ignores the effect of CP. Although the system can automatically self-clean, in the real plant, CP reduces the productivity and makes the effect of some phenomena such as water hammer more severe. Therefore, in this dissertation, CP will be analyzed and counted in the linearized system.

Table 1 The RO model parameters

Parameters	Value	Unit
V	0.04	m3
ρ	1000	Kg/m3
v_f	10	m/s
A_p	$1.27x10^{-4}$	M2
A	30	M2
K_m	$9.128x10^{-9}$	s/m
C_f	10000	Mg/L
a	0.5	
T	25	^oC
R	0.993	
μ	-12.135	
β	151.442	

θ	0.2641
K_w	9.218×10^{-12}
K_s	1.948×10^{-7}
k	2.4007×10^{-6}

4.3.3 Nonlinear analysis

The problems of nonlinear systems are hard to be solved because of the complexity and particularity of each plant. Up to now, no analytical solution has been devised for them. Although some powerful methods have been developed for the analysis and design of nonlinear systems, they all have their limitations. Therein, the phase plane (phase portrait) analysis is widely used in the engineering.

In this paper, the nonlinear analysis is carried out under steady state condition. Brackish water with concentration 10000 mg/L is constantly fed to the system at a velocity of 10 m/s. The ideal temperature is 25°C. As seen in Fig. 30A, the phase plane is the plot of two variables v_c and v_b for a large number of initial conditions, with constant parameters and fix control input values. This phase plane shows a stable node at equilibrium point (4.511,1.123). It means this system is a stable system. From any given initial values or perturbations of v_c and v_b, they will finally converge to the equilibria. The figure also shows some areas where the trajectories are almost straight lines, indicating faster convergences than those of in the other areas. The faster convergences physically increase the system stability.

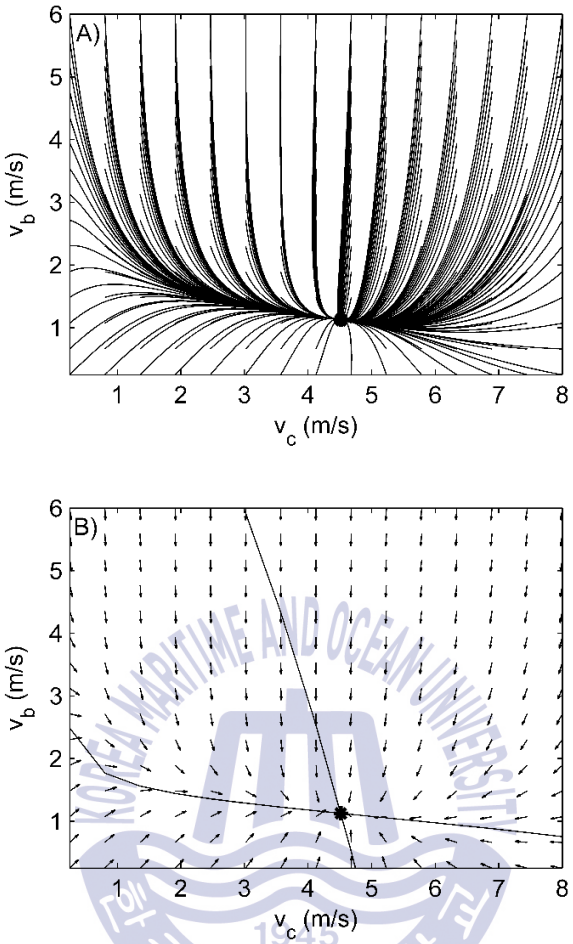

Fig. 30 The phase plane (A) and nullclines (B) of the nonlinear RO system

The position of the equilibrium point also agrees with the nullclines plot in Fig. 30B. In this figure, two nullclines are defined by $dv_c/dt = 0$ on one hand and $dv_b/dt = 0$ in the other hand. The intersection of these curves corresponds to the equilibrium point where $dv_c/dt = 0$ and $dv_b/dt = 0$ simultaneously. From the graph of the nullclines, it is possible to infer whether or not a system will be bistable. It can be seen that the nullclines only intersect in one place. Hence, one can conclude that the system is not bistable, and there is only one equilibrium point. The vector fields in all the four regions delimited by these nullclines converge to the equilibria, indicating a stable node at the point.

Note that v_c and v_b represent flow velocities through concentration and bypass valve respectively, physical considerations restrict them to positive real numbers. Therefore, the phase portrait of v_c and v_b only poses positive values of these variables.

4.3.4 Concentration polarization

In cross-flow RO process, solute rejected by the membrane forms a boundary layer of high concentration at the membrane surface. The thickness of this layer increases axially along the operation time and the length of filtration channel. This phenomenon is called CP. It reduces the effective driving force and product water flow. Ignoring of CP as in Bartman *et al*. (2009) makes the results unreal. Therefore, in this section, CP is counted, and its influence on performance ratio is considered and simulated.

There have been many studies on CP such as Niemi and Polasaari (1993) and Kimura (1995). In these studies, CP layer is simplified as a uniform layer over the membrane surface so that the CP index can be calculated using:

$$\mathrm{CP} = \frac{C_m - C_p}{C_f - C_p} = e^{\left(\frac{J_w}{k}\right)} \tag{78}$$

where C is the concentration, the subscript m indicates membrane wall, p refers to product side and f the feed side, k the feed-side solute mass transfer coefficient and J_w the permeate flux, which is given in the following equation.

$$J_w = K_w(P_s - \Delta\pi) \tag{79}$$

where K_w is the water permeability coefficient of the membrane

Noting that the salt flux through the membrane is also given in irreversible thermodynamics model as:

$$J_s = C_p J_w = K_s (C_m - C_p) \tag{80}$$

where K_s is the salt permeability coefficient of the membrane

Clearly, from Eqs. (74) and (77), the permeate water concentration (product water quality) is calculated by:

$$C_p = C_f \left(\frac{e^{\left(\frac{J_w}{k}\right)}}{\frac{J_w}{K_s} + e^{\left(\frac{J_w}{k}\right)}} \right) \tag{81}$$

When CP is included, the component C_f in Eq. (74) should be replaced by C_m. During the operation of RO plant, the CP index is increasing, and C_m is also getting higher. It will result in the increasing of the osmotic pressure, the velocities through two valves and the product water concentration, as well as the decreasing of the product water flow. Fig. 31 illustrates the effects of CP and feed concentration on concentrate flow velocity and system performance ratio at steady state values of the two control inputs.

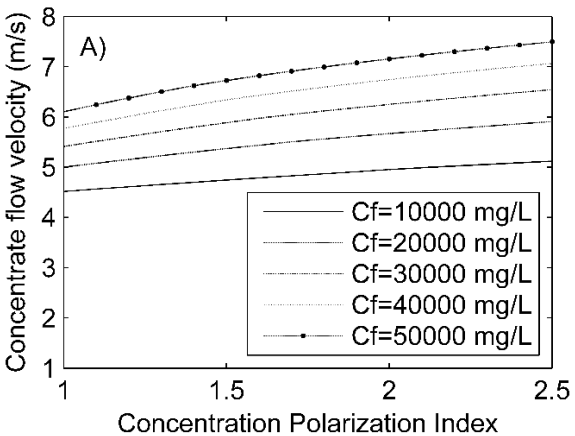

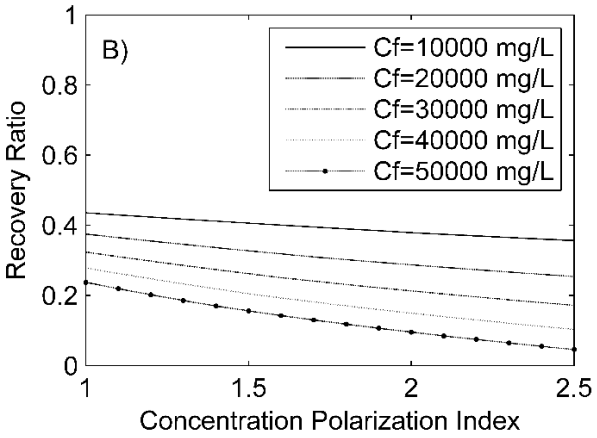

Fig. 31 CP index affects (A) on the concentration flow and (B) on the recovery ratio

It can be seen that when the feed concentration and CP index increases, the equilibrium value of concentrate flow velocity also increases. However, there is no bifurcation point. It is also worth noting that the recovery ratio, which is the ratio between product water and feed water, is decreasing with increasing feed concentration (Fig. 31B). When the performance (recovery) ratio reaches a certain low threshold (less than 20%), cleaning process should be carried out to guarantee system efficiency and economic costs. With the influence of CP in the high concentrate seawater RO plant, the cleaning process must be carried out more often.

4.4 Water hammer phenomenon

4.4.1 Water hammer, column separation and vaporous cavitation

Water hammer is the phenomenon occurring when there is a sudden starting or stopping of liquid flow. During the sudden shutdown of a pump or closure of a valve, there will be the formation of large pressure variations, cavitation, vibrations and column separation. In water hammering, kinetic energy of the moving fluid is converted into potential energy, causing waves of pressure and flow velocity back to

the fluid source. As a consequence, there is a pressure rise and fall and the pattern is repeated until the transients decay. These shock waves can also be of sufficient magnitude to cause physical damages to pipes, equipment and personnel.

Joukowsky is considered as the first scientist to study about water hammering. In 1898 he derived his famous law about instantaneous water hammer. It states that the piezometric head rises an amount ΔH resulting from a fast closure of a downstream valve.

$$\Delta H = \frac{aV_0}{g} \tag{82}$$

where a is the wave speed, V0 the initial flow velocity and g the gravitational acceleration.

The time closure T_c calculated to be less than $2L/a$ will cause a water hammer. Where L is the pipe length.

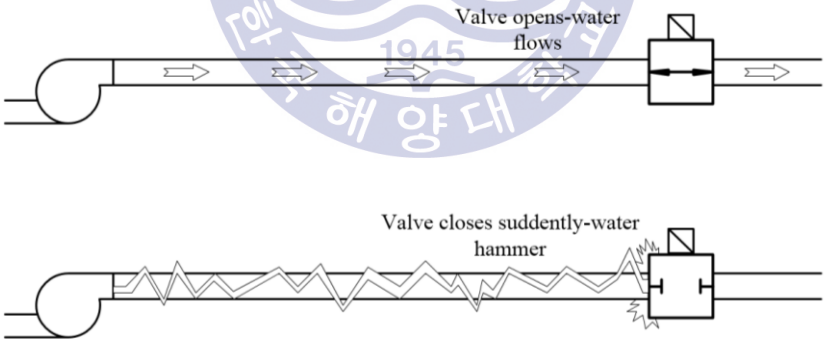

Fig. 32 Water hammer phenomenon

Column separation was first observed and analyzed by Joukowsky in 1900. Column separation is the breaking of liquid in fully filled pipelines. This may occur in a water-hammerring or at specific locations such as high points, knees or changing in diameters, when the pressure in a pipeline drops lower than vapor pressure of that

liquid, as shown in Fig. 33. Note that the atmospheric pressure equal to 1 atm while the vapor pressure of water at 25°C is about 0.03 atm. In this phenomenon, liquid columns are separated by a vapor cavities that grow and diminishes when the dynamics of the system change. The collision of two liquid columns, or of liquid columns with closed ends, may cause very large and nearly instantaneous rises in pressure. These pressure rises travel through the pipelines and create heavy loads for hydraulic machinery, pipes and supporting structures (Bergant, 2006).

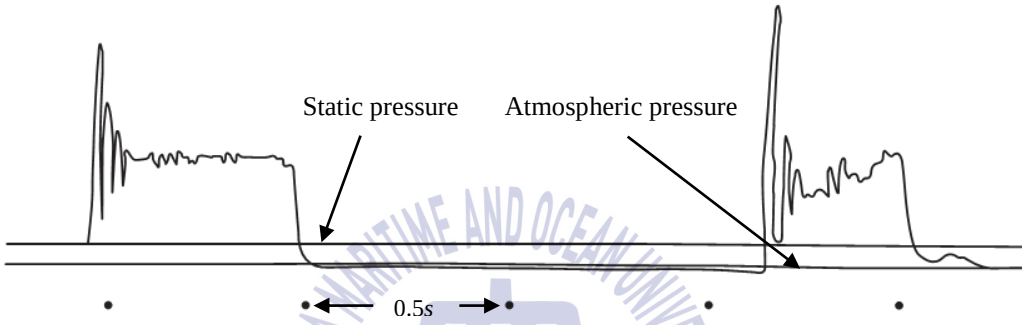

Fig. 33 Pressure record exhibiting column separation [Adapted from Joukowsky (1900)]

Vaporous cavitation exists when column separation occurs. In case the rising pressure is not enough to break pipes, cavitation still cause the wear in system equipment, finally resulting in leaks and ruptures. The phenomenon can be explained by the collapsing voids that implode near to a metal surfaces causing cyclic stress through repeated implosion. This results in surface fatigue of the metal causing a type of wear which is often called cavitation.

There are two type of vaporous cavitation, which depends on the magnitude of the void fraction of the vapor within the liquid occurring when column separation happens. It is defined by the ratio between the volume of the vapor V_v to the total volume of the liquid-vapor mixture V_m (Wallis, 1969):

$$\alpha_v = V_v / V_m \tag{83}$$

If α_v is large ($\alpha_v \approx 1$), it is call the local large vapor cavitation. If α_v is very small, it will be call the distributed small cavitation.

4.4.2 Water hammer analysis and simulation

In some RO systems that utilize feed flow reversal as that of Bartman *et al*. (2009), the valves close and open very often. With flow velocity greater than 1.5 m/s and high operating pressure, by manipulating the valves, or a sudden RO plant shutdown, water hammer often happens, and the transient pressure will be significantly high. Therefore, water hammer phenomenon in such RO system must be sufficiently realized for RO plant design and to avoid plant damages or failure.

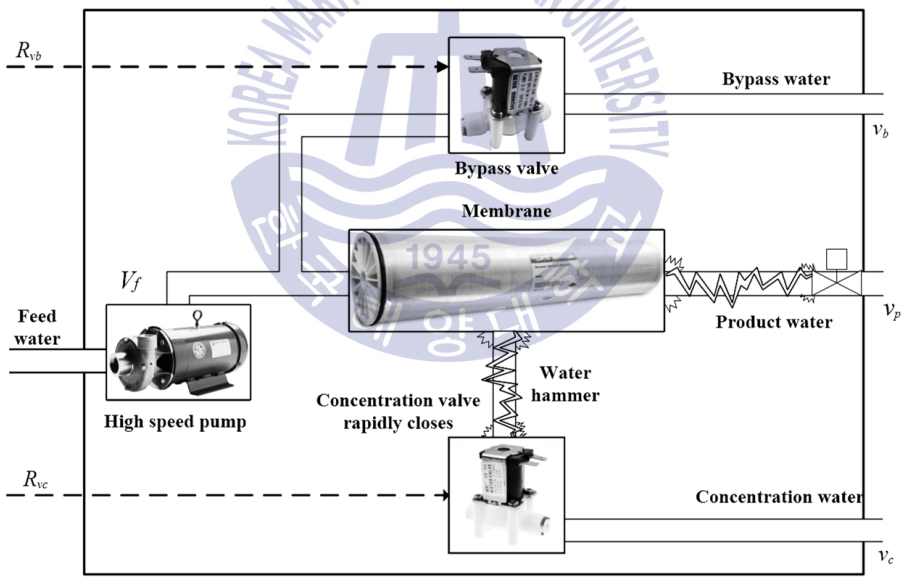

Fig. 34 Cases of water hammer in RO system

The theory of water hammer was introduced and developed very early as in Parmakian (1963), and Chaudhry (1987). There exist some inherited studies and simulations about water hammer such as in Saikia & Sarma (2006) and Saemi (2014). The governing equations of water hammer are adapted from continuity and

momentum in unsteady flow along a pipe. They include two partial differential equations (PDEs) with respect to time and pipe's length, as given in Juneseok (2008) as follow:

$$\frac{\partial Q}{\partial t} + gA\frac{\partial H}{\partial x} + \frac{f}{2D}Q|Q| = 0 \tag{84}$$

$$\frac{\partial H}{\partial t} + \frac{a^2}{gA}\frac{\partial Q}{\partial x} = 0 \tag{85}$$

where x is the pipe's length, $Q = AV$ the discharge flow, $H = P/\rho g$ the piezometric head, f the friction factor, D the pipe internal diameter, and a is the wave speed, which is calculated by

$$a = \sqrt{\frac{K_f}{\rho(1 + c\frac{K_f D}{eE})}} \tag{86}$$

with K_f is the bulk modulus of fluid elasticity, ρ the density of the liquid, e the pipe thickness, E the Young's modulus of pipe elasticity, $c = 1\text{-}\nu/2$, ν is the Poisson's ratio. The Q^2 term is changed to $Q|Q|$ so that the sign of the velocity can be considered.

Noted that the governing equations are nonlinear PDEs. There is no analytical solution for this problem. Therefore, numerical methods such as finite-differences should be used to solve these equations. The approach employed in this paper is the McCormack method which was first applied by Chaudhry and Hussaini (1985). This method adopts second-order explicit models for the analysis of single liquid transient flows, based on the characteristic boundary lines defined by $dx/dt = \pm a$ ($C+$,$C-$). This algorithm uses predictor and corrector steps to solve the problem of PDEs. The values of variables determined in the predictor part are used for the corrector part. The solution yields the pressure head, $H(x,t)$ and discharge flow, $Q(x,t)$ at any intersection of space node i and time level j.

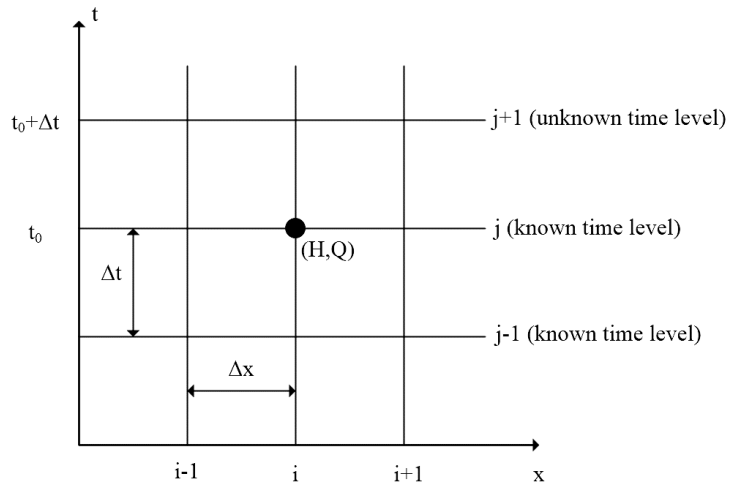

Fig. 35 The McCormack numerical method scheme

In the first alternative, the intermediate values of head and flow are calculated through the predictor part (Juneseok, 2008):

$$H_i^* = H_i^j - \frac{\Delta t}{\Delta x}\frac{a^2}{gA}(Q_{i+1}^j - Q_i^j) \tag{87}$$

$$Q_i^* = Q_i^j - \frac{\Delta t}{\Delta x} gA(H_{i+1}^j - H_i^j) - RQ_i^j \left|Q_i^j\right| \Delta t,\ (1 \le i \le n) \tag{88}$$

Then the new values of head and flow are obtained through the corrector part:

$$H_i^{j+1} = \frac{1}{2}\left[(H_i^j + H_i^*) - \frac{\Delta t}{\Delta x}\frac{a^2}{gA}(Q_i^* - Q_{i-1}^*)\right] \tag{89}$$

$$Q_i^{j+1} = \frac{1}{2}\left[(Q_i^j + Q_i^*) - \frac{\Delta t}{\Delta x} gA(H_i^* - H_{i-1}^*) - RQ_i^* \left|Q_i^*\right| \Delta t\right],\ (2 \le i \le n+1) \tag{90}$$

The equations for the second alternative are written in similar way but with the reverse direction of the spatial finite-difference approximation. Specifically, the equation for predictor part is written as:

$$H_i^* = H_i^j - \frac{\Delta t}{\Delta x}\frac{a^2}{gA}(Q_i^j - Q_{i-1}^j) \tag{91}$$

$$Q_i^* = Q_i^j - \frac{\Delta t}{\Delta x} gA(H_i^j - H_{i-1}^j) - RQ_i^j \left|Q_i^j\right| \Delta t, \ (2 \le i \le n+1) \tag{92}$$

and the corrector part:

$$H_i^{j+1} = \frac{1}{2}\left[(H_i^j + H_i^*) - \frac{\Delta t}{\Delta x}\frac{a^2}{gA}(Q_{i+1}^* - Q_i^*) \right] \tag{93}$$

$$Q_i^{j+1} = \frac{1}{2}\left[(Q_i^j + Q_i^*) - \frac{\Delta t}{\Delta x} gA(H_{i+1}^* - H_i^*) - RQ_i^* \left|Q_i^*\right| \Delta t \right], \ (1 \le i \le n) \tag{94}$$

The inclusion of boundaries is an important aspect of the numerical methods since errors appearing at a boundary will be propagated throughout the computational domain and lead to instabilities. The values of *H* and *Q* can be solved at the interior points. However, at the boundaries, *H* and *Q* cannot be calculated since there is no grid point outside the computational domain. Therefore, the boundary conditions need to be included in the analysis by using the characteristic equations as follow (Chaudhry and Hussaini, 1985):

When $\lambda^+ = \frac{dx}{dt} = a$

$$C+: \left(\frac{\partial H}{\partial t} + \lambda^+ \frac{\partial H^+}{\partial x} \right) + \frac{a}{gA}\left(\frac{\partial Q}{\partial t} + \lambda^+ \frac{\partial Q^+}{\partial x} \right) + \frac{af}{2gDA} Q|Q| = 0 \tag{95}$$

When $\lambda^{-} = \frac{dx}{dt} = -a$

$$C-: \left(\frac{\partial H}{\partial t} + \lambda^{-} \frac{\partial H^{-}}{\partial x} \right) - \frac{a}{gA} \left(\frac{\partial Q}{\partial t} + \lambda^{-} \frac{\partial Q^{-}}{\partial x} \right) - \frac{af}{2gDA} Q|Q| = 0 \qquad (96)$$

where the characteristic line $C+$ is valid for downstream and $C-$ is for upstream boundary and λ is the Lagrange multiplier.

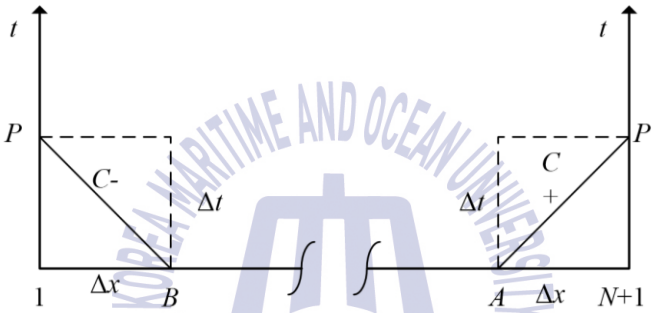

Fig. 36 Characteristic lines at boundaries

4.4.2.1 Water hammer in spiral wound membrane of RO system

The water flow inside the spiral wound membrane module can be simplified as the flow in a rectangular membrane as shown in Fig. 37.

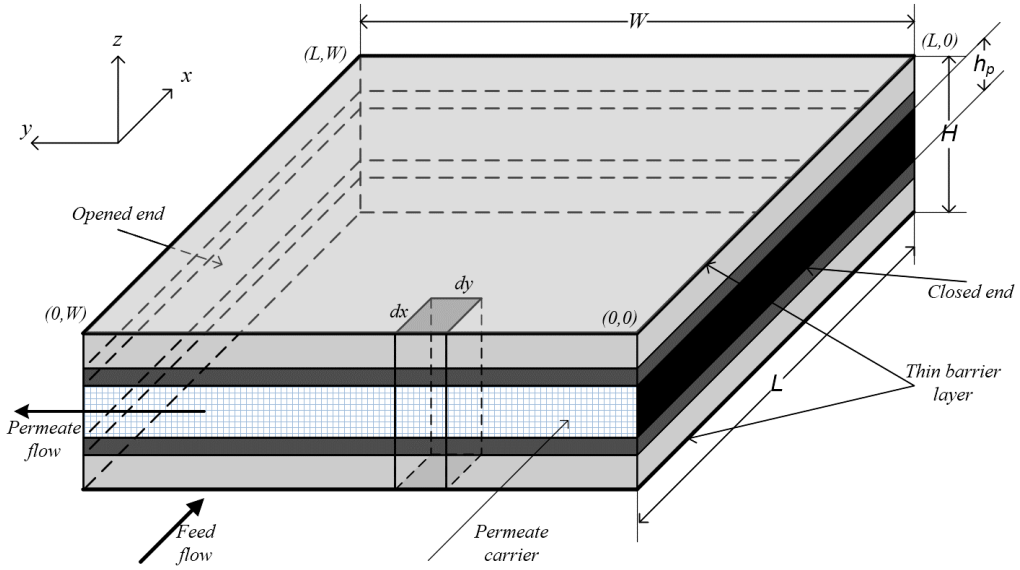

Fig. 37 Unwound RO membrane mechanism [Adapted from Avlonitis *et al*., (2010)]

The feed water is fed into the membrane along *x* direction, while the permeate water is flowing along a permeate channel from the close end to the open end, in *y* direction. The permeate carrier which is laid between two membrane layers to form a leaf. The leaf is glued in three sides and the opened side is connected to the collecting tube. Since there is no flow along the *x* direction in the permeate channel, the pressure in this direction is assumed constant. The local permeate velocity and local permeate pressure are given in Avlonitis *et al*., (2010) as:

$$v_p = \frac{2qK_wK_m \sinh\frac{y}{q}}{h_p\left[K_m + K_wW(c_f + fx)\right]\cosh\frac{w}{q}}\left[P_d - Wc_f + \frac{c_f v_f k_{fb}\mu}{f}\ln\frac{c_f}{c_f + fx} - Wfx\right] \quad (97)$$

$$P_p(y) = \frac{2k_{fp}\mu K_m K_w q^2}{h_p(K_m + K_w Wc_f)}(\Delta P - Wc_f)\left(1 - \frac{\cosh\frac{y}{q}}{\cosh\frac{W}{q}}\right) + P_p(0,W) \quad (98)$$

where K_w is the water permeability coefficient, K_m the total mass transfer coefficient, c_f the feed concentration, μ the viscosity of the feed solution, W the width of the membrane, k_{fp} the friction coefficient in the permeate channel, h_p the height of the permeate channel, $q = \sqrt{h_p / 2K_w k_{fp}\mu}$, $f = (c_c\text{-}c_f)/L$, $P_l = P_f(0,W) - P_p(0,W)$ the lost pressure, x and y the distance along x and y axes, and a is the wave velocity.

Providing that there is a valve at the end of the permeate tube of a RO system. Suppose the valve is closed suddenly so that the flow near the valve is completely stopped. However, the permeate water in the membrane leaf still flow with velocity $u_p(x,y)$ at each point of the membrane. This make the water near the valve compressed and the pressure is increasing rapidly, called hammer phenomenon. The transient pressure at each point inside the membrane leaf is calculated as the following equation (Avlonitis *et al*., 2010):

$$\Delta P(x, y) = \rho a v_p(x, y) \tag{99}$$

4.4.2.2 Simulation result

In this paper, water hammer phenomenon in RO system is simulated at equilibrium condition with a sudden closure of concentration valve. Assume that the valve is 25 m away from the pump and 5 m away from the membrane, and all components are in the same horizontal plane. The steady state value of system pressure is 31.57 bar and that of velocity through concentration valve is 4.511 m/s. The wave profiles of internal pressure and velocity waves at the membrane are simulated as in Fig. 38.

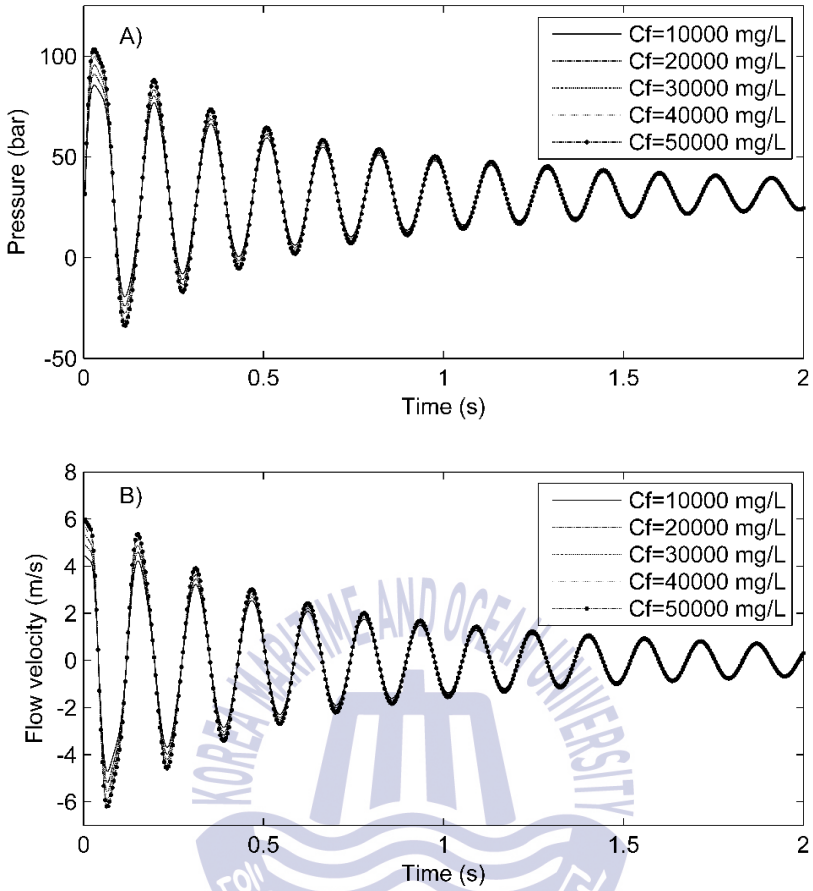

Fig. 38 Water hammer wave profile of the transient pressure (A) and the concentration flow velocity (B)

It can be observed that the magnitude of the first pressure wave is the maximum one and can be very much higher than the initial pressure, while that of the first velocity wave only equals to the initial flow velocity through concentration valve. The pressure profile depends on initial pressure and flow velocity, the elasticity of the fluid and pipe, the density of the fluid, the diameter and thickness of the pipe and the valve closing time. Specifically, the maximum pressure is 103.4 bar, which is 3.27 times as big as the steady state one. This results in a huge hammering force acting on the valve, the pipe, and the membrane. This behavior can lead to safety issues if the pressure exceeds the safety rating of system components. Especially,

this pressure can destroy the membrane since the maximum working pressure of membranes are about 80 bars.

The result in Fig. 38A agrees with the famous fundamental Joukowski equation (Joukowski, 1904) to calculate the maximum pressure in water hammer:

$$P_{\max} = \rho a \Delta V + P_s \tag{100}$$

where ΔV is the velocity change of water in the pipeline.

Eq. (100) shows that the water hammer pressure depends on the characteristic of the fluid and the pipe, and the system operating status just before the water hammer happen.

It is known that CP phenomenon makes the velocity through concentration valve increase. It means under the effect of CP, the transient pressure in water hammer will be much higher, as illustrated in Fig. 39. For the feed seawater with a high concentration greater than 40000 mg/L and CP index greater than 2, the transient pressure will be greater than 100 bar, depicted by the bright area of the pressure surface in Fig. 39. Hence, the CP phenomenon can cause more serious problems to RO system if it is not sufficiently considered in the design and control of the process.

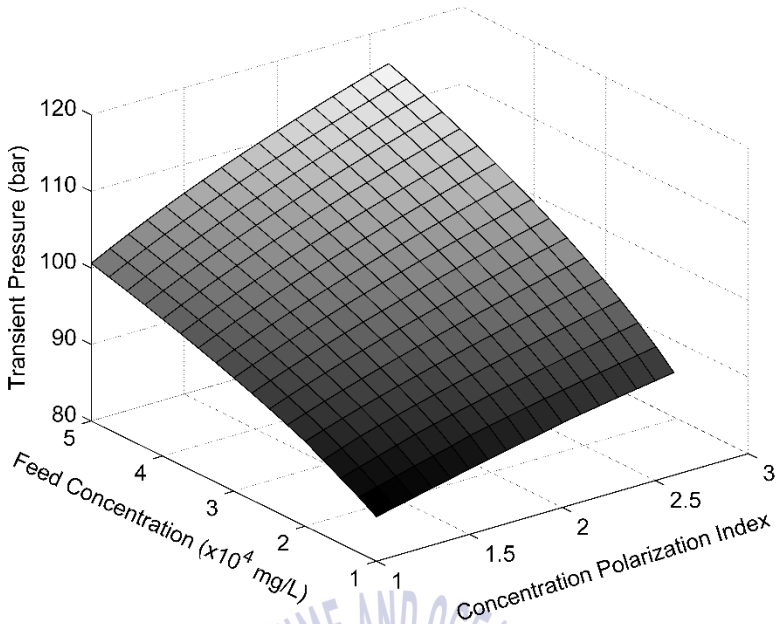

Fig. 39 The transient pressure *vs* CP index and feed concentration in water hammer

4.4.3 Prevention of water hammer effect

Water hammer is an undesired phenomenon, whose effects need to be rejected as much as possible. There are some methods can diminish water hammer. Those approaches include designing the discharge pipes with lower flow velocity, increasing the inertia moment of the pump, installing surge tanks, air chambers or non-return valve in the piping system, and adding pressure control valve (Choon et al., 2005). One of the simpler and efficient methods to minimize the damaging of water hammer is to install the bypass pipe like that in the current model. Whenever there is a sudden closure of the concentrate valve, the system pressure will jump immediately to a very high value (see Fig. 38). In order to prevent damages, the bypass valve needs to be opened in time to discharge the transient pressure. This duty must be carried out in milliseconds. Furthermore, the transient pressure profile is a wave of alternative positive and negative pressure. Hence, the bypass valve must be alternatively opened and closed in a manner so that system pressure is kept stable

and safe. It is a hard job, and it needs a powerful controller to regulate the system. In the next section, designers introduce a robust H_∞ controller to handle this problem.

4.5 RO linearization

4.5.1 Nominal linearization

The nonlinear analysis showed that the nonlinear behavior of the system around it unique equilibrium point is a stable node. Since there are many limitations on controlling of a nonlinear system, the system can be linearized in the vicinity of its equilibrium to utilize some good control theory for a linear system.

In the current RO system, besides the product water flow and system pressure, product water concentration is added as the third output for linearized systems. These three outputs are the most common controlled variables in RO systems.

Consider nonlinear differential equations given in Eqs. (72-73) as follow:

$$\begin{aligned} \dot{x}(t) &= f(x(t), u(t)) \\ y(t) &= g(x(t), u(t)) \end{aligned} \tag{101}$$

where

$\dot{x} = \begin{bmatrix} \dot{v}_c \\ \dot{v}_b \end{bmatrix}, u = \begin{bmatrix} R_{vc} \\ R_{vb} \end{bmatrix}, y = \begin{bmatrix} F_p \\ P_s \\ C_p \end{bmatrix}$, $f(x,u)$, and $g(x,u)$ are given in Eqs. (72), (73), (74), (76), and (81), respectively.

Providing that the system equilibrium family including the equilibrium input u^*(5000, 310), the equilibrium point x^*(4.511, 1.123) and the constant output y^*(2.369e3, 3.15e6, 180). Starting a little bit away from x^* and applying slightly different input from u^*, the constant output will be slightly shifted away from y^*, where the deviations are expressed as:

$$\begin{aligned}\delta_x(t) &:= x(t) - x^* \\ \delta_u(t) &:= u(t) - u^* \\ \delta_y(t) &:= y(t) - y^*\end{aligned} \tag{102}$$

Substituting into Eq. (74) yields:

$$\begin{aligned}\dot{\delta}_x(t) &= f(\delta_x(t) + x^*, \delta_u(t) + u^*) \\ \delta_y(t) &= g(\delta_x(t) + x^*, \delta_u(t) + u^*)\end{aligned} \tag{103}$$

By applying a Taylor expansion of the right hand side in Eq. (103), neglecting all higher order terms,

$$\dot{\delta}_x(t) \approx f(x^*, u^*) + \left.\frac{\partial f}{\partial x}\right|_{\substack{x=x^* \\ u=u^*}} \delta_x(t) + \left.\frac{\partial f}{\partial u}\right|_{\substack{x=x^* \\ u=u^*}} \delta_u(t) \tag{104}$$

$$\delta_y(t) \approx g(x^*, u^*) + \left.\frac{\partial g}{\partial x}\right|_{\substack{x=x^* \\ u=u^*}} \delta_x(t) + \left.\frac{\partial g}{\partial u}\right|_{\substack{x=x^* \\ u=u^*}} \delta_u(t) \tag{105}$$

Noting that $f(x^*,u^*) = 0$, the state-space constant matrices are calculated using:

$$A := \left.\frac{\partial f}{\partial x}\right|_{\substack{x=x^* \\ u=u^*}}, B := \left.\frac{\partial f}{\partial u}\right|_{\substack{x=x^* \\ u=u^*}}, C := \left.\frac{\partial g}{\partial x}\right|_{\substack{x=x^* \\ u=u^*}}, D := \left.\frac{\partial g}{\partial u}\right|_{\substack{x=x^* \\ u=u^*}} \tag{106}$$

whose the partial components are particularized in the appendix *A*.

The linear system which is so-called the Jacobian linearization of the original nonlinear system about the equilibrium point (x^*,u^*) is displayed as

$$\begin{aligned}\dot{\delta}_x(t) &= A\delta_x(t) + B\delta_u(t) \\ \delta_y(t) &= C\delta_x(t) + D\delta_u(t)\end{aligned} \tag{107}$$

Having the state-space matrices, the transfer function from the inputs to outputs is calculated using $G(s) = C(sI-A)^{-1}B+D$, as follow

$$G(s)=\begin{bmatrix} \dfrac{T_{11}s+K_{11}}{s^2+2\xi\omega_n s+\omega_n^2} & \dfrac{T_{12}s+K_{12}}{s^2+2\xi\omega_n s+\omega_n^2} \\ \dfrac{T_{21}s+K_{21}}{s^2+2\xi\omega_n s+\omega_n^2} & \dfrac{T_{22}s+K_{22}}{s^2+2\xi\omega_n s+\omega_n^2} \\ \dfrac{T_{31}s+K_{31}}{s^2+2\xi\omega_n s+\omega_n^2} & \dfrac{T_{32}s+K_{32}}{s^2+2\xi\omega_n s+\omega_n^2} \end{bmatrix} \tag{108}$$

where the nominal values of the parameters in the transfer function are listed in Table 2 and the respective parameters are given in the Apendix B.

Table 2 RO model parameter variations

Parameters	Min. values	Nominal values	Max. values	Unit
T_{11}	10.61	11.61	13.61	min
K_{11}	26.75	31.75	37.75	unitless
T_{12}	10.61	11.61	12.61	min
K_{12}	34.26	38.26	42.26	unitless
T_{21}	1.664	2.664	3.664	min
K_{21}	3.03	8.03	11.03	unitless
T_{22}	1.339	2.339	3.339	min
K_{22}	5.05	7.05	9.05	unitless
T_{31}	-3.792	-2.792	-1.792	min
K_{31}	-8.633	-7.633	-6.633	unitless
T_{32}	-3.792	-2.792	-1.792	min
K_{32}	-10.197	-9.197	-8.197	unitless
ω_n	4.48	4.70	4.9	rad.s^{-1}
ξ	1.04	1.068	1.15	unitless

4.5.2 Uncertainty modeling

The varying of the parameters in Table 2 can be lumped into $W_M\Delta$ structure and displayed as an input multiplicative uncertainty as in the dashed block in Fig. 42. In this framework Δ is used to model the uncertainty kind and level of RO unit, and W_M is the uncertainty weighting function. The uncertainty in this model is assumed to be real and structured. It stands for all the mismatch uncertainty in the system. The perturbed plant is extracted and simply written as follows:

$$\tilde{G}_r = G_r(I + \Delta W_M) \tag{109}$$

where $\Delta = \begin{bmatrix} \delta_1 & 0 \\ 0 & \delta_2 \end{bmatrix}$ and $W_M = \begin{bmatrix} W_{M11} & 0 \\ 0 & W_{M22} \end{bmatrix}$

The set of perturbed plant is also defined as

$$\Pi = \left\{ \tilde{G}_r \mid \tilde{G}_r = G_r(I + \Delta W_M), \bar{\sigma}(\Delta) \le 1 \ ^{\forall}\omega \right\} \tag{110}$$

The perturbed system boundary $l_M(j\omega)$ at each frequency which includes the possible plant $\tilde{G}_r \in \Pi$ is defined by Skogestad et al. (2005) as follow:

$$\begin{aligned} l_M(j\omega) &= \max \bar{\sigma}\left(\Delta(j\omega) W_M(j\omega)\right) \\ &= \max \bar{\sigma}\left[G_r^{-1}(j\omega)\left(\tilde{G}_r(j\omega) - G_r(j\omega)\right)\right] \end{aligned} \tag{111}$$

When max singular value $\bar{\sigma}(\Delta) = 1$, the weighting function W_M is chosen to cover the boundary $l_M(j\omega)$ that satisfies:

$$\underline{\sigma}\left(W_M(j\omega)\right) \ge l_M(j\omega) \ ^{\forall}\omega \tag{112}$$

The set of l_M and elements of weighting function W_M in Eqs. (111) and (112) are plotted in Fig. 40. It can be seen that weighting function elements bound all the possible l_M.

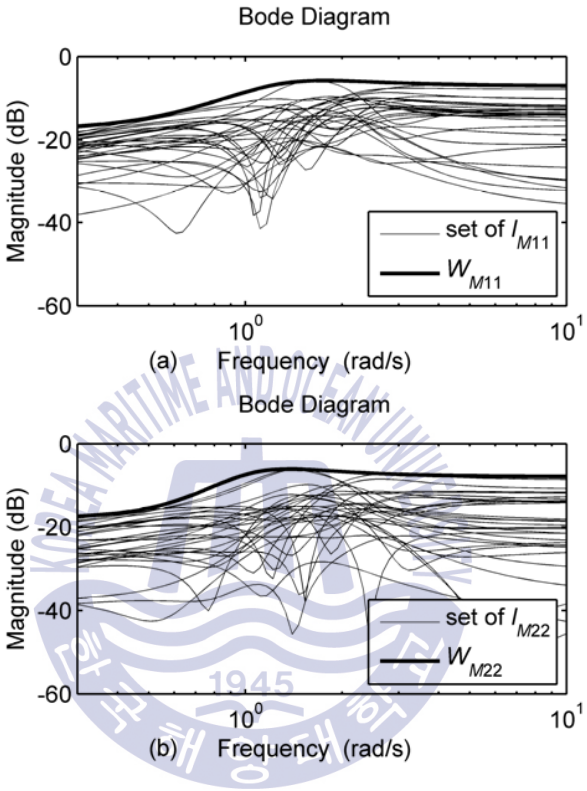

Fig. 40 The Bode plots of uncertainty weighting function W_M and l_M : (a) W_{M11} and the set of l_{M11} in the first channel; (b) W_{M22} and the set of l_{M22} in the second channel.

4.5.3 Parametric uncertainty linearization

The state-space matrices in Eq. (106) and the transfer function in Eq. (108) are based on nominal parameter. In fact, the real RO system is an uncertain system with variable membrane concentration $C_{m,}$ due to CP phenomenon. Note that in this real system, the feed concentration C_f in Eq. (74) is replaced by the membrane concentration C_m, whose value can vary up to $2.6C_f$. Using the approach in Sam-sang & Seok-kwon (2002), the variation of C_m can be modeled as:

$$C_m = \bar{C}_m(1 + E\Delta_m) \tag{113}$$

where $\bar{C}_m$ is the nominal value, $-1 \le \Delta_m \le 1$, and E indicates the maximum percent of variation from nominal value. In this system, since C_f = 10000 mg/L, then $\bar{C}_m$ = 18000 and E = 0.44 are chosen to perform the range of possible variation.

The uncertain state variable model due to CP is now considered as:

$$\begin{bmatrix} \dot{x}(t) \\ y(t) \end{bmatrix} = \begin{bmatrix} A + \Delta_1 A_1 & B + \Delta_1 B_1 \\ C + \Delta_1 C_1 & D + \Delta_1 D_1 \end{bmatrix} \begin{bmatrix} x(t) \\ u(t) \end{bmatrix}$$
$$= \left(\underbrace{\begin{bmatrix} A & B \\ C & D \end{bmatrix}}_{\text{nominal matrix}} + \Delta_1 \underbrace{\begin{bmatrix} A_1 & B_1 \\ C_1 & D_1 \end{bmatrix}}_{\text{uncertain matrix}} \right) \begin{bmatrix} x(t) \\ u(t) \end{bmatrix} \tag{114}$$

Using the uncertain model of C_m as in Eqs. (112) and (113), the components of the uncertain matrix are calculated and given in the appendix *B*. Then the uncertain matrix can be factorized using singular value decomposition as:

$$E_1 = \begin{bmatrix} A_1 & B_1 \\ C_1 & D_1 \end{bmatrix} = \begin{bmatrix} K_1 \\ L_1 \end{bmatrix} \begin{bmatrix} M_1 & N_1 \end{bmatrix} \tag{115}$$

where $E_1 = USV^*$, $\begin{bmatrix} K_1 \\ L_1 \end{bmatrix} = US^{1/2}$, and $\begin{bmatrix} M_1 & N_1 \end{bmatrix} = S^{1/2}V^*$

From Eqs. (114) and (115), a real linear system G_r with the extra connections to the uncertainty, the input w_1 and the output z_1 (see Fig. 41), can be represented as

$$\begin{bmatrix} \dot{x} \\ \hline y \\ \cdots \\ z_1 \end{bmatrix} = \left[\begin{array}{c|c} A_r & B_r \\ \hline C_r & D_r \end{array}\right] \begin{bmatrix} x \\ \hline u \\ \cdots \\ w_1 \end{bmatrix} = \underbrace{\left[\begin{array}{c|c:c} A & B & K_1 \\ \hline C & D & L_1 \\ \cdots & \cdots & \cdots \\ M_1 & N_1 & 0 \end{array}\right]}_{G_r} \begin{bmatrix} x \\ \hline u \\ \cdots \\ w_1 \end{bmatrix} \tag{116}$$

Note that the shorthand notation for the transfer function from u and w_1 to y and z_1 is defined as:

$$G_r = \left[\begin{array}{c|c} A_r & B_r \\ \hline C_r & D_r \end{array}\right] = C_r(sI - A_r)^{-1}B_r + D_r \tag{117}$$

The calculated values of G_r are also given in appendix *B*.

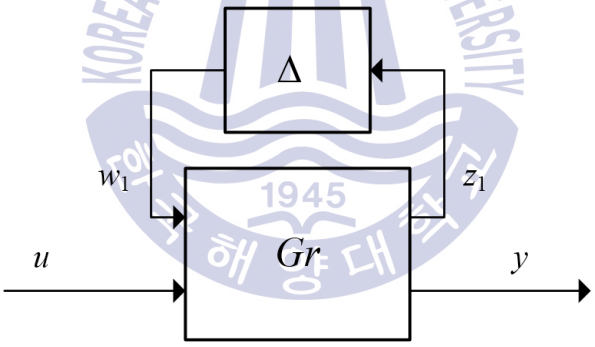

Fig. 41 The real RO system with uncertain parameter C_m

4.6 Robust H_∞ controller design for RO system

4.6.1 Control of uncertain RO system

Beside the parametric uncertainty caused by some parameter variations such as C_m in section 4.5.3, the robust controlling of RO system should consider unmodelled uncertainty (unmodelled dynamic) as depicted in Fig. 42. The unmodelled dynamic

represented by W_M and Δ_M, comes from some assumptions, approximations when modelling the system or from the ignoring of some factors in the real system. This kind of uncertainty can be modelled at the input (such as in this study), output or parallel of the system. Furthermore, external disturbances and sensors noises always exist in the operating system.

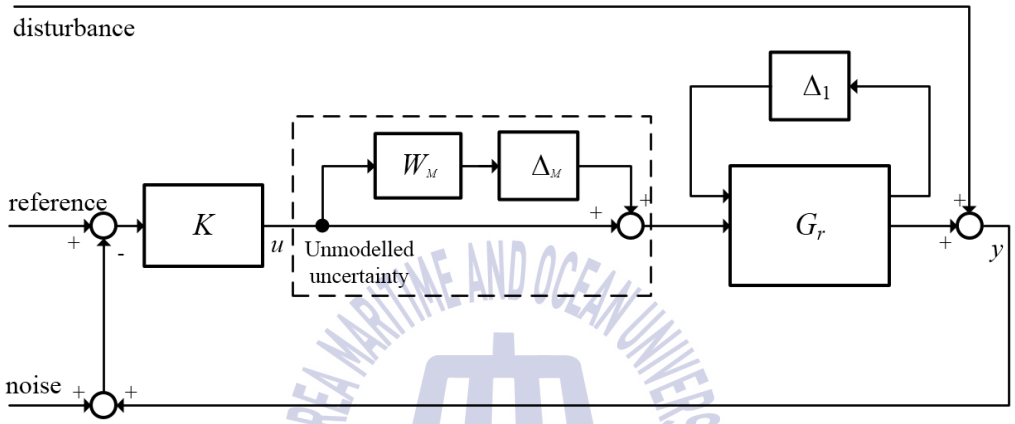

Fig. 42 Control scheme of uncertainty RO system

The measured output will be affected by sensor noise signals, normally in high frequency. These feedback signals will be compared with the desired reference to give the error which is fed into the controller *K*. The controller is said to be robust if it can deal with both parametric and unmodelled uncertainty, with disturbance and noise meanwhile satisfy the requirement criterions for robustness such as those presented in the next section.

4.6.2 Robustness analysis and H_∞ controller design

In modern multivariable control, robust H_∞ controller has been proved its ability to deal with the systems with high uncertainties. In this paper, based on small gain theorem and μ-synthesis (Doyle, 1982), the mixed robust H_∞-μ theory is applied to control the current uncertainty RO system. In this framework, it is necessary to

develop a generalized plant P accounting all possible affecting factors. In the block diagram (see Fig. 43), besides the parameter uncertainty block Δ_1, designers also introduce unmodelled uncertainty at system input. They stand for some modeling mismatches under the linearization process and unmodelled dynamics of actuators. A performance weighting function W_P is added at the output of the system to perform the level of the performance requirement. Δ_P is the fictitious perturbation representing the $H\infty$ performance specification of the μ-synthesis framework in Doyle (1982). The generalized plant also accounts some real inputs such as disturbance d, sensor noise n and reference r, accompanied by their weighting function W_d, W_n and W_r, respectively. Especially, water hammering is considered as disturbance d. Therefore, the simulation result of water hammering in section 3 is accounted into the control design. The controller is successfully designed if it can deal with water hammering, noises and uncertainties while satisfies robust performance and stability requirements.

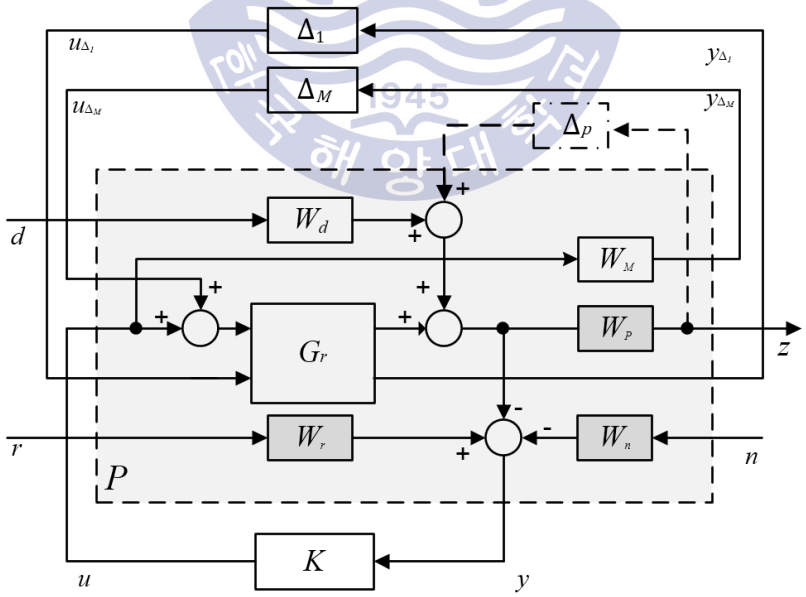

Fig. 43 Generalized plant P

The generalized plant P is further written as:

$$\begin{bmatrix} y_{\Delta_1} \\ y_{\Delta_M} \\ z \\ \hline y \end{bmatrix} = P \begin{bmatrix} u_{\Delta_1} \\ u_{\Delta_M} \\ d \\ n \\ r \\ \hline u \end{bmatrix} \tag{118}$$

where

$$P = \left[\begin{array}{cccccc|c} 0 & G_r & 0 & 0 & 0 & 0 & 0 \\ 0 & 0 & 0 & 0 & 0 & 0 & W_M \\ W_P & 0 & W_P G_r & W_P W_d & 0 & 0 & W_P G_r \\ W_P & 0 & W_P G_r & W_P W_d & 0 & 0 & W_P G_r \\ \hline -I & 0 & G_r & -W_d & -W_n & W_r & -G_r \end{array}\right] = \left[\begin{array}{c|c} P_{11} & P_{12} \\ \hline P_{21} & P_{22} \end{array}\right] \tag{119}$$

Note that the uncertainty block Δ_μ including three sub blocks, has the structure as depicted in Fig. 44. In order to use μ-synthesis for structured uncertainty, the closed-loop transfer matrix that connects the generalized plant P with the controller K via a lower linear fractional transformation. N is calculated as follow:

$$\begin{aligned} N &= F_l(P,K) = P_{11} + P_{12}K(I - P_{22}K)^{-1}P_{21} \\ &= \left[\begin{array}{cc|ccc} G_r & 0 & 0 & 0 & 0 \\ 0 & -W_M T_i & -W_M K S_o W_d & -W_M K S_o W_n & W_M K S_o W_r \\ \hline 0 & W_P G_r S_i & W_P S_o W_d & -W_P T_o W_n & -W_P T_o W_r \end{array}\right] \\ &= \left[\begin{array}{c|c} N_{y_{\Delta\mu}u_{\Delta\mu}} & N_{y_{\Delta\mu}w} \\ \hline N_{zu_{\Delta\mu}} & N_{zw} \end{array}\right] \end{aligned} \tag{120}$$

where

$$S_i = (I + KG_r)^{-1},\ S_o = (I + G_r K)^{-1},\ T_i = KG_r(I + KG_r)^{-1},\ T_o = G_r K(I + G_r K)^{-1},$$

are so-called the input, output sensitivity and complementary sensitivity functions, respectively.

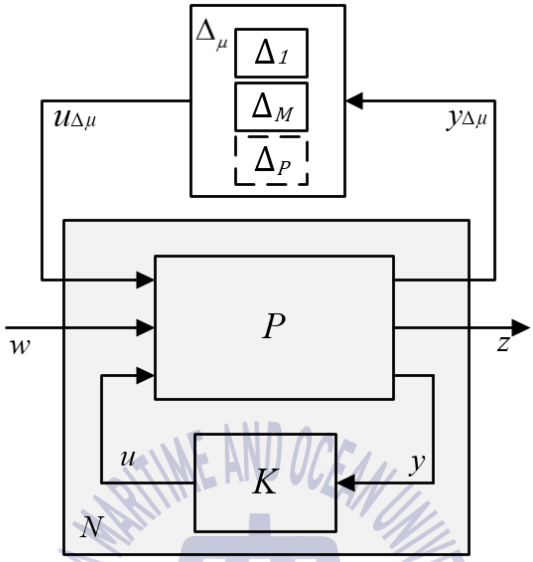

Fig. 44 N-$\Delta\mu$ structure

According to small gain theorem and μ-synthesis (Doyle, 1982), nominal performance, robust stability and robust performance conditions are satisfied for the control system if the weighting functions W_P, W_M and the optimal controller K are calculated so that the follow inequalities hold, respectively:

$$\|W_M T_i\|_\infty < 1 \;\Leftrightarrow\; \mu_\Delta(N_{11}(j\omega)) < 1, \;^\forall\omega \tag{121}$$

$$\|W_P S_o W_d\|_\infty < 1 \Leftrightarrow \mu_\Delta(N_{22}(j\omega)) < 1, \;^\forall\omega \tag{122}$$

$$\begin{aligned} &\left\|F_u(N,\Delta_\mu)\right\|_\infty = \left\|N_{zw} + N_{zu_{\Delta\mu}}\Delta_\mu(I - N_{y_{\Delta\mu}u_{\Delta\mu}}\Delta_\mu)^{-1}N_{y_{\Delta\mu}w}\right\|_\infty < 1, \\ &\forall\Delta_\mu, \|\Delta_\mu\|_\infty < 1 \Leftrightarrow \mu_{\Delta_\mu}(N) < 1, \;^\forall\omega \end{aligned} \tag{123}$$

where $\mu_{\Delta_\mu}(N)$ is the structured singular value of the closed-loop transfer matrix N defined in section 2.3.3.

4.7 Simulation result and discussion

The objective of the robust H_∞ controller in this study is to cope with system uncertainties, noises and to attenuate the transient pressure in water hammer phenomenon. It is known that the membrane concentration C_m is variable during the operation time, and there exist unmodelled uncertainties in the modeling process. All the uncertainties in this RO system are represented by the parameter variations of the linearized transfer function as shown in Table 2. The uncertainties are chosen based on the experimental reference (Chaaben & Andouls, 2008); however, with larger ranges. It means the requirements for controller design in simulation condition is more stringent than those in real system. For the sake of clarity, the designers built three models named as nom, min, and max model using nominal, minimum, and maximum parameters in Table 1, respectively. These models stand for the perturbed system with uncertainties. The controller is expected to control all three models without big differences in the performances, eliminate at least 50% of transient pressure caused by water hammer effect and attenuate more than 70% of noises.

For the robust control synthesis, the suitable weighting functions are chosen. Based on those functions, the controller K has been designed to satisfy the condition given in Eqs. (121-123). It is given in Appendix C. Then the transient responses of the closed-loop system are examined. Structured singular values of nominal performance, robust stability and robust performance are plotted in Fig. 44. It can be observed that all the requirements for stability and performance in Eqs. (121-123) are satisfied, where all the maximum values are less than 1. The peak of nominal performance, robust stability and robust performance plots are 0.63, 0.52 and 0.86, respectively. The meaning of these number can be explained as follows: the nominal performance with no uncertainty is easily satisfied since the peak is 0.63, being for from 1. For robust stability, the uncertainty size can increase by a factor of 1/0.52 = 1.92 before the worst-case uncertainty yields instability. Consequently, the peak 0.86 of $\mu\Delta_\mu(N)$ shows that even with 1/0.86 = 1.16 larger uncertainty, the perturbed

system still be stable. If the uncertainty level gets higher than this limit, the performance will become worse.

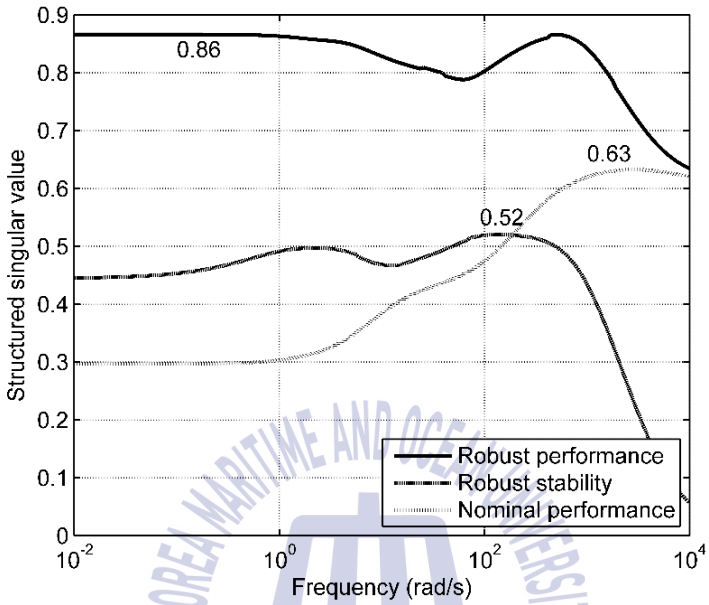

Fig. 45 Structured singular value plots of the stability and performance for RO system

The responses of the closed-loop systems are illustrated in Fig. 46. From the plot, we can see that there are only slight differences between the three mentioned models. All the responses are fast enough with rising times less than 1 second and there are no overshoots. It means whatever values of the parameters given in Table 2 are, the controlled system is still in good operation. Normally, the permeate water concentration less than 500 mg/L is acceptable. Fig. 46C indicates good quality product water is guaranteed. Note that the product water concentration and flow are inversely related. It means there is a trade-off between product quality and quantity. Therefore in this simulation, only the product water flow is chosen as controlled variable, in accompany with the system pressure. Especially, Fig. 46B shows that the response of the system pressure is less than 0.2s, which is very fast. It makes sense

since the system pressure is the direct variable having effect on the other variables. Controlling the system pressure is the key in system performance. The transient responses prove that the controller effectively control the system and deal with the given uncertainties.

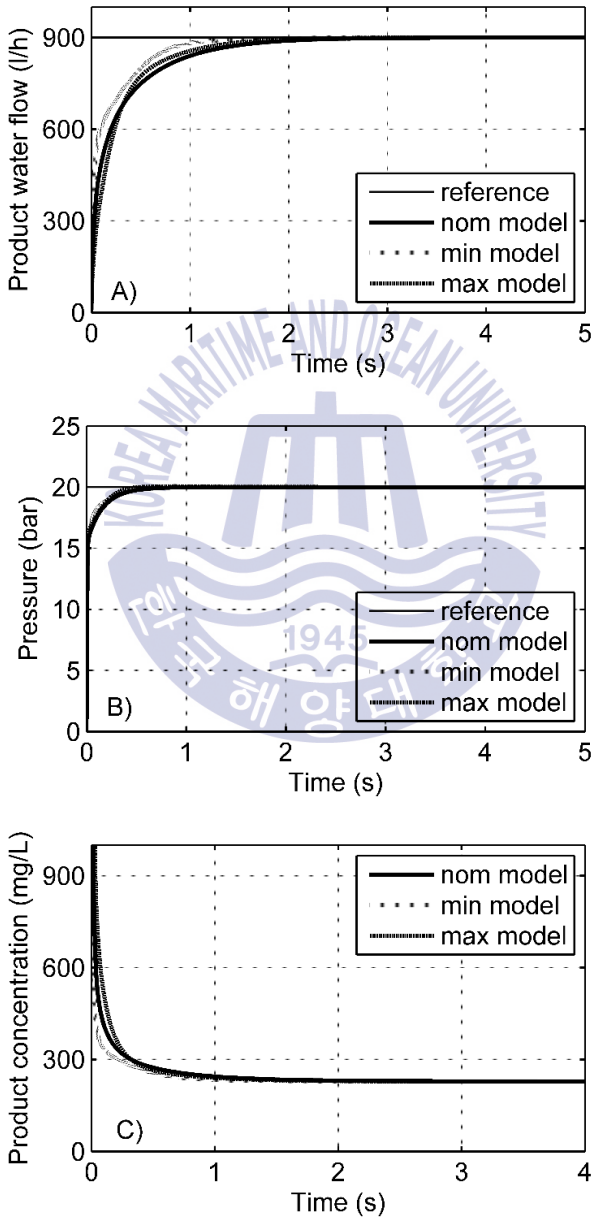

Fig. 46 Transient responses of the controlled system

In the real operation time, the measured outputs are always distorted by sensor noises. Noises often happen in high frequency range. The distortion caused by noises can be attenuated with different levels depending on controllers. In the following simulation, one noise signal at 102 rad/s is introduced in the first channel and another one at 3103 rad/s is pushed into the second channel to check the responses of two controlled variables. Note that since the system pressure is the direct controlled variable, its sensor should operate in higher frequency. Fig. 47 shows that about 90% and 80% of sensor noises are rejected, respectively. It means the controller can protect the process from large distortion caused by noises.

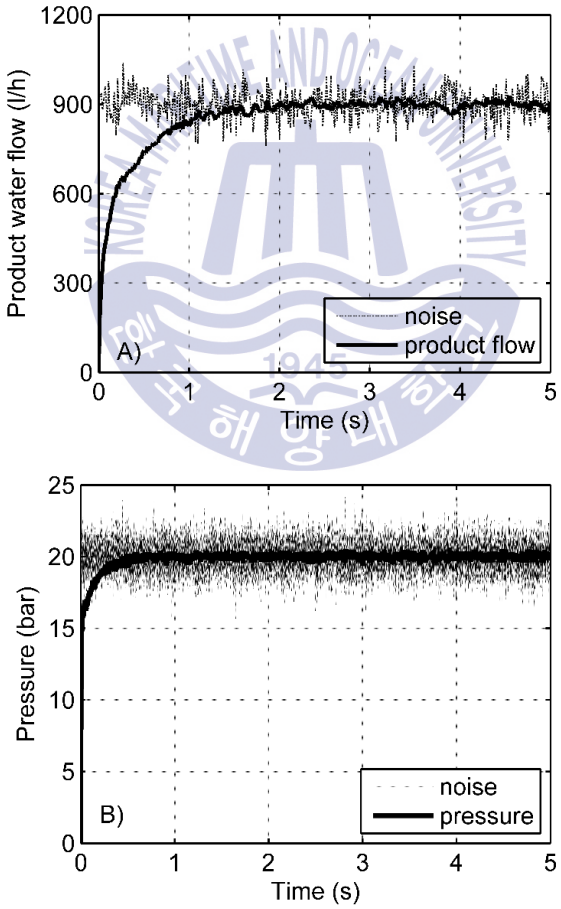

Fig. 47 Noise responses

The most interesting concern is the ability of disturbance attenuation of the controller. In this simulation, the transient pressure caused by water hammer effect is introduced as a disturbance to the system. As discussed, this transient pressure has damping wave profile and the magnitude of the first pressure wave is very high. Only powerful controllers can handle this kind of disturbance to protect the system from damages or eliminate some sounds coming out.

In this simulation, the water hammer is supposed to happen at 0.5^{th} second. The initial system pressure is 31.57 bar. The simulated condition is chosen as the worst case with the feed water concentration C_f = 50000 mg/L. The performance of the controller is illustrated in Fig. 48. The illustration shows that without the controller, the top pressure in the first wave is calculated at 103.4 bar. Under the effect of the controller, this top pressure is reduced to 61.9 bar. It means 58% of the disturbance is eliminated. This result is superior comparing to the best result presented in literature, which is 33.33%. The elimination is also seen in the aspect of time. The controlled transient pressure only happens in a halftime comparing to the uncontrolled one.

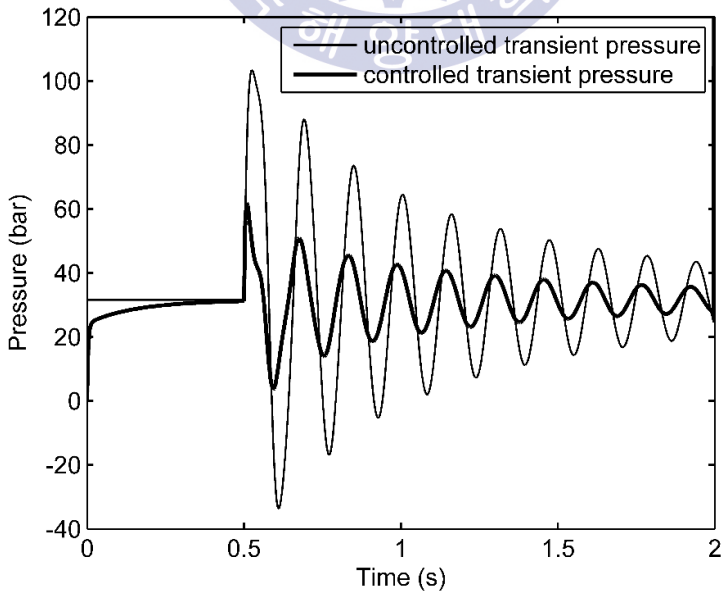

230

Fig. 48 Water hammer attenuation ability

From Fig. 48 one can observe that even though the transient pressure has the wave profile with positive and negative values, the system is regulated effectively. It is done as the result of the controller alternately closes and opens the bypass valve in a manner being opposite to the value of the transient pressure. Note that the vacuum pressure is harmful to the RO system in the aspect that it can cause erosion. Therefore, not only high positive pressure wave but also negative ones must be regulated.

The safest way is to include a pressure reducing valve (PRV) and a check valve at the discharge pipe. The PRV is to combine with the controlled bypass valve to optimally reduce the transient pressure. The check valve is to allow air to be sucked into the pipe under vacuum conditions. The combination between the controlled bypass and safety valves will give the best performance for the RO system.

4.8 Conclusion

In this section, the reverse osmosis system is carefully studied, including the nonlinear analysis, water hammer simulation, polarization concentration calculation. Based on the analysis, the mixed robust H_∞ and μ-synthesis controller are successfully designed and applied to control the RO system under uncertainties, disturbance and noises. Especially, water hammer is considered as a disturbance in the simulation. The simulation results show that the controller can eliminate 58% of transient pressure and keep the system safe, avoiding membrane spoiling, vapor cavitation and column separation. It also has good performance in dealing with uncertainties and noises.

Chapter 5. Robust gain scheduling control of activated sludge process

5.1 Introduction about activated sludge process

Nowadays, wastewater treatment (WWT) is a very active research area. Wastewater can originate from domestic, industrial, commercial or agricultural activities, surface runoff, stormwater, or from the combination of them. The most popular method in WWT plants is the activated sludge process (ASP), which directly removes the contaminants in the sewage through the biological process (Jeppsson, 1996). The basis of the process lies in maintaining a mixture of several microorganisms transforming the biodegradable pollutants (substrate) into new biomass. The ASP has the advantage of producing a high quality effluent for reuse purposes and maintenance costs. It is widely used by large cities and industrial zones where large volumes of wastewater must be highly treated economically. The process is also a good choice for small communities and facilities.

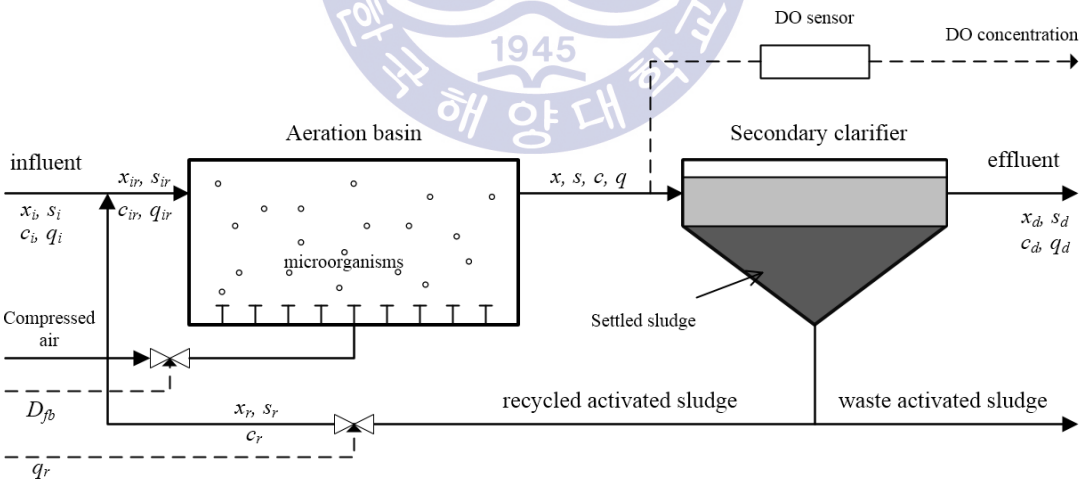

Fig. 49 Block diagram of an activated sludge process

The block diagram of an activated sludge process is illustrated in Fig. 49. The system includes an aeration basin with diffuser system, a secondary clarifier (settler)

where the solids settle and are separated from treated wastewater, and pumps for recycled and waste activated sludge.

The activated sludge consists of a mixed community of microorganisms, about 59% of bacteria and 5% of higher organisms such as protozoa, rotifers…The most predominant microorganisms are aerobic bacteria, which need oxygen for their operation. Rotifers and nematodes are most frequently found in systems with long aeration periods.

Amoeboid forms, the flagellates, and the ciliates are the most protozoans in a working sludge. Amoeboid predominates in young sludge. The flagellates are free-swimmers and predominate in light mixed liquors during high food condition. Their presence usually indicates poor effluent quality. Free-swimming ciliates predominate when the food to microorganisms (F:M) ratio decreases. Stalked ciliates predominate when there is an abundance of bacteria, giving good-quality effluent. Filamentous bacteria can cause the sludge no to settle properly, called bulking. These bacteria flourish when the excess sludge is not wasted at the proper rate.

In ASP, screened wastewater is mixed with varying amount of recycled sludge containing a high concentration of microorganisms taken from the secondary clarifier, and it becomes a product called mixed liquor. This liquor is then mixed in the aeration system including aeration basin and diffuser is to provide oxygen to the microorganisms. The aeration system makes wastewater pollutants contact with the microorganism to treat the wastewater and reduce the pollutants. The microorganisms are utilized to convert organic and certain inorganic matter from wastewater into cell mass. The microorganisms used oxygen to break down organic matter (food) for their growth and survival. Over time and as wastewater moves through the aeration basin, food (BOD) decreases and cell mass (mix liquor suspended solids-MLSS) increases. By the time the mixed liquor reaches the end of the basin, the microorganisms have used most of the organic matter to produce new cell mass.

In the bottom of the clarifier, the cell mass is settled to form a blanket of activated sludge, separated from clearer water. The settled sludge which is also called activated

sludge, is partly returned into the basin as RAS (returned activated sludge) and wasted to become fertilizer. The returned activated sludge is to provide a concentrated population of microorganisms back into the aeration basin. The effluent is sent out for further treatment if required.

In the biological reactor, the dissolved oxygen (DO) affects the production of the bioprocess. Too-high DO concentration will lead to a waste of energy, and lower efficiency of the procedure. In case of too-low DO concentration, the activity of microorganism is weak, which leads to the concentration of pollutant in the outflow is high or leftovers, and the outflow could not reach the standard level, and become stinking, harming the environment.

5.1.1 State variables

The state variables included in the ASM1 are the fundamental components that act upon the process, but they are not always measurable or interpretable in many practical applications. Therefore, some composite variables can be calculated from the state variables in order to combine them into forms that are typically measured in reality, such as COD (Chemical Oxygen Demand), TSS (Total Suspended Solids) and TN (Total Nitrogen).

It is known that the ASM1 model allows us to describe phenomena of organic matter and nitrogen removal. In fact, the main classification in the model state variables is in organic matter, expressed in terms of COD, and nitrogen compounds. In summary, the total COD balance of ASM1 is given in the following diagram:

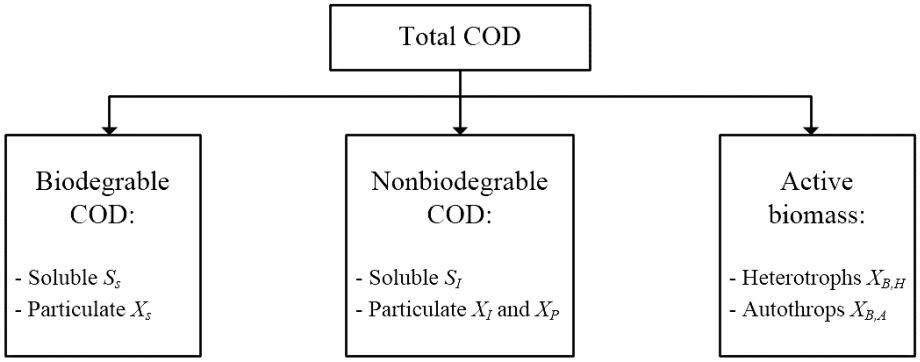

Fig. 50 COD components in ASM1 model

where the components are explained as follows:

S_S is the readily biodegradable solute. It is assumed to be made up of simple soluble molecules easily absorbed by the organisms and metabolized for energy and synthesis. X_S is the slowly biodegradable particulate, consisting of relatively complex molecules that require enzymatic breakdown prior to absorption and utilization.

S_I is the soluble inert and X_I the particulate inert. They are nonbiodegradable organic matter which are biologically inert and pass through the system without change in their form and concentration. S_I leaves the system through the secondary clarifier effluent, whereas X_I enmeshed in the settled sludge and leaves the system mainly through the removal of excess sludge.

$X_{B,H}$ is the heterotrophic biomass and $X_{B,A}$ is the autotrophic biomass. Heterotrophs are considered to growth in both anoxic and aerobic environments, whereas autotrophs can only growth in aerobic environment. Anoxic growth of X_{BH} and aerobic growth of X_{BA} are also known as denitrification and nitrification process, respectively.

X_P is an extra component included to take into account the inert particulate arising from cell decay.

The total Nitrogen compound in the system (Mulas, 2006) is given as:

$$TN = S_{NO} + S_{NH} + S_{ND} + X_{ND} + 0.086(X_{BH} + X_{BA}) + 0.06(X_P + X_I) \text{ [gN/m3]} \quad (124)$$

where S_{NO} is the nitrification of ammonia to nitrate nitrogen.

It is considered as a single step process. S_{NH} is the free and saline ammonia nitrogen. S_{ND} is the soluble biodegrable organic nitrogen and X_{ND} is the particulate biodegrable organic nitrogen.

Beside the state variables in the balances of total COD and nitrogen, the last two components described in the ASM1 are the dissolved oxygen concentration (S_O), and the alkalinity (S_{ALK}). The alkalinity does not affect any other processes in the model.

5.1.2 ASM1 processes

In ASP, two major types of microorganisms carry out the biological reactions: heterotrophs and autotrophs. The reactions taking place in the ASM1 was briefly described by Jeppsson (1996) as follow.

- The aerobic growth of heterotrophs exerts oxygen and results in a production of heterotrophic biomass. The growth rate depending on the concentration of both readily biodegradable substrate (S_S) and dissolved oxygen (S_O). This process is the main contributor to the production of new biomass and COD removal. Ammonia is used as nitrogen source for synthesis and is incorporated into the cell mass.

$$S_S + S_O + S_{NH} \rightarrow X_{BH} \quad (125)$$

- The anoxic growth of heterotrophs (denitrification) occurs in aqueous environment without dissolved oxygen with nitrate as the terminal electron acceptor, with S_S the substrate and resulting in heterotrophs biomass and nitrogen gas. Ammonia serves as nitrogen source for cell mass synthesis.

$$S_S + S_{NO} + S_{NH} \rightarrow X_{BH} \quad (126)$$

- Aerobic growth of autotrophs (nitrification): Ammonia is oxidized to nitrate via a single-step process (nitrification) resulting in production of autotrophic biomass and giving rise to an associated oxygen demand. Ammonia is also used as the nitrogen source for synthesis and incorporated into the cell mass. The process has a marked effect on the alkalinity (both from the conversion of ammonia into biomass and by the oxidation of ammonia to nitrate) and the total oxygen demand. The growth rate is very slow.

$$S_O + S_{NH} \rightarrow X_{BA} + S_O \quad (127)$$

- The decay of heterotrophs is modelled on the death-regeneration hypothesis proposed by Dold et al. (1980). The organisms die at a certain rate and a portion of the material is considered to be nonbiodegradable adding up to the X_P fraction. The remainder adds up to slowly biodegradable X_S. Organic nitrogen associated with X_S becomes available as particulate organic nitrogen X_{ND}.

$$X_{BH} \rightarrow X_P + X_S + X_{ND} \quad (128)$$

- The decay of autotrophs takes exactly the same modelling approach as the decay of the heterotrophs.

$$X_{BA} \rightarrow X_P + X_S + X_{ND} \quad (129)$$

- The ammonification of soluble organic nitrogen regards the conversion of S_{ND} into S_{NH} by a first order process mediated by active heterotrophs.

$$S_{ND} \rightarrow S_{NH} \quad (130)$$

- In the hydrolysis of entrapped organics, slowly biodegradable substrate trapped in the sludge mass is broken down, producing S_S for the organisms to growth. The process is modelled on the basis of reaction kinetics and occurs in aerobic and anoxic environments. The rate of hydrolysis is reduced under anoxic conditions compared to aerobic conditions by a factor $\eta h < 1$.

$$X_S \rightarrow S_S \tag{131}$$

- In the hydrolysis of entrapped organic nitrogen, X_{ND} is broken down to soluble organic nitrogen at a rate defined by the hydrolysis reaction for entrapped organics.

$$X_{ND} \rightarrow S_{ND} \tag{132}$$

It should be noted that S_I and X_I are not included in any conversion process. However, they must be considered because they are included in the COD computation. The processes happening in ASM1 model are summarized graphically in Fig. 51.

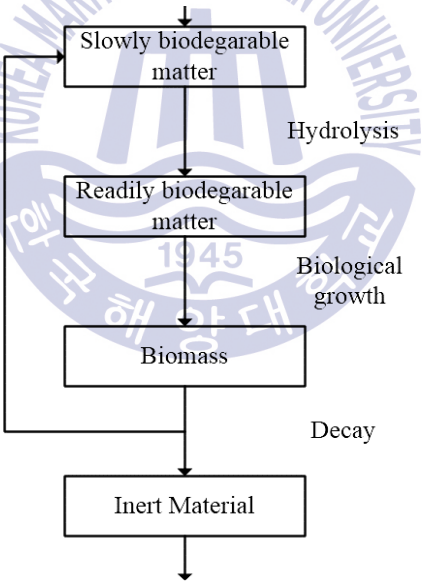

Fig. 51 Biological process renewal scheme

5.1.3 The control problem of activated sludge process

The real-time control of the activated sludge faces some complex problems due to the changing nature of the microbiological processes taking place in the bioreactor,

the variability of the input flow and concentration, and the complex interactions between different microorganisms.

Nevertheless, effective operation can be achieved by regulation of substrate and other product levels and the maintenance of DO in the process above minimum acceptable conditions. The system is multivariable in nature, however, taking into account the fact that the time scale in which the oxygen operates is in minutes while the substrate and other components evolve in the range of hours, it is possible to decompose the control problem in two different layers, isolating the DO control from the other ones that can be considered as disturbances.

As in the operation of ASP, oxygen is consumed by the microorganisms, it becomes necessary to add enough oxygen to the water in order to comply with the required minimum dissolved oxygen concentration (Roman *et al*., 2012). The DO concentration can be controlled by mean of aerators and RAS flow. The operation of aerators accounts for 50–90% of the total energy demand of a treatment plant. Aerators can be divided into two main types: mechanical aerators and fine-bubble diffused aeration, depicted in Fig. 52. The former is turbines moved by electrical motors that represent the main energy and maintenance costs. The latter uses compressor to inject air through submerged diffusers, which is short-called diffuser.

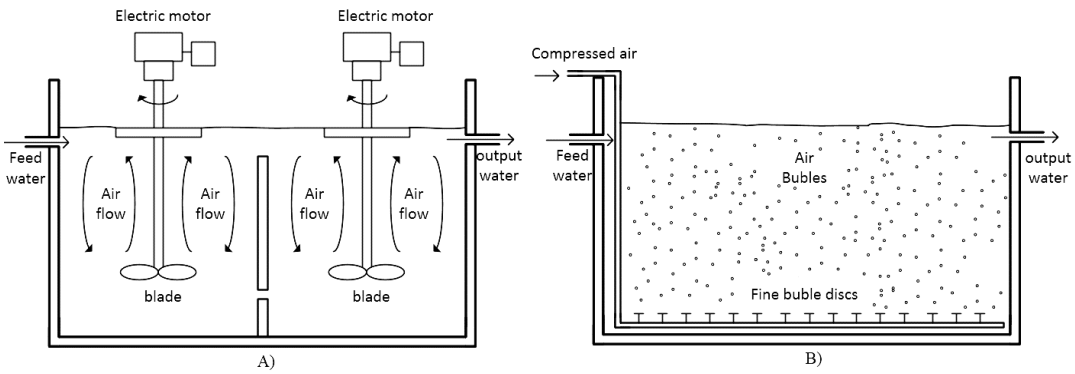

Fig. 52 Two main type of aerators. A) mechanical aerator and B) fine-bubble diffused aeration

Nowadays, the diffuser is used more popular in ASP since it is more efficiently in transfer oxygen. The measurement of the efficiency is expressed in term of standard aeration efficiency (SAE), which factors in pressure and efficiency of the mechanical equipment required to achieve a factor of oxygen transfer. The standard aeration efficiency is the amount of oxygen transferred per unit of energy consumed. Table 3 shows a brief summary of estimated SAE values for common types of aeration equipment used for biological treatment. Aerator types include high- and low-speed surface aerators, submersed jet aerators, fine-bubble disc diffusers, and high density low flux (HDLF) fine-bubble diffusers.

Table 3 Efficiency ranges for various types of aeration equipment (Tchobanoglous *et al*., 2003)

Type	SAE, kg O_2/kWh
Low-speed surface aerators	1.5-2.1
High-speed surface aerators	1.1-1.4
Submersed jet aerators	0.9-1.4
Fine-bubble diffusers, discs	2-7
HDLF fine-bubble diffusers	3-8

The RAS control is also very important to the ASP. The RAS distributes the required microorganisms for the aeration basin to work in proper condition. Since the RAS is pumped back to the aeration basin and eventually flows back to the clarifier, if the RAS flow is too high, it will eventually cause a high hydraulic load on the clarifier, preventing solids from settling. If the RAS flow is too low, the solid will build up and finally spill over the clarifier weirs into the effluent.

5.2 System modelling

ASM1 model is decentralized and nonlinear due to the presence of Monod kinetics equations. In order to design the controller, the process is modelled in the

compound form, which classifies all the components in three group: dissolved oxygen (DO), active microbial biomass (X) and the substrate (S). The compound model can be found in Moreno (1991), which is also based on ASM1. In this model, the DO time evolution is expressed by a dynamic mass balance where the oxygen accumulation equates the oxygen supplied by the aerators and the oxygen consumed by the microorganisms, given by the oxygen uptake rate, and a transport term:

$$\frac{dc}{dt} = K_{la} D_{fb} (c_s - c) - OUR - q(c - c_{ir}) / V \tag{133}$$

where

$$c_{ir} = (c_i q_i + c_r q_r) / q \tag{134}$$

c is the DO concentration in the reactor, c_s refers to the DO saturation level at the working temperature, D_{fb} indicates the aeration factor, OUR is the oxygen uptake rate, c_{ir} the DO concentration of the flow into the reactor, c_i the input flow concentration, c_r the sludge recycled flow concentration, q the input flow rate, q_r the sludge recycled flow rate, K_{la} dilution constant and V the reactor working volume. The DO concentrations in the input flow and the sludge recycled flow are considered constant: c_i = 2 mg/L and c_r = 0.

The aeration factor D_{fb}, is normalized varying between 0 and 1 representing the percent of maximum power of the fine-bubble diffused system.

The oxygen uptake rate (OUR) plays an important role in the dynamic of the DO as it represents the rate at which oxygen is consumed by the microorganisms, with one term proportional to the activity of the microorganisms and another one to its concentration:

$$\mathrm{OUR} = K_x \mu_s x s + K_0 x \tag{135}$$

Here x is the biomass concentration in the bioreactor (mg/L), s corresponds to the substrate concentration (mg/L) and the other parameters can be taken as constants with values $K_0 = 0.2 \times 10{-}3\ h^{-1}$, $K_x = 0.01$L/mg, $s = 4.079 \times 10^{-4\ h-1}$. The dynamics of the biomass x and substrate s in the bioreactor can be described by Cristea *et al*. (2011):

$$\frac{dx}{dt} = \mu_x \frac{s}{K_s + s} x - K_{dx} \frac{x^2}{s} + \frac{q}{V}(x_{ir} - x) \tag{136}$$

$$\frac{ds}{dt} = -\frac{1}{\alpha} \mu_x \frac{s}{K_s + s} x + K_{dx} \frac{x^2}{s} + K_{cs} x + \frac{q}{V}(s_{ir} - s) \tag{137}$$

where

$$x_{ir} = \frac{x_i q_i + x_r q_r}{q}, s_{ir} = \frac{s_i q_i + s_r q_r}{q}, q = q_i + q_r \tag{138}$$

And the simulation parameters are given in Table 4.

Table 4 ASP model parameters

Parameters	Value	Unit
K_o	$0.2x10^{-3}$	h^{-1}
K_x	0.01	L/mg
K_{dx}	10^{-5}	h^{-1}
K_{ds}	10^{-5}	h^{-1}
K_{cx}	$1.33x10^{-4}$	h^{-1}
K_{cs}	$0.27x10^{-4}$	h^{-1}
K_{la}	0.4	h^{-1}
μ_s	$4.079x10^{-4}$	h^{-1}
μ_x	0.1085	h^{-1}
α	0.5948	
V	5996	m^3
c_s	10.92	mg/L
ci	2	mg/L
cr	0	

5.3 Model linearization

ASP is complex and difficult to control. However, effective operation can be achieved by regulation of substrate and other product levels and the maintenance of DO in the process above minimum acceptable conditions. Therefore, the DO concentration is one of the principal parameters in an ASP. The amount of oxygen supplied for the aeration basin should be equal to the amount required by the microorganism to oxidize the organic material. Another potential measured variable is substrate concentration in the recycle stream. The system is multivariable in nature, however, taking into account the fact that the time scale in which the oxygen operates is in minutes while the substrate and other components evolve in the range of hours,

it is possible to decompose the control problem in two different layers, isolating the DO control from the other ones that can be considered as disturbances (Cristea *et al.*, 2011). In this study, DO is chosen as the control variable. DO is controlled by the fine-bubble diffused aeration system. In order to linearize the process as a controllable system, the recycle-stream flow rate is chosen as the second manipulated variable.

$$\begin{aligned} \dot{x}(t) &= f(x(t), u(t)) \\ y(t) &= g(x(t), u(t)) \end{aligned} \tag{139}$$

where $\dot{x} = \begin{bmatrix} c \\ x \\ s \end{bmatrix}, u = \begin{bmatrix} D_{fb} \\ q_r \end{bmatrix}, y = \begin{bmatrix} c \\ x \end{bmatrix}$

The Jacobian linearization is carried a little bit away from equilibrium point x^*(2, 2550, 8.4) and equilibrium input u^*(0.29, 1325), and equilibrium output y^*(2), the components of the linear system are calculated using:

$$A \triangleq \left.\frac{\partial f}{\partial x}\right|_{\substack{x=x^* \\ u=u^*}}$$

$$= \begin{bmatrix} -\frac{q_i}{5996} - 0.3368 & -2.3324\text{e-}04 & -0.0107 \\ 0 & -\frac{q_i}{5996} - 0.1852 & 8.9746 \\ 0 & -0.0578 & \frac{q_i}{5996} - 14.6034 \end{bmatrix} \tag{140}$$

$$B \triangleq \left.\frac{\partial f}{\partial u}\right|_{\substack{x=x^* \\ u=u^*}} = \begin{bmatrix} 3.356 & -0.0004 \\ 0 & 0.3976 \\ 0 & -0.001 \end{bmatrix} \tag{141}$$

$$C \triangleq \left.\frac{\partial g}{\partial x}\right|_{\substack{x=x^* \\ u=u^*}} = \begin{bmatrix} 1 & 0 & 0 \\ 0 & 1 & 0 \end{bmatrix} \tag{142}$$

$$D \triangleq \left.\frac{\partial g}{\partial u}\right|_{\substack{x=x^* \\ u=u^*}} = \begin{bmatrix} 0 & 0 \\ 0 & 0 \end{bmatrix} \tag{143}$$

where the symbolic partial matrices *A*, and *B* are given in Appendix D.

The scheduled parameter is the influent flow. It can be seen that the dynamics of the system changes depending on the parameter q_i in the matrix *A*. Through the linearization, the nonlinear system is transformed to a linear parameter-varying system, which is used to design a controller.

5.4 Robust gain-schedule controller design for activated sludge process

Conventional activated sludge is an aerobic process. The microorganism need free oxygen to convert food into energy for their growth. For optimal performance, it is very important to provide enough oxygen into the aeration tank. Typically, the dissolved oxygen (DO) concentration in aeration tank is kept stable at 2 mg/L. However, in waste water treatment plants, the influent water flow rate varies in large ranges during daily and weekly operation time. As seen in the Fig. 53 (Cristea *et al.*, 2011), the variation range of the feed water is from 900-2100 m^3/h. In this study, the feed water is let to be random number in the range of [500-6000]. This variation will cause big fluctuations in the DO concentration without an effective controller. The aim of the controller is to keep the DO concentration stable at 2 mg/l in spite of the variation of feed water.

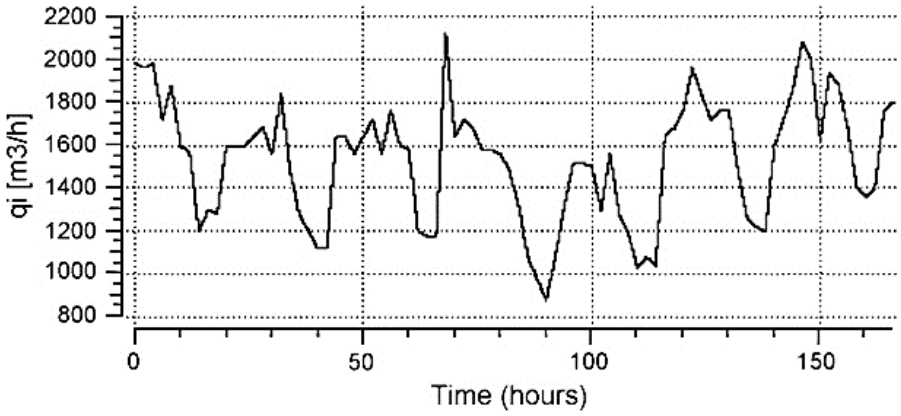

Fig. 53 The reference variation in influent flow (Cristea *et al*., 2011)

From the linearization, the linear system G is given under state space form as:

$$\begin{cases} \begin{bmatrix} \dot{c} \\ \dot{x} \\ \dot{s} \end{bmatrix} = A \begin{bmatrix} c \\ x \\ s \end{bmatrix} + B \begin{bmatrix} F_a \\ q_r \end{bmatrix} \\ y = C \begin{bmatrix} c \\ x \\ s \end{bmatrix} \end{cases} \tag{144}$$

where A, B, C are given in Eqs (139-142)

In this case, the feed water q_i is the schedule parameter. The feed water flow is easy to measure. Consequently, three parameter A_{11}, A_{22}, A_{33} in the state-space matrix A are variable in their ranges as follow:

$$-0.687 \le A_{11} \le -0.487;\ \ 0.115 \le A_{22} \le 0.749;\ \ 0.872 \le A_{33} \le 1.744 \tag{145}$$

From the state-space equation, it can be seen that the dynamics of the system is changed depend on the variation of q_i. The system is a LPV one and can be described using affine parameter-dependent representation as follow:

$$G(q_i)=\begin{cases} E(q_i)\dot{x}=A(q_i)x+Bu \\ y=Cx \end{cases} \tag{146}$$

where $A(q_i)$ and $E(q_i)$ are affine matrices and $q_i = (\, q_{i1}, q_{i2}, q_{i3}) = (\, A_{11}, A_{22}, A_{33})$ are real parameters based on A_{11}, A_{22}, A_{33}, respectively.

The LPV system $G(q_i)$ then can be expressed in the form:

$$G(q_i)=\left[\begin{array}{c|c} A(q_i)+jE(q_i) & B \\ \hline C & 0 \end{array}\right]=S_0+\sum_{j=1}^{3} q_{ij}S_j,\; S_j=\left[\begin{array}{c|c} A_j+jE_j & B_j \\ \hline C_j & D_j \end{array}\right] \tag{147}$$

where

$$S_0=\left[\begin{array}{ccc|cc} 0 & -2.332\text{x}10^{-4} & -0.01 & 3.356 & -4.2\text{x}10^{-4} \\ 0 & 0 & 8.974 & 0 & 0.0397 \\ 0 & -0.0578 & 0 & 0 & -0.001 \\ \hline 1 & 0 & 0 & 0 & 0 \\ 0 & 1 & 0 & 0 & 0 \end{array}\right] \tag{148}$$

$$S_1 = \left[\begin{array}{ccc|cc} -1 & 0 & 0 & 0 & 0 \\ 0 & 0 & 0 & 0 & 0 \\ 0 & 0 & 0 & 0 & 0 \\ \hline 0 & 0 & 0 & 0 & 0 \\ 0 & 0 & 0 & 0 & 0 \end{array}\right], \; S_2 = \left[\begin{array}{ccc|cc} 0 & 0 & 0 & 0 & 0 \\ 0 & -1 & 0 & 0 & 0 \\ 0 & 0 & 0 & 0 & 0 \\ \hline 0 & 0 & 0 & 0 & 0 \\ 0 & 0 & 0 & 0 & 0 \end{array}\right]$$

$$S_3 = \left[\begin{array}{ccc|cc} 0 & 0 & 0 & 0 & 0 \\ 0 & 0 & 0 & 0 & 0 \\ 0 & 0 & -1 & 0 & 0 \\ \hline 0 & 0 & 0 & 0 & 0 \\ 0 & 0 & 0 & 0 & 0 \end{array}\right] \tag{149}$$

The above representation is equal to:

$$G(q_i) = S_0 + A_{11}S_1 + A_{22}S_2 + A_{33}S_3 \tag{150}$$

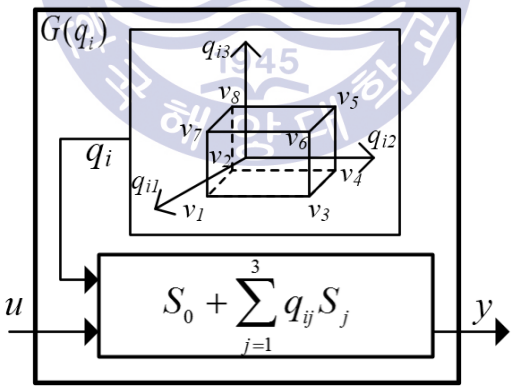

Fig. 54 The affine parameter-dependent representation of the activated sludge system

The robust gain scheduled controller design for the ASP from now become similar to H_∞ controller synthesis. From the block diagram of the control system as in Fig. 55, it's necessary to create a generalized plant P including the LPV system G, the gain scheduled controller K and weighting functions. The weighting functions are

chosen to scale the respective signals depending on the control goals. In this study, control error and control effort are weighted and chosen to be included in the optimization so that the control system satisfies the desired DO concentration with minimum energy consumption.

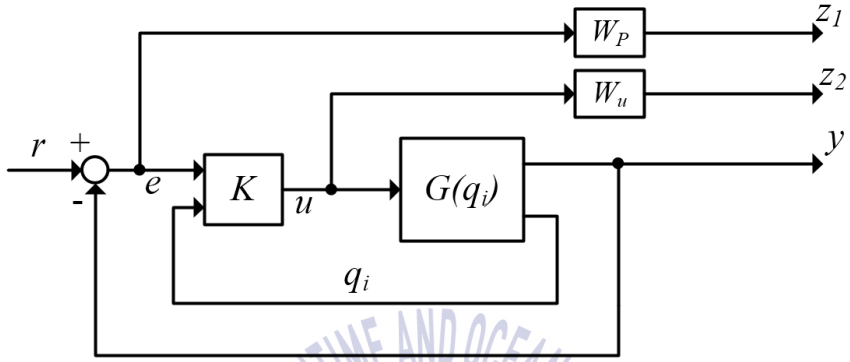

Fig. 55 Block diagram of the control system

From the control block diagram, a generalized plant P is created by grouping the LPV system $G(q_i)$, the weighting functions W_p and W_u, and the external factor such as reference r and noise n. The generalized plant is illustrated as the grey block in Fig. 56. It is further written as in Eq. (151).

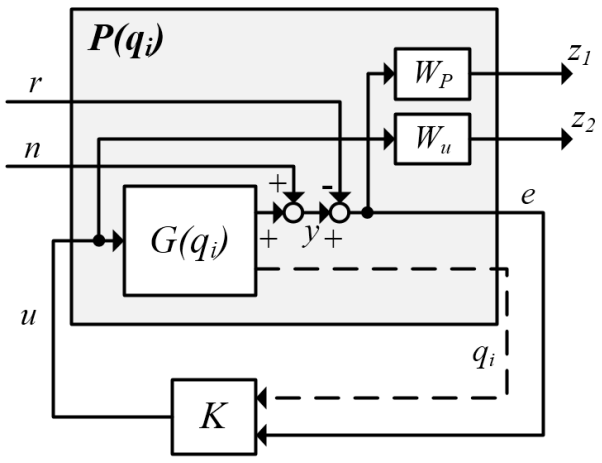

Fig. 56 The parameterized generalized plant P

$$\begin{bmatrix} z_1 \\ z_2 \\ \hline e \end{bmatrix} = \underbrace{\left[\begin{array}{cc|c} -W_p & W_p & -W_pG \\ 0 & 0 & W_u \\ \hline -I & I & -G \end{array}\right]}_{P} \begin{bmatrix} n \\ r \\ \hline u \end{bmatrix} = \left[\begin{array}{c|c} P_{11} & P_{12} \\ \hline P_{21} & P_{22} \end{array}\right] \begin{bmatrix} n \\ r \\ \hline u \end{bmatrix} \tag{151}$$

In order to formulate the robust criterion for controller design, the grouping of the generalized plant and the controller K is carried out by a lower linear fractional transformation (LFT) as depict in Fig. 57. The LFT is further express as follow:

$$F_l(P,K) = P_{11} + P_{12}K(I - P_{22}K)^{-1}P_{21} = \begin{bmatrix} -W_pS_o & W_pS_o \\ -W_uKS_o & W_uKS_o \end{bmatrix} \tag{152}$$

where $S_o = (I + GK)^{-1}$ is the output sensitivity function, and it has the relation with the complementary sensitivity function $T_o = GK(I + GK)^{-1}$ such that $S_o + T_o = I$

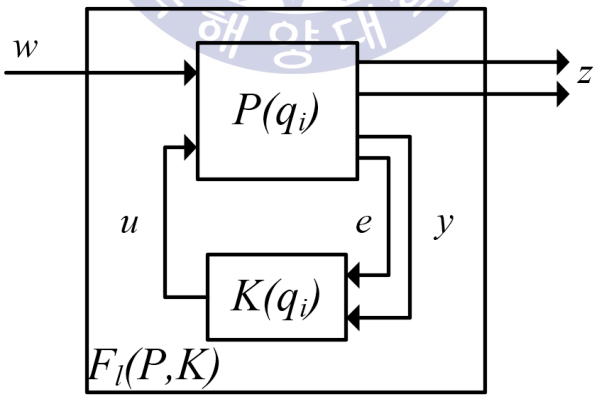

Fig. 57 Lower LFT configuration

In term of control synthesis, all these specifications can be summarized by the following optimal problem: find the weighting functions and the gain scheduled controller K s.t.

$$\left\| \begin{matrix} W_P S \\ W_u KS \end{matrix} \right\|_\infty \le 1 \tag{153}$$

which is called an S/KS mixed sensitivity problem. The problem is equal to solve the LFT of the generalized system P and the controller K (see Fig. 57) s.t.

$$\left\| F_l(P,K) \right\|_\infty \le 1 \tag{154}$$

In the routine of controller design, the weighting functions are chosen as follow to optimize the problem:

$$W_P = \frac{15}{s+10^{-2}}, W_u = \frac{5}{s+0.2} \tag{155}$$

Then the chosen weighting functions are applied at the final stage to synthesize a gain scheduled controller K which is optimized for each value of the scheduled parameter $q_{i,}$ and it can auto tune whenever q_i varies in its range. At any possible value of q_i, the controller has it respective dynamics and the optimal problem is still satisfied. The gain scheduled controller therefore is not as complex as H_∞ robust controller which is synthesized for entire set of parameter uncertainty simultaneously. Consequently, the former is more focus and effective for the control system.

In this study, $\left\| \begin{matrix} W_P S \\ W_u KS \end{matrix} \right\|_\infty = 0.59 < 1$, which is very good value since there will be a large margin before the control system comes to its worst case.

5.5 Simulation result and discussion

It is known that the DO concentration in ASP should be kept stable at 2 mg/l to guarantee the best performance for the system. Too high DO concentration leads to a waste of energy and too low DO concentration will weaken the activity of the microorganism and the input waste water is not enough treated, resulting in a low-quality effluent.

In Cristea *et al*. (2011), three motors were chosen as the mechanical aerators. They are scheduled by a hybrid MPC to alternately operate in on/off manner to keep DO concentration at 2 mg/l and minimize the consumed energy. The result in Fig. 58 shows that even the controller can keep the DO concentration above 2 mg/L, there are still a lot of fluctuation. For more stringent output water, the above controlled system is not satisfied. It also means the energy consumption is not minimized.

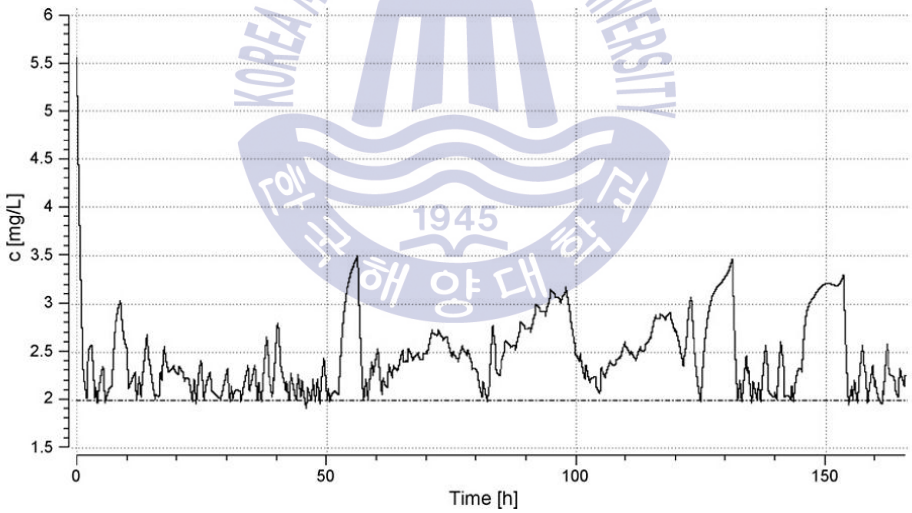

Fig. 58 Variant DO concentration at effluent in Cristea *et al*. (2011)

In this study, the fine-bubble diffuser continuously discharges compressed air into the aeration tank. The air flow and RAS flow are controlled by the gain scheduled controller so that the DO concentration is kept stable at 2 mg/l under large variations of the input water flow. To illustrate the ability of the gain scheduled controller in dealing with parameter variation (q_i in this study), the simulation was carried on using 50 random values of feed water flow q_i. Fig. 59 shows that all the sample

responses have rising time less than 0.15 h = 9 min and there is no considered difference between them. The steady state errors are zeros. This is a very good result since the output water's quality is guaranteed in the best condition. It proves that the designed controller can handle the long-range variation of the feed water.

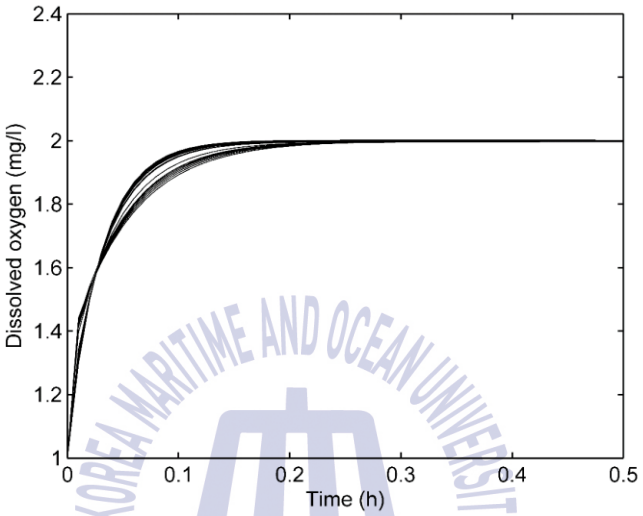

Fig. 59 The set of transient responses of the control ASP under parameter variation

Since the controller dynamics is changing according to the parameter variation, one of the advantages of the gain scheduled controller is its ability to be applied for nonlinear system. In this study, designer built a nonlinear model of ASP in Simulink environment to test the control system under influent variation. Two responses are plotted in Fig. 60. The firs is the DO response of the system without the controller and the second is the one controlled by the designed controller. The result shows that without the controller, the DO concentration is varied in big magnitudes due to influent changes. Being controlled by the gain scheduled controller, the DO concentration is kept stable at exactly 2 mg/l and the rising time is very short with a slight overshoot. It proves that the achieved controller can be applied for the real nonlinear ASP.

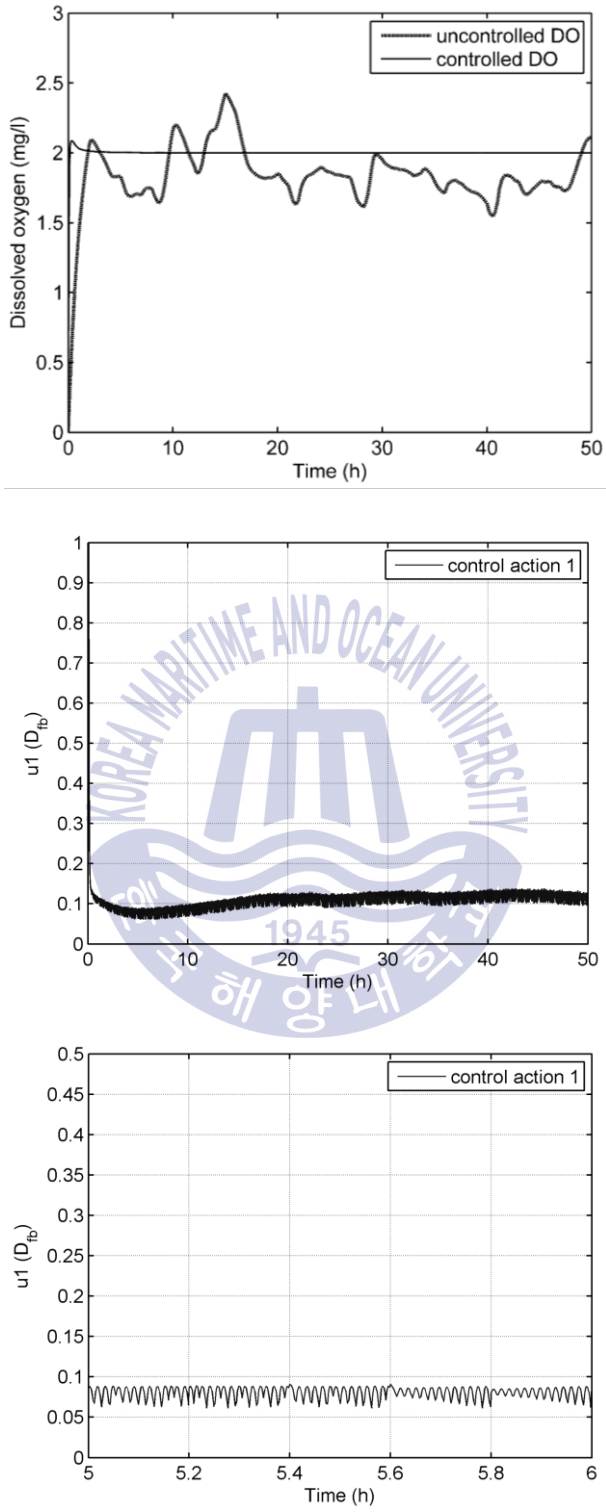

Fig. 60 Nonlinear response of DO concentration (up), control action u_1 (middle) and magnified u_1 (down)

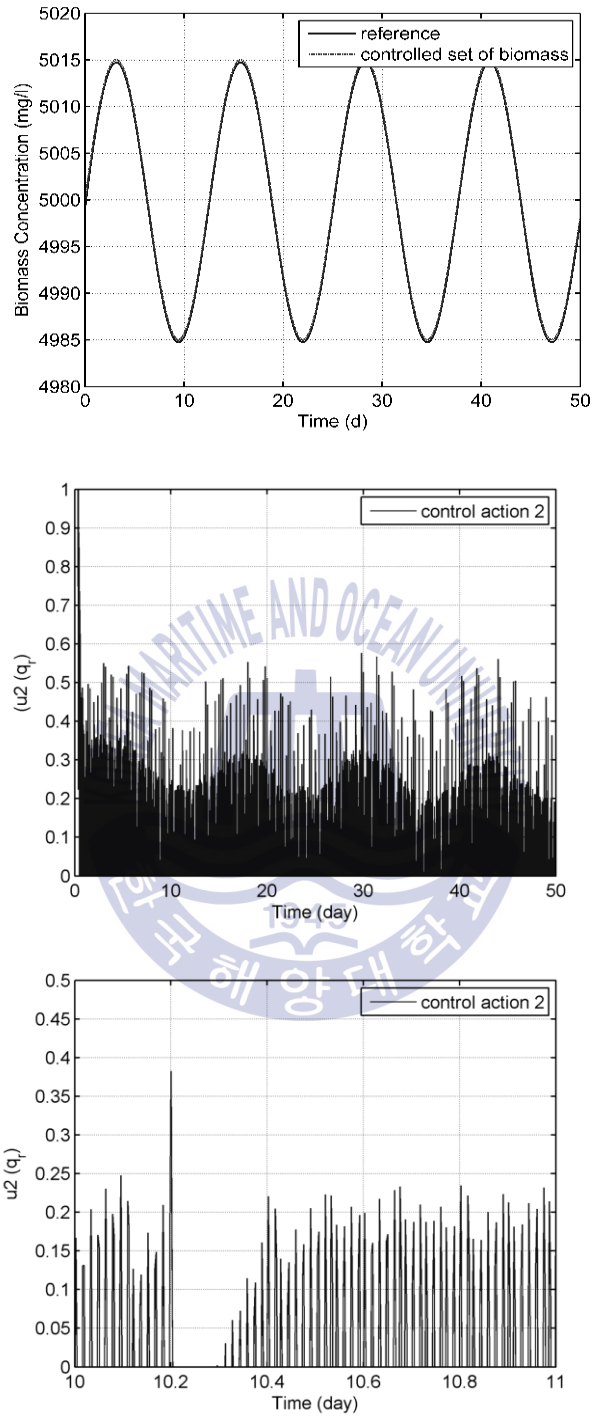

Fig. 61 Nonlinear response of biomass concentration (up), control action u_2 (middle) and magnified u_2 (down)

At high frequency ranges where the measurement noises happen, the controller is designed so that the value of *KS* is small to reduce the effects of noises. Therefore, beside the ability to eliminate disturbance caused by parameter uncertainty, the controller can also attenuate sensor noises. In order to illustrate this ability, white noise is introduced into the system as in Fig. 61. Simulation result shows that the response is fluctuated but in very slight magnitudes compared to the noise magnitudes. It can be conclude that most of noises are attenuated and the control system is unsusceptible to noise.

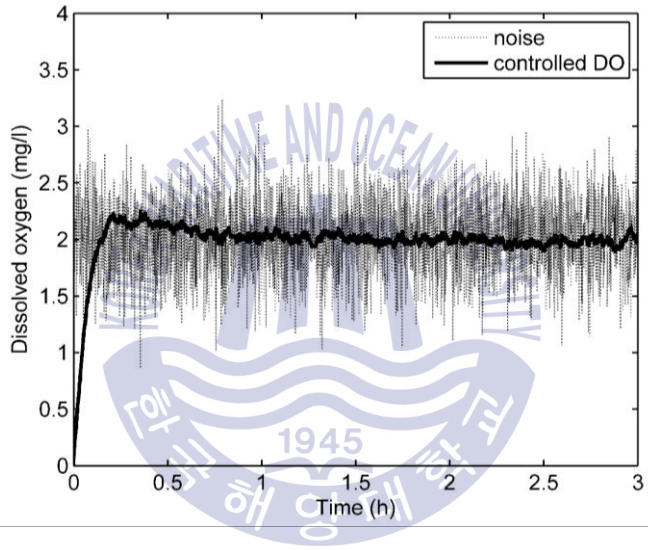

Fig. 62 Noise response of nonlinear controlled system

5.6 Conclusion

In this section, the ASP is linearized as an LPV system, due to large variation in the influent flow rate. A robust gain scheduling controller is successfully designed to regulate the DO concentration at 2 mg/L under the parameter variation and noise. The controller is tested for both the linearized and nonlinear system. The simulation results show that the controller is very active and can help to optimize the energy consumption for the ASP.

Chapter 6. Observer-based loop-shaping control of anaerobic digestion

6.1 Introduction

The sludge rejected from activated sludge process is not safe for the environment. It needs further treatment. The most widely employed method for sludge treatment is anaerobic digestion (AD). AD is a well-known process for renewable energy production. In this process, about 40% to 60% of the organic solids is decomposed into biogas. The chemical composition of the gas is 60-65% methane (CH4), 30-35% carbon dioxide (CO2), plus small quantities of H2, N2, H2S and H2O. Of these, methane is the most valuable because it is a hydrocarbon fuel (giving 36.5 MJ/m3 in combustion).The remainder is dried and becomes fertilizer or residual soil-like material. The process happens in the environment without oxygen, that's why it is called anaerobic dioxide.

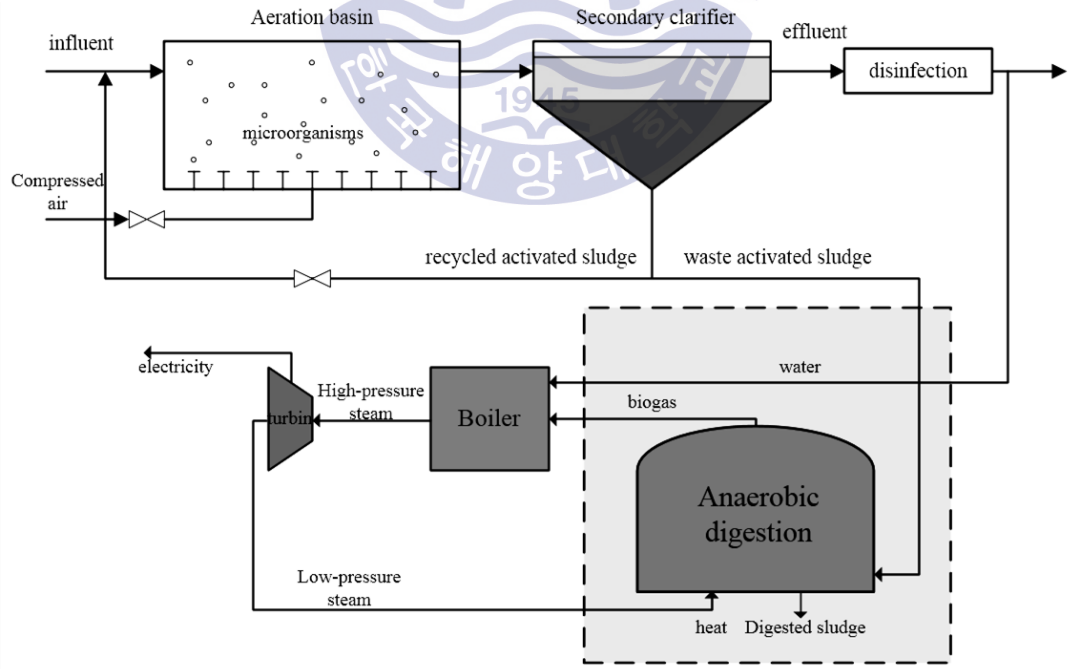

Fig. 63 The diagram of activated sludge and anaerobic digestion system

6.1.1 Control problem in anaerobic digestion

Controlled inputs or manipulated variables in automatic control of AD process should have quick and significant impacts on the process. In AD process, depend on the application, control variables can be methane flow rate, chemical oxygen demand (COD) concentration in the effluent or volatile fatty acid (VFA) while feeding rate is the most common manipulated variable. By using feeding rate as manipulate variables, it is possible to simultaneously regulate the retention time and organic loading rate, allowing microbial communities in the system to adapt to some disturbances. The feeding rate can be represented by dilution rate which is the ratio between the flow rate of the substrate and liquid volume of the digester.

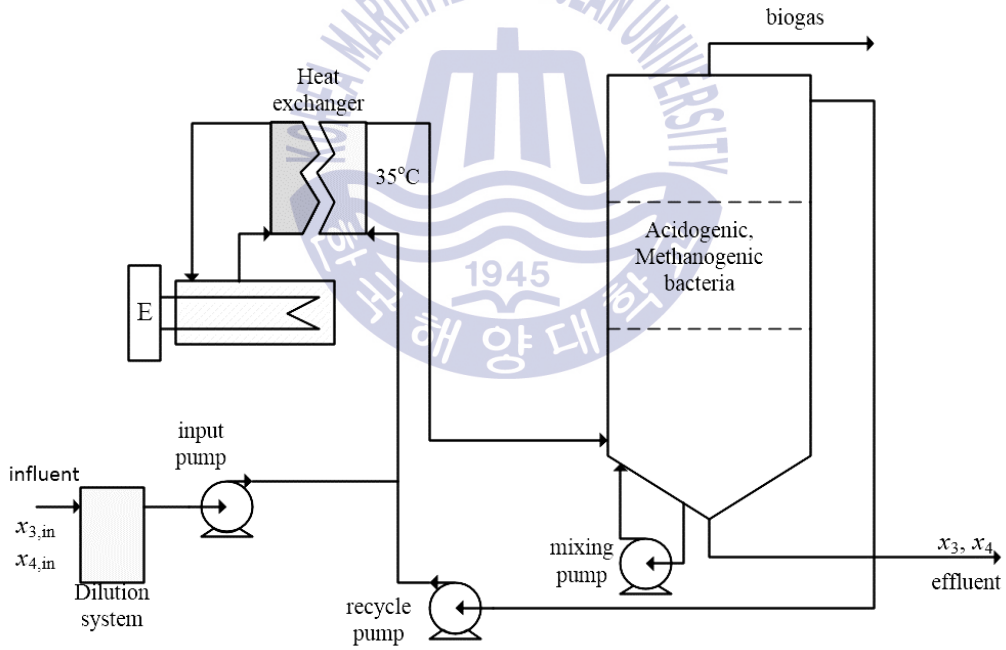

Fig. 64 The diagram of an anaerobic digestion system.

For industrial scale AD plants, basic parameters such as pH, temperature, mixed liquor level, gas pressure, mixed liquor and biogas flow rate, should be monitored on-line. However, in fact, on-line monitoring was not performed in many industrial

scale plants. According to Spanjers and Lier (2006), only 10% among 400 industrial scale AD plants worldwide are equipped with on-line analysis of COD, TOC, VFAs, alkalinity, and biogas composition. It could be explained from the complexity in operation and maintenance of the advanced analyzers or sensors. Additionally, high capital and operation costs of these state-of-the art devices make it economically unattractive for AD operators to embrace the technology.

For plants with on-line monitoring systems, real-time control was rare and even the periodical data analysis was skipped. For the plants with real-time controllers, the control system was simple, time-based, equipped with on–off controller.

Therefore, in this section, a robust loop-shaping controller is designed based on a robust observer to control the COD concentration under disturbances and to observe VFA, in case of there is no equipment to measure this parameter.

6.2 System modelling

The system is modelled based on the fourth-order model relating the mass balances of acidogenic, methanogenic bacteria, chemical oxygen demand and volatile fatty acids (Estrella *et al.* 2013) as follow:

$$\dot{x}_1 = (\mu_1(x_3) - \alpha D)x_1 \tag{156}$$

$$\dot{x}_2 = (\mu_2(x_4) - \alpha D)x_2 \tag{157}$$

$$\dot{x}_3 = (x_{3,in} - x_3)D - k_1\mu_1(x_3)x_1 \tag{158}$$

$$\dot{x}_4 = (x_{4,in} - x_4)D + k_2\mu_1(x_3)x_1 - k_3\mu_2(x_4)x_2 \tag{159}$$

$$\mu_1(x_3) = \mu_{1\max}\frac{x_3}{x_3 + K_{s1}}$$
$$\mu_2(x_4) = \mu_{2\max}\frac{x_4}{x_4 + K_{s2} + \left(x_4 / K_{I2}\right)^2} \tag{160}$$

where x_1 represents the acidogenic bacteria concentration (g/L); x_2 is the methanogenic bacteria concentration (g/L); x_3 the chemical oxygen demand (COD), x_4 the volatile fatty acids concentration (VFA, mmol/L), $x_{3,in}$ and $x_{4,in}$ denote the inlet concentrations, $\mu_1(x_3)$ and $\mu_2(x_4)$ are the growth rates of acidogenic and methanogenic bacteria, respectively.

Table 5 Parameter of the AD system.

Parameter	Value	Unit
α	0.5	
k_1	42.14	
k_2	116.5	mmol/g
k_3	268	mmol/g
μ_{1max}	0.05	h^{-1}
μ_{2max}	0.031	h^{-1}
K_{S1}	7.1	g/L
K_{S2}	9.28	mmol/L
K_{I2}	16	mmol/L
$x_{3,in}$	16	g/L
$x_{4,in}$	68.78	g/L

The system is highly nonlinear and very difficult to be controlled due to the interconnection between the state variables. From the nonlinear model, the system is linearized using the parameter in Table 5 to achieve a LTI system, based on which the control synthesis is designed. The manipulated variable is the dilution D, which is performed by adding water to influent sludge. The controlled variable is the COD concentration, and the observed state is VFA concentration.

6.3 Controller design

6.3.1 $H\infty$ loop-shaping controller

In the robust control approach, the control objective is to stabilize not only the nominal plant G, but also the set of perturbed plant $G_{p.}$ using a dynamic feedback controller K. A loop-shaping technique allows the system designer to specify closed-loop objectives by shaping the loop gains. If the function W_1 and W_2 are the pre- and post compensators, respectively, then the shaped plant with its coprime factorization is given by:

$$G_s(s) = W_2(s)G(s)W_1(s) = M_s^{-1}N_s \tag{161}$$

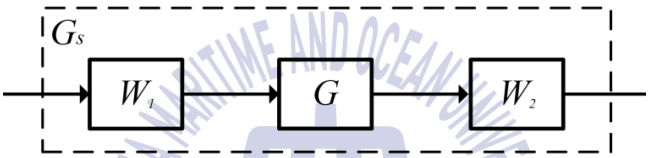

Fig. 65 Shaped close-loop system.

where W_2 is the identity matrix and W_1 is a diagonal matrix which is used to shape the frequency response of the nominal model and to specify the closed-loop behaviors. Typically, the loop gains have to be large at low frequencies for good disturbance rejection at both the input and output of the plant, and small at high frequencies for noise rejection. In addition, the desired opened-loop shapes are chosen to be approximately -20 dB/decade roll-off around the crossover frequency to achieve desired robust stability, gain and phase margins, overshoot and damping.

In this section, the shaping functions W_1 is chosen as:

$$W_1(s) = \left(\frac{s+20}{s+10^{-3}} \right)^2 \tag{162}$$

So that the shaped plant has the shape as in Fig 66. Since the system operates in very low frequency range, it is shaped only in this frequency to eliminate the effect of disturbance.

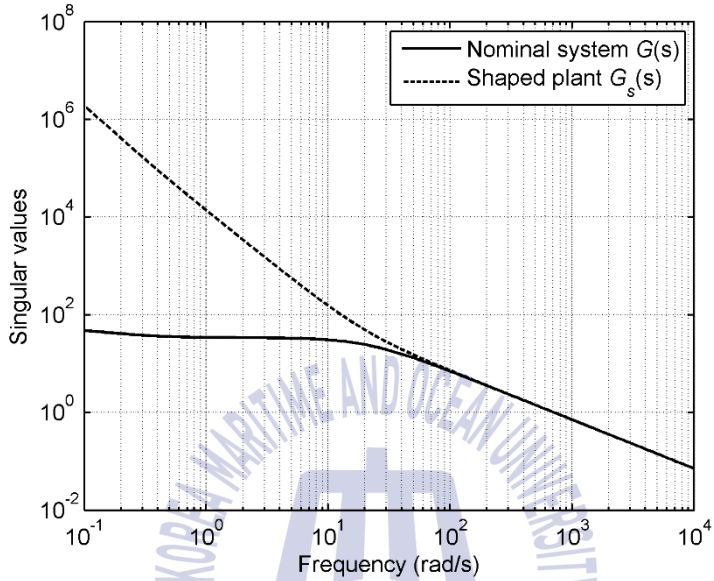

Fig. 66 The singular value plot of the nominal and shaped loop

6.3.2 Coprime factor uncertainty

Robust stability bounds in terms of the H_∞ norm are conservative if there are many perturbation blocks at different position in AD system. To get tighter bounds for AD system, the uncertainties are described using the left coprime factorization (LCF) (McFarlane and Glover 1992) as depicted in the dashed rectangle in Fig. 67. In this structure, uncertainty blocks enter and exit from the same position. Therefore, they can be combined to form a full perturbation block.

Note that in the coprime factor uncertainty (CFU) description in Fig. 67, there is no weighting block. The description is based on addictive perturbations to the LCF. The robust stabilization problem is to stabilize the set of perturbed plants:

$$G_p = (M_s + \Delta_M)^{-1}(N_s + \Delta_N), \quad \left\| \begin{bmatrix} \Delta_N & -\Delta_M \end{bmatrix} \right\|_\infty \le \varepsilon \tag{163}$$

where $M_s^{-1}N_s = G_s$ is the normalized LCF of the shaped plant, ε is the stability margin, M_s, N_s, Δ_M and $\Delta_N \in \Re H_\infty$.

6.3.3 Control synthesis

For stringent tracking problem in AD system, one-degree-of-freedom controller will not be sufficient to meet both requirements for reference tracking and disturbance rejection. Hence, a dynamic 2-DOF controller is proposed using Hoyle et al. (1991) approach. The 2-DOF feedback control scheme is depicted schematically in Fig. 67.

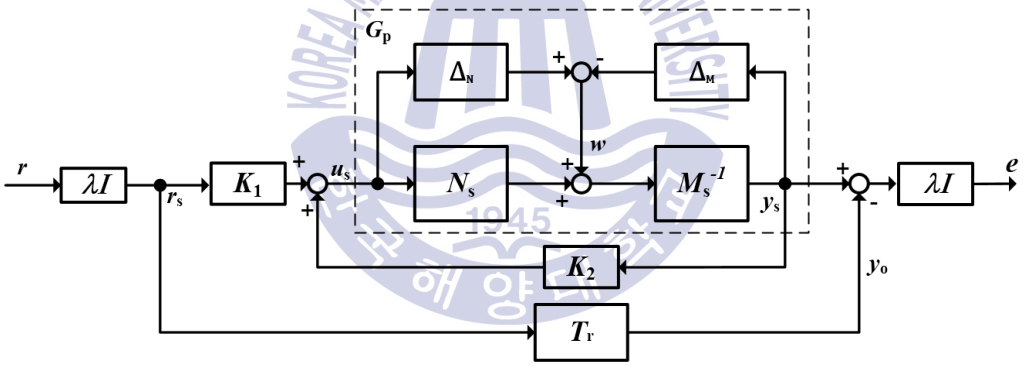

Fig. 67 2-DOF design configuration with coprime plant perturbation.

The 2-DOF controller includes the feedback part K_2 that satisfies the requirements of internal and robust stability, disturbance rejection, measurement noise attenuation and sensitivity minimization; and the pre-compensator K_1 that optimizes the response of the overall system to the command input such that the output of the system would be close to that of a chosen ideal system T_r. More explicitly, T_r represents some desired closed-loop transfer function between reference input and output

The shaped plant is supposed to be strictly proper, with a stabilizable and detectable state-space realization

$$G_s = \left[\begin{array}{c|c} A_s & B_s \\ \hline C_s & 0 \end{array}\right] \tag{164}$$

And the desired (reference) closed-loop transfer function

$$T_r = \left[\begin{array}{c|c} A_r & B_r \\ \hline C_r & 0 \end{array}\right] \tag{165}$$

To form the standard control configuration, a generalized plant P is defined as:

$$\begin{bmatrix} u_s \\ y_s \\ e \\ \hline r_s \\ y_s \end{bmatrix} = \underbrace{\left[\begin{array}{cc:c} 0 & 0 & I \\ M_s^{-1} & 0 & G_s \\ \lambda M_s^{-1} & -\lambda^2 T_r & \lambda G_s \\ \hdashline 0 & \lambda I & 0 \\ M_s^{-1} & 0 & G_s \end{array}\right]}_{P} \begin{bmatrix} w \\ r \\ \hline u_s \end{bmatrix} \tag{166}$$

P is further calculated as:

$$P = \left[\begin{array}{cc|cc:c} A_s & 0 & 0 & Z_c C_s^T & B_s \\ 0 & A_r & B_r & 0 & 0 \\ \hline 0 & 0 & 0 & 0 & I \\ C_s & 0 & 0 & I & 0 \\ \rho C_s & -\rho^2 C_r & 0 & \rho I & 0 \\ \hline 0 & 0 & \rho I & 0 & 0 \\ 0 & 0 & 0 & I & 0 \end{array}\right] \triangleq \left[\begin{array}{c|cc} A & B_1 & B_2 \\ \hline C_1 & D_{11} & D_{12} \\ C_2 & D_{21} & D_{22} \end{array}\right] \tag{167}$$

The 2-DOF loop-shaping controller in Fig. 67 can be separated into a state estimator (observer) and a state feedback controller. According to Walker (1996),

the state feedback stabilizing controller K(s) satisfying $\|F_{\mathrm{L}}(P,K)\|_{\infty}<1$ has the following equations:

$$K(s):\begin{cases}\dot{\hat{x}}_s = A_s\hat{x}_s + H_s(C_s\hat{x}_s - y_s) + B_s u_s \\ \dot{x}_r = A_r x_r + B_r r \\ u_s = -B_s^T X_{\infty 11}\hat{x}_s - B_s^T X_{\infty 12} x_r\end{cases} \tag{168}$$

where $X_{\infty 11}$ and $X_{\infty 12}$ are elements of

$$X_{\infty} = \begin{bmatrix} X_{\infty 11} & X_{\infty 12} \\ X_{\infty 21} & X_{\infty 22}\end{bmatrix} \tag{169}$$

in which $X_{\infty} \geq 0$ is a solution to the following algebraic Riccati equation:

$$X_{\infty}A + A^T X_{\infty} + C_1^T C_1 - \bar{F}^T(\bar{D}^T \bar{J}\bar{D})\bar{F} = 0 \tag{170}$$

where

$$\bar{F} = (\bar{D}^T \bar{J}\bar{D})^{-1}(\bar{D}^T \bar{J}C + B^T X_{\infty}) \tag{171}$$

$$\bar{D} = \begin{bmatrix} D_{11} & D_{12} \\ I_w & 0\end{bmatrix} \tag{172}$$

$$\bar{J} = \begin{bmatrix} I_z & 0 \\ 0 & \gamma^2 I_w\end{bmatrix} \tag{173}$$

The observer-based control system is depicted in Fig. 68.

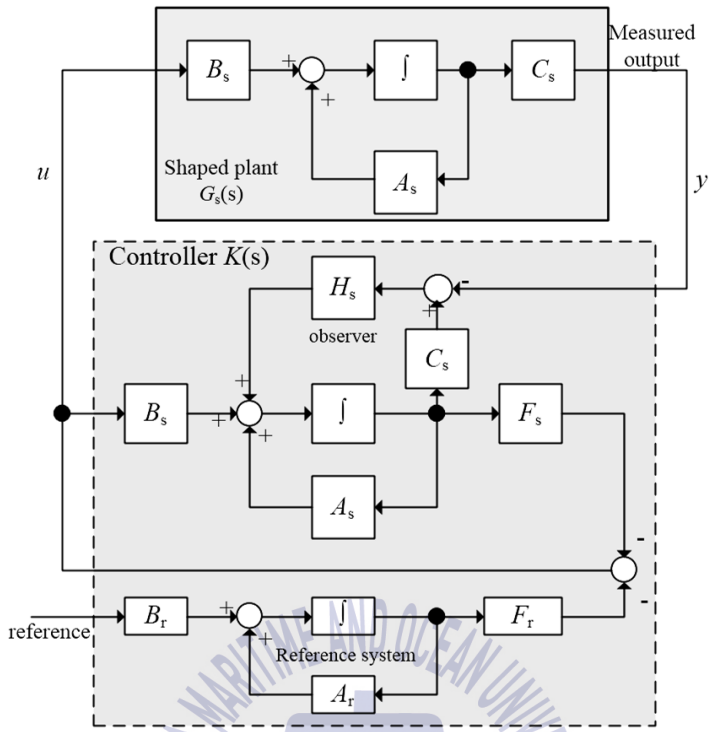

Fig. 68 Structure of the two degree-of-freedom H_∞ loop-shaping controller.

Noting that

$$F_s \triangleq B_s^T X_{\infty 11} \tag{174}$$

$$F_r \triangleq B_s^T X_{\infty 12} \tag{175}$$

And the observer is calculated by solving following equation:

$$H_s = -Z_s C_s^T \tag{176}$$

where Z_s is the appropriate solutions to the generalized algebraic Riccati equation:

$$(A - BS^{-1}D^{T}C)Z + Z(A - BS^{-1}D^{T}C)^{T} - ZC^{T}R^{-1}CZ + BS^{-1}B^{T} = 0 \quad (177)$$

with

$$R = I + DD^{T}, \; S = I + D^{T}D \quad (178)$$

6.4 Simulation result

Fig. 69 shows the response of the COD concentration under the effect of disturbance. It can be seen that the COD concentration has only some slight changes due to large disturbances. It means the COD is kept stable at desired value, despite the large disturbances. The variation in COD is also eliminated whenever the disturbance values are stable. The control action is also plotted in this figure, which shows some changes to bring the COD back to the desired value.

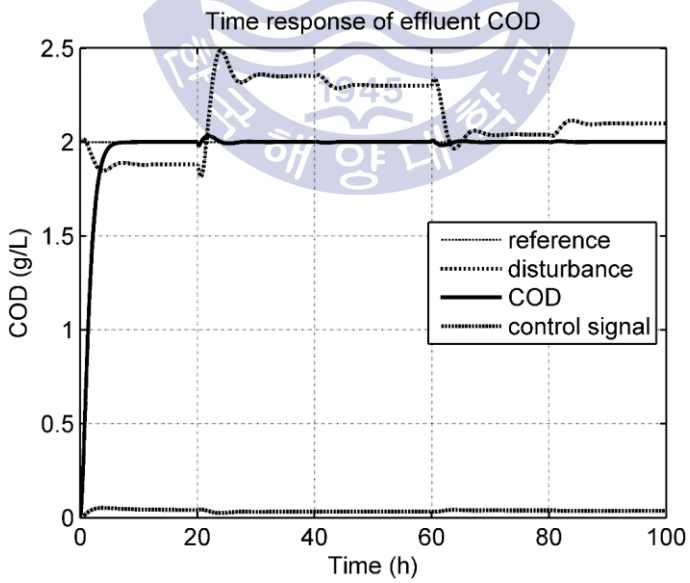

Fig. 69 The response of COD concentration under disturbance

Fig. 70 shows the performance of the observer on the estimation of VFA state and Fig. 71 shows the magnification at initial time of Fig. 70. Assuming that the initial value of the real VFA is 60 mmol/l and that of the estimated VFA is 30 mmol/l. It can be observed that the estimated state can track the real state in very short time, in other words, immediately. The estimated error is 0 and the tracking is perfect.

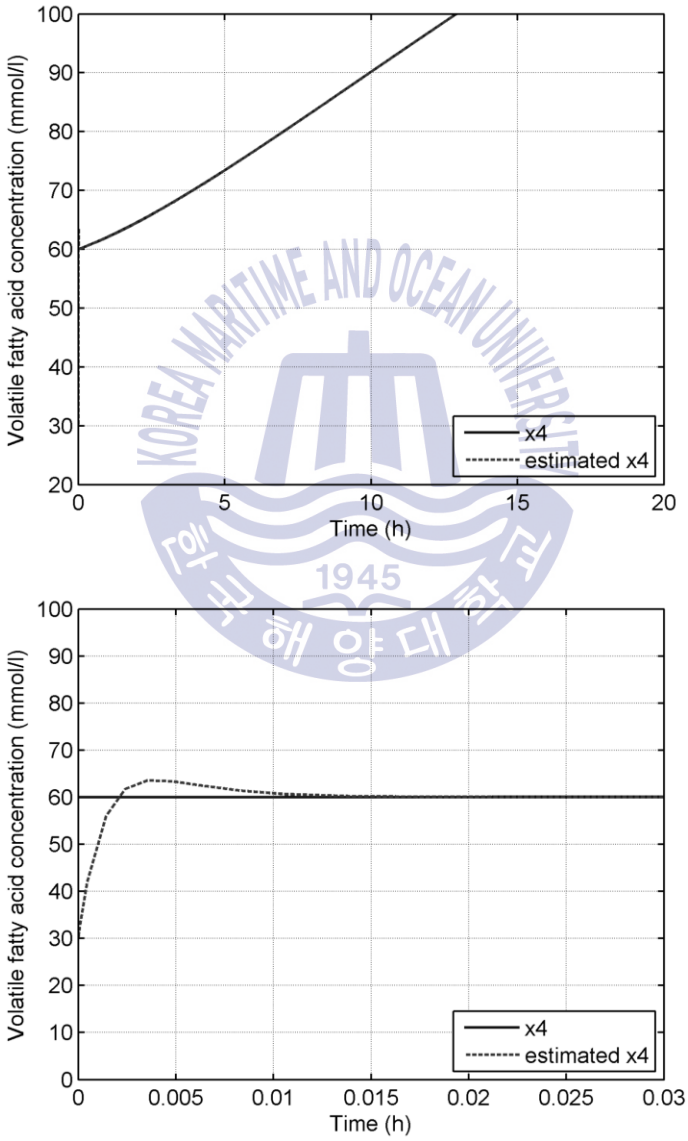

Fig. 70 The VFA estimation (upper) and its magnification (lower)

6.5 Conclusion

By using the coprime uncertainty, the control system accounted for any kind of uncertainty that can exist in ASP. The loop-shaping procedure allows designer to shape the system as desired. The 2-DOF controller gives some flexibilities in the robustness satisfaction and reference tracking. The above performances prove that the observer based H_∞ loop-shaping controller is very active. Based on this control configuration, the COD can be robustly regulated and the VFA value can be exactly estimated, overcoming the limitation of difficulty in the implementation of complex and expensive sensors or analyzers.

Chapter 7. Conclusion

Nowadays, when water demand is rapidly increasing and water sources are exhausted, water treatment becomes a very urgent problem all over the world. Therefore, water area need more studies and contributions to guarantee enough productivity and lower water cost. This dissertation contribute for water treatment are by successfully applying high level control algorithms to robustly manipulate the water treatment plants.

The water treatment plants being controlled in this study include RO and ASP system. Each of the system is approximated from their respective nonlinear differential equation. The nonlinear behaviors of RO system are carefully examined. Especially, the water hammer phenomenon is well analyzed. The analysis shows the potential danger of water hammering to the system. Water hammering is consider as disturbance to the system and give some insights into the control design. The uncertainty in RO system is modelled using linear state-space parametric uncertainty framework plus unmodelled dynamics. Hence, this is a kind of general uncertainty model for RO system. The simulation shows that the robust mixed $H\infty$-μ controller can cope with large parametric and unmodelled uncertainty, as well as sensor noises. Especially, it can attenuate 58% of transient pressure caused by water hammer and can regulate the system in short time. Using this controller will help reduce the cleaning process, prolong the membranes life and lower product cost. The comprehensive analyses, linearization with parametric uncertainty, and the robust controller have remarkable contributions and are needed for the safe operation of any RO system.

The RO system is linearized as an LTI system while the ASP system with measurable scheduling parameter is modelled as an LPV system. Due to the large variation in the influent flow, which is considered as a scheduling parameter, the robust gain scheduling controller is applied to control the ASP system. In this control system, the dynamic of the controller is changing with the scheduling parameter, giving the best result for ASP system along its operation time. The simulation also

shows that the control system give the identic responses for different perturbed systems to keep the DO concentration stable and can deal with noise as well. In AD, since some state variables such as VFA...are very complicated to be measured, the robust observer based-controller is designed which is original from the 2 DOF loop-shaping controller, to regulate the COD concentration and estimate the VFA concentration. This kind of controller is useful for AD since the analyzers and sensors are very difficult to be embraced.

Finally, through this dissertation, the three high level robust control techniques are successfully designed to control two water treatment plants: RO-the desalination system and ASP-the wastewater treatment system. The controllers can regulate the plants under very harsh conditions such as high uncertainty, big disturbance such as water hammer and flow variation, as well as estimate some state variables. They help to protect the system, prolong the life of instruments, find a solution in the case lack of instruments, increase productivity and contribute on lowering the product water cost for people. Furthermore, the study and analysis of the two water treatment plants also introduce many knowledge about water treatment system and excite more consciousness of scientists and investors to cooperate in water treatment area giving more low cost water for people.

References

Abbas, A., 2006. Model predictive control of a reverse osmosis desalination unit. *Desalination*, 194, pp.268–280.

Alatiqi, I. M., Ghabris, A. H., & Ebrahim, S., 1989. System identification and control of reverse osmosis desalination. *Desalination*, 75, pp.119–140

Alatiqi, I., Ettouney, H., & El-Dessouky, H., 1999. Process control in water desalination industry: an over view. *Desalination*, 126, pp.15–32.

Ali, M. A., Ajbar, A., Ali, E., & Alhumaizi, K., 2010. Robust model-based control of a tubular reverse-osmosis desalination unit. *Desalination*, 255, pp.129–136.

Apkarian, P., & Gahinet, P., 1995. A Convex Characterisation of Gain-Scheduled H∞ Controllers. *IEEE Transactions on Automatic Control*, 40, pp.853–140864.

Apkarian, P., Gahinet, P., & Becker, G., 1995. Shelf-scheduled H∞ control of linear parameter-varying systems: a design example. *Automatica*, 31(9), pp.1256–1261.

Avlonitis, S.A., Avlonitis, D. A., Kralis, K., & Metaxa, A., 2010. Water hammer simulation in spiral wound reverse osmosis membranes. *Desalination and Water Treatment*, 13, pp.74–81.

Bartman, A. R., McFall, C.W., Chritofides, P. D., & Cohen, Y., 2009. Model-predictive control of feed flow reversal in a reverse osmosis desalination process. *Journal of Process Control* 19, pp.433–442.

Baroni, P., Bertanza, G., Collivignarelli, C., & Zambarda, V., 2006. Process improvement and energy saving in a full scale wastewater treatment plant: Air supply regulation by a fuzzy logic system. *Environmental Technology*, 27(7), pp.733–746.

Bastin, G., & Dochain, D., 1990. *On line Estimation and Adaptive Control of Bioreactors*, Elsevier Science Publishers, Amsterdam.

Becker, G., Packard, A., Philbrick, D., & BALAS, G., 1993. Control of Parametrically-Dependent Linear Systems: A Single Quadratic Lyapunov Approach. *Proceedings of the American Control Conference*, San Francisco, pp.2795–2799.

Becker, G., & Packard, A., 1994. Robust Performance of Linear Parametrically Varying Systems Using Parametrically-dependent Linear Feedback. *Systems & Control Letters*, 23, pp.205–215.

Beraud, B., Lemoine, C., & Steyer, J. P., 2009. Multiobjective Genetic Algorithms for the Optimisation of Wastewater Treatment Processes. In CarmoNicoletti, M. & Jain, L. C., *Computational Intelligence Techniques for Bioprocess Modelling, Supervision and Control*, Springer-Verlag Berlin Heidelberg, Germany.

Chaaben, A. B., & Andouls, R., 2008. MIMO modelling approach for a small photovoltaic reverse osmosis desalination system. *Research Unit RME, INSNT North Urban Centre*, BP 676, 1080, Tunis, Tunisia.

Chaudhry, M. H., & Hussaini, M. Y., 1985. Second-Order Accurate Explicit Finite-Difference Schemes for Water Hammer Analysis. *ASME Journal of Fluids Engineering*, 107, pp.523–529.

Chaudhry, M. H., 1987. Applied Hydraulic Transients. *Van Nostrand Reinhold*, New York.

Choon, T. W., Aik, L. K., Aik, L. E. & Hin, T. T., 2005. Investigation of water hammer effect through pipeline system. *International Journal on Advanced Science, Engineering and Information Technology*, 2, pp.48–53.

Cristea, S., de Prada, C., Sarabia, D., & Gutierrez, G. 2011. Aeration control of a wastewater treatment plant using hybrid NMPC. *Computer and Chemical Engineering*, 35, pp.638–650.

Davis K., & Leighton, D., 1987. Shear-induced transport of a particle layer along a porous wall. *Chemical Engineering Science,* 42 pp.275–281.

Dold, P. L., Ekama, G. A. & Marias, G. V. R., 1980. A general model for the activated sludge process. *Water Technology*, 12, pp.47–77.

Doyle, J., 1978. Guaranteed margins for LQG regulators. *IEEE transactions on Automatic Control* 23, pp.756–757.

Doyle, J., 1982. Analysis of feedback systems with structured uncertainty. *IEE Proceeding of Control Theory Application,* 129**,** pp.242–250.

Eckenfelder, W. W., 1955. Process design of aeration systems for biological waste treatment. *Presented at 48th Annual Meeting of American Institute of Chemical Engineering*

Ferreira, E. C., & Feyo de Azevedo, S., 1996. Adaptive linearising control of bioreactors. *Proceedings of Control 96, UKACC- International Conference on Control*, pp.1184-1189, Exeter, U.K., 2-5 September.

Flores-Estrella, R., Quiroz, G., Mendez-Acosta, H. O., and Femat, R., 2013. Hinf control of Anaerobic Digester for Winery Industry Wastewater treatment. *Industrial Engineering Chemistry Research*, 52, pp.2625–2632.

Fountoukidis, E., Marouls Z. B., & Marinos-Kouris, D., 1989. Modeling of calcium sulphate fouling of reverse osmosis membranes. *Desalination* 72 pp.294–318.

Gambier, A., Wellenreuther, A., & Badreddin, E., 2006. Optimal control of a reverse osmosis desalination plant using multi-objective optimization. In: *Proceedings of the 2006 IEEE International Conference on Control Applications*, Munich, Germany, October 4-6.

Gambier, A., Krasnik, A., & Badreddin, E., 2007. Dynamic modelling of a RO desalination plant for advanced control purposes. *American Control Conferences*, 7(9), pp.4854–4859.

Georgieva, P. G. & Feyo De Azevedo, S., 1999. Robust control design of an activated sludge process. *International Journal of Robust Nonlinear Control*, 9, pp.949–967.

Glover, K., 1984. All Optimal Hankel Norm Approximation of Linear Multivariable Systems, and Their L_{∞}-error Bounds. *International Journal of Control*, 39(6), pp.1145–1193.

Gujer, W., Henze, M., Mino, T., van Loosdrecht, M.C.M., 1999. Activated Sludge Model No. 3. *Water Science and Technology*, 39(1), 183–193

Henze, M., Grady, C. P. L., Gujer, W., Marais, G. V. R., & Matsuo, T., 1986. Activated Sludge Model No. 1. *International Association on Water Pollution Research and Control*, London, England.

Holenda, B., Domokos, E., Rédey, Á. & Fazakas, J., 2008. Dissolved oxygen control of the activated sludge wastewater treatment process using model predictive control. *Computer and Chemical Engineering*, 32(6), pp.1270–1278.

Ingildsen, P., 2002. *Realising full-scale control in Wastewater treatment systems*. Ph.D. Lund University.

Jafar, M., & Zilouchian, A., 2002. Real-time implementation of a fuzzy logic controller for a seawater RO plant. In*: Proceedings of the 5th biannual world, Automation Congress*, Orlando, Florida, USA, June.

Jeppsson, U., 1996. *Modelling aspects of wastewater treatment processes*. Ph.D. Lund Institute of Technology.

Johnson, G., 1980. Overview of theories for water and solute trans-port in UF/RO membrane. *Desalination*, 35, pp.21–38.

Juneseok, L., 2008. *Two issues in premise plumbing: contamination intrusion at service line and choosing alternative plumbing material*. Ph.D. the Faculty of the Virginia Polytechnic Institute and State University.

Joukowski, N., 1904. Water Hammer, translated by Miss O. Simin. *Proceedings of American TFnier TForA's Assoc*, 24, pp.365–368.

Kim, G., Park, J., Kim, J., Lee, H. & Heo, H., 2009. PID control of reverse osmosis desalination plant using immune-genetic algorithm. *ICROS-SICE International Joint Conference*, Fukuoka International Congress Center, Japan, August 18-21.

Kimura, S., 1995. Analysis of reverse osmosis membrane behaviors in a long-term verification test. *Desalination*, 100, pp.77–84.

Krause, K., Böcker, K., & Londong, J., 2002. Simulation of a nitrification control concept considering influent ammonium load. *Water Science and Technology*, 45(4–5), pp.413–420.

Lawrence A.W., and McCarty P. L., 1970. Unified basis for biological treatment design and operation. *Journal of the Sanitary Engineering Division — ASCE*, 96(SA3), pp.757–778.

Lee, K. P., Arnot, T. C., & Mattia, D., 2011. A review of reverse osmosis membrane materials for desalination-Development to date and future potential. *Journal of Membrane Science*, 370, pp.1–22.

Masahide, T., & Shoji, K., 2000. Estimation of transport parameters of RO membranes for seawater desalination. *American Institute of Chemical Engineers Journal*, 46(10), pp.1967–1973.

Meyer, U., & Pöpel, H. J., 2003. Fuzzy-control for improved nitrogen removal and energy saving in WWT-plants with pre-denitrification. *Water Science and Technology*, 47(11), pp.69–76.

Mazid, M., 1984. Mechanisms of transport through reverse osmosis membranes. *Separation Science and Technology*, 19, 357.

McFall, C. W., Bartman, A., Christofides, P. D., & Davis, J. F. 2007 Fault-tolerant control of a reverse osmosis desalination process. *8th International IFAC Symposium on Dynamics and Control of Process Systems*, Cancún, Mexico, June 6-8.

McFall, C. W., Bartman, A., Christofides, P. D., & Cohen, Y. 2008 Control of a reverse osmosis desalination process at high recovery. *American Control Conference*, Seattle, Washington, USA, June 11-13.

Moreno, R., 1991. *Control predictivo no lineal en depuración aerobia*. M.S. Universitat Autónoma de Barcelona.

Mulas, M., 2006. *Modelling and control of Activated sludge processes.* Ph.D. Dottorato Di Ricerca in Ingegneria Industriale Eniversita Degli Studi di Cagliari.

Niemi, H., & Polasaari, S., 1993. Calculation of permeate flux and rejection in simulation of ultrafiltration and reverse osmosis processes. *Journal of Membrane Science*, 84, pp.123–137.

O'Brien, M., Mack, J., Lennox, B., Lovett, D., & Wall, A., 2011. Model predictive control of an activated sludge process: A case study. *Control Engineering Practice*, 19(1), pp.54–61.

Packard, A., 1994. Gain-Scheduling via Linear Fractional Transformations. *Systems & Control Letters*, 22, pp.79–92.

Parmakian, J., 1955. *Water-Hammer Analysis*, Prentice-Hall, Inc., Englewood Cliffs, N. J. (Dover Reprint, 1963).

Pfafflin, J. R., & Ziegler, E. N., 2015. *Encyclopedia of Environmental Science and Engineering*, 5th edn, Taylor & Francis.

Rathore, N. S., Kundariya, N., & Narain, A., 2013. PID controller tuning in reverse osmosis system based on particle swarm optimization. *International Journal of Science and Research Publications*, 3(6), pp.351–358.

Riverol, C., & Pilipovik, V., 2005. Mathematical modeling of perfect decoupled control system and its application: A reverse osmosis desalination industrial-scale unit. *Journal of Automated Methods and Management in Chemistry*, 2, pp.50–54.

Robertson, M. W., Watters, J. C., Desphande, P. B., Assef, P. B. & Alatiqi, I. M., 1996. Model based control for reverse osmosis desalination processes. *Desalination*, 104, pp.59–68.

Roman, M., Slisteanu, D., & Bobasu, E., 2012. Wastewater Treatment Bioprocesses: Modeling Issues and Simulation. *In Proceeding of the Asian Conference on Sustainability, Energy & the Environment*, Osaka, Japan.

Rugh, W., & Shamma, J., 2000. Research on gain scheduling. *Automatica* 36, pp.1401–1425.

Saikia, M. D., Sarma, A. K., 2006. Simulation of water hammer flows with unsteady friction factor. *Journal of Engineering and Applied Sciences*, 1, pp.35–40.

Saemi, S. D., Raisee, M., Cervantes, M. J., & Nourbakhsh, A., 2014. Computation of laminar and turbulent water hammer flows. *6th European Conference on Computational Fluid Dynamics*, Barcelona, Spain.

Sam-sang, Y., & Seok-kwon, J., 2002. Controller design and analysis for automatic steering of passenger cars. *Mechatronics*, 12, pp.427–446.

Sanchez, A., & Katebi, M. R., 2003. Predictive control of dissolved oxygen in an activated sludge wastewater treatment plant. *In Proceedings of the European Control Conference*, Cambridge, UK, 1-4 September.

Serralta, J., Ribes, J., Seco, A., & Ferrer, J., 2002. A supervisory control system for optimising nitrogen removal and aeration energy consumption in wastewater treatment plants. *Water Science and Technology*, 45(4-5), pp.309–316.

Shamma, J. S., 1988. *Analysis and design of gain scheduled control systems*. Ph.D. Massachusetts Institute of Technology, Department of Mechanical Engineering.

Skogestad, S., and Postlethwaite, I., 2005. *Multivariable feedback control: analysis and design*, 2nd edn, Josn Wiley & Sons, Ltd., Chichester, West Sussex PO19 8SQ, England.

Soltanieh, M., Gill, W. N., 1981, Review of reverse osmosis membranes and transport model. *Chemical Engineering Communications*, 12, 279.

Slater, C. S., Zielinski, J. M., Wendel, R. G., & Uchrin, C. G., 1985. Modeling of small scale reverse osmosis system. *Desalination*, 52(3), pp.267–84.

Spanjers, H., Lier, J. B. V., 2006. Instrumentation in anaerobic treatment – research and practice. *Water Science and Technology*, 53, pp.63–76.

Tchobanoglous, G., Burton, F. L., and Stensel, H. D., 2003. *Wastewater Engineering: Treatment and Reuse*, McGraw-Hill Education, London, UK.

Thornton, A., Sunner, N., & Haeck, M., 2010. Real time control for reduced aeration and chemical consumption: a full scale study. *Water Science and Technology*, 61(9), pp.2169–2175.

Vrecko, D., Hvala, N., & Carlsson, B., 2003. Feedforward-feedback control of an activated sludge process: a simulation study. *Water Science and Technology*, 47(12), pp.19–26.

Vrecko, D., Hvala, N., Stare, A., Strazar, M., Levstek, M., Cerar, P., & Podbevsek, S., 2006. Improvement of ammonium removal in activated sludge process with feedforward feedback aeration controllers. *Water Science and Technology*, 53(4), pp.125–132.

Walker, D. J., 1996. On the structure of a two-degree-of-freedom Hinf loop shaping controller. *International Journal of Control*, 63(6), pp.1105–1127.

Weijers, S., 2000. *Modelling, identification and control of activated sludge plants for nitrogen removal*. Ph.D. Technische Universiteit Eindhoven.

Wu, F., & Dong, K., 2006. Gain-scheduling control of LFT system using parameter-dependent Lyapunov functions. *Automatica*, 42, pp.39–50.

Yamanaka, O., Obara, T., & Yamamoto, K., 2006. Total cost minimization control scheme for biological wastewater treatment process and its evaluation based on the COST benchmark process. *Water Science and Technology*, 53(4-5), pp.203–214.

Yong, M., Yongzhen, P., & Shuying, W., 2005. Feedforward-feedback control of dissolved oxygen concentration in a predenitrification system. *Bioprocess and Biosystem Engineering*, 27(4), pp.223–228.

Yong, M., Yong-zhen, P., Xiao-lian, W., & Shu-ying, W., 2006. Intelligent control aeration and external carbon addition for improving nitrogen removal. *Environmental Modelling & Software*, 21(6), pp.821–828.

Zames, G., 1981. Feedback and optimal sensitivity: Model reference transformations, multiplicative seminorms and approximate inverses. *IEEE Transactions on Automatic Control*, AC-26:301–320.

Zames, G., & Francis, B. A., 1983. Feedback, minimax sensitivity, and optimal robustness. *IEEE Transactions on Automatic Control*, 28, pp.585–600.

Zhang, P., Yuan, M., & Wang, H., 2008. Improvement of nitrogen removal and reduction of operating costs in an activated sludge process with feedforward-cascade control strategy. *Biochemical Engineering Journal*, 41(1), pp.53–58.

Zhou, K., Khargonekar, P. P., Stoustrup, J., & Niemann, H. H., 1992. Robust stability and performance of uncertain systems in state space. In *Proceedings of the 31st IEEE Conference: on Decision and Control*, Tucson, AZ, pp.662–667.

Appendices

Appendix A

Symbolic linearized partial matrices

$$
\begin{aligned}
A_{11} &= -\frac{A_p^2}{SK_m} - \frac{A_p}{\rho V} C_f \beta T (1-a) \frac{(1-R) + R(v_f - v_b)}{v_c^2} - \frac{A_p}{V} R_{v_c} v_c \\
A_{12} &= -\frac{A_p^2}{SK_m} - \frac{A_p}{\rho V} C_f \beta T (1-a) R \\
A_{21} &= -\frac{A_p^2}{SK_m} - \frac{A_p}{\rho V} C_f \beta T (1-a) \frac{(1-R) + R(v_f - v_b)}{v_c^2} \\
A_{22} &= -\frac{A_p^2}{SK_m} - \frac{A_p}{\rho V} C_f \beta T (1-a) R - \frac{A_p}{V} R_{v_b} v_b
\end{aligned}
\tag{A.1}
$$

$$
\begin{aligned}
B_{11} &= -\frac{1}{2} \frac{A_p}{V} v_c^2 \\
B_{12} &= 0 \\
B_{21} &= 0 \\
B_{22} &= -\frac{1}{2} \frac{A_p}{V} v_b^2
\end{aligned}
\tag{A.2}
$$

$$C_{11} = -A_p.36.10^5$$

$$C_{12} = -A_p.36.10^5$$

$$C_{21} = -\frac{\rho A_p}{SK_m} - C_f \beta T (1-a) \frac{(1-R) + R(v_f - v_b)}{v_c^2}$$

$$C_{22} = -\frac{\rho A_p}{SK_m} - C_f \beta T (1-a) R$$

$$C_{31} = C_f \frac{K_w \frac{\rho A_p}{SK_m} e^{\left(\frac{J_w}{K}\right)} \left(1 - e^{\left(\frac{J_w}{K_s}\right)}\right)}{\left(\frac{J_w}{K_s} + e^{\left(\frac{J_w}{K}\right)}\right)^2} \tag{A.3}$$

$$C_{32} = C_f \frac{K_w \frac{\rho A_p}{SK_m} e^{\left(\frac{J_w}{K}\right)} \left(1 - e^{\left(\frac{J_w}{K_s}\right)}\right)}{\left(\frac{J_w}{K_s} + e^{\left(\frac{J_w}{K}\right)}\right)^2}$$

$$D = \begin{bmatrix} 0 & 0 \\ 0 & 0 \\ 0 & 0 \end{bmatrix} \tag{A.4}$$

Appendix B

Calculated values of linearized matrices

$$A = \begin{bmatrix} -5.31 & -2.016 \\ -2.3 & -5.03 \end{bmatrix}, B = \begin{bmatrix} -0.0254 & 0 \\ 0 & -0.0254 \end{bmatrix}$$

$$C = \begin{bmatrix} -457.2 & -457.2 \\ -104.88 & -92.08 \\ 109.91 & 109.91 \end{bmatrix}, D = \begin{bmatrix} 0 & 0 \\ 0 & 0 \\ 0 & 0 \end{bmatrix} \tag{B.1}$$

$$G(s)=\begin{bmatrix} \dfrac{11.61s+31.75}{s^2+10.34s+22.09} & \dfrac{11.61s+38.26}{s^2+10.34s+22.09} \\ \dfrac{2.66s+8.03}{s^2+10.34s+22.09} & \dfrac{2.33s+7.05}{s^2+10.34s+22.09} \\ \dfrac{-2.79s-7.63}{s^2+10.34s+22.09} & \dfrac{-2.79s-9.19}{s^2+10.34s+22.09} \end{bmatrix}$$

$$=\begin{bmatrix} \dfrac{T_{11}s+K_{11}}{s^2+2\xi\omega_n s+\omega_n^2} & \dfrac{T_{12}s+K_{12}}{s^2+2\xi\omega_n s+\omega_n^2} \\ \dfrac{T_{21}s+K_{21}}{s^2+2\xi\omega_n s+\omega_n^2} & \dfrac{T_{22}s+K_{22}}{s^2+2\xi\omega_n s+\omega_n^2} \\ \dfrac{T_{31}s+K_{31}}{s^2+2\xi\omega_n s+\omega_n^2} & \dfrac{T_{32}s+K_{32}}{s^2+2\xi\omega_n s+\omega_n^2} \end{bmatrix} \tag{B.2}$$

$$A_1=\begin{bmatrix} -0.41 & -0.21 \\ -0.41 & -0.21 \end{bmatrix}, B_1=\begin{bmatrix} 0 & 0 \\ 0 & 0 \end{bmatrix}$$

$$C_1=\begin{bmatrix} 0 & 0 \\ -1.3\text{x}10^5 & -6.79\text{x}10^4 \\ 0 & 0 \end{bmatrix}, D_1=\begin{bmatrix} 0 & 0 \\ 0 & 0 \\ 0 & 0 \end{bmatrix} \tag{B.3}$$

$$G_r=\left[\begin{array}{cc|cc:cc} -5.31 & -2.016 & -0.0336 & 0 & -0.0012 & -0.051 \\ -2.3 & -5.03 & 0 & -0.0023 & -0.0012 & -0.051 \\ \hline -457.2 & -457.2 & 0 & 0 & 0 & 0 \\ -104.88 & -92.08 & 0 & 0 & -382.96 & 0 \\ 109.91 & 109.91 & 0 & 0 & 0 & 0 \\ \hdashline 339.45 & 17.3 & 0 & 0 & 0 & 0 \\ 0.033 & -0.66 & 0 & 0 & 0 & 0 \end{array}\right] \tag{B.4}$$

Appendix C

The weighting functions and analytical controller *K*

$$W_M = \begin{bmatrix} \dfrac{0.5s+0.78}{s+3.46} & 0 \\ 0 & \dfrac{0.52s+1.2}{s+3.47} \end{bmatrix} \tag{C.1}$$

$$W_P = \begin{bmatrix} \dfrac{0.8s+1.5}{5.5s+10^{-4}} & 0 \\ 0 & \dfrac{4.8s+35}{6.5s+10^{-4}} \\ 0 & 0 \end{bmatrix} \tag{C.2}$$

$$K = \begin{bmatrix} K_{11} & K_{12} \\ K_{21} & K_{22} \\ K_{31} & K_{32} \end{bmatrix} \tag{C.3}$$

where:

$$\begin{aligned}
K_{11} &= \frac{0.03s^6 + 5.05\text{x}10^5 s^5 + 2.81\text{x}10^7 s^4 - 7.05\text{x}10^9 s^3 - 1.96\text{x}10^{11} s^2 - 3.68\text{x}10^{11} s - 5.67\text{x}10^7}{s^6 + 8315s^5 + 7.25s^4 + 1.57\text{x}10^9 s^3 + 6.9\text{x}10^{10} s^2 + 2.11\text{x}10^7 s + 1610} \\
K_{12} &= \frac{0.8s^6 + 775s^5 + 5.58\text{x}10^7 s^4 + 1.45\text{x}10^{10} s^3 + 4.35\text{x}10^{11} s^2 + 8.2\text{x}10^{11} s + 1.26\text{x}10^8}{s^6 + 8315s^5 + 7.25s^4 + 1.57\text{x}10^9 s^3 + 6.9\text{x}10^{10} s^2 + 2.11\text{x}10^7 s + 1610} \\
K_{21} &= \frac{0.11s^6 + 6.76\text{x}10^5 s^5 + 1.23\text{x}10^9 s^4 + 1.39\text{x}10^{11} s^3 + 3.09\text{x}10^{12} s^2 + 6.73\text{x}10^{12} s + 1.01\text{x}10^9}{s^6 + 8315s^5 + 7.25s^4 + 1.57\text{x}10^9 s^3 + 6.9\text{x}10^{10} s^2 + 2.11\text{x}10^7 s + 1610} \\
K_{22} &= \frac{1.23s^6 - 1.74\text{x}10^4 s^5 - 9.95\text{x}10^7 s^4 - 6.63\text{x}10^9 s^3 + 1.26\text{x}10^{12} s^2 + 8.62\text{x}10^{12} s + 1.3\text{x}10^9}{s^6 + 8315s^5 + 7.25s^4 + 1.57\text{x}10^9 s^3 + 6.9\text{x}10^{10} s^2 + 2.11\text{x}10^7 s + 1610} \\
K_{31} &= \frac{-0.02s^6 - 1.28\text{x}10^5 s^5 - 2.14\text{x}10^7 s^4 - 2.09\text{x}10^8 s^3 - 1.05\text{x}10^9 s^2 + 2.35\text{x}10^5 s + 59.72}{s^6 + 8315s^5 + 7.25s^4 + 1.57\text{x}10^9 s^3 + 6.9\text{x}10^{10} s^2 + 2.11\text{x}10^7 s + 1610} \\
K_{32} &= \frac{-0.16s^6 + 398.7s^5 - 1.25\text{x}10^7 s^4 - 3.29\text{x}10^9 s^3 - 1.11\text{x}10^{11} s^2 - 3.29\text{x}10^7 s - 2444}{s^6 + 8315s^5 + 7.25s^4 + 1.57\text{x}10^9 s^3 + 6.9\text{x}10^{10} s^2 + 2.11\text{x}10^7 s + 1610}
\end{aligned} \tag{C.4}$$

Appendix D

Symbolic linearized partial matrices of ASP

$$A=\begin{bmatrix} -K_{la}D_{fb}-\dfrac{q_i+q_r}{V} & -K_X\mu_S S-K_0 & -K_X\mu_S X \\ 0 & \mu_X\dfrac{S}{K_S+S}-2K_{dx}\dfrac{X}{S}-\dfrac{q_i+q_r}{V}-K_{cx} & \mu_X\dfrac{K_S X}{(K_S+S)^2}+K_{dx}\dfrac{X^2}{S^2} \\ 0 & -\dfrac{1}{\alpha}\mu_X\dfrac{S}{K_S+S}+2K_{dx}\dfrac{X}{S}+K_{cs} & -\dfrac{1}{\alpha}\mu_X\dfrac{K_S X}{(K_S+S)^2}-K_{dx}\dfrac{X^2}{S^2}-\dfrac{q_i+q_r}{V} \end{bmatrix}$$

where

$$A_{11}=\frac{\partial f_1}{\partial c}\quad A_{12}=\frac{\partial f_1}{\partial x}\quad A_{13}=\frac{\partial f_1}{\partial s}$$
$$A_{21}=\frac{\partial f_2}{\partial c}\quad A_{22}=\frac{\partial f_2}{\partial x}\quad A_{23}=\frac{\partial f_2}{\partial s},\quad B=\begin{bmatrix} K_{la}(c_s-c) & \dfrac{c_r-c}{V} \\ 0 & \dfrac{X_r}{V} \\ 0 & \dfrac{S_r}{V} \end{bmatrix}$$
$$A_{31}=\frac{\partial f_3}{\partial c}\quad A_{32}=\frac{\partial f_3}{\partial x}\quad A_{33}=\frac{\partial f_3}{\partial s}$$